Effects of the Geometric Modifications on the Shear Layer Excitation Source in Co-Axial Side Branches

by

Omar S. Hammad

A thesis submitted to the School of Graduate and Postdoctoral Studies in partial fulfillment of the requirements for the degree of

Master of Applied Science

in

Mechanical Engineering

Faculty of Engineering and Applied Science

University of Ontario Institute of Technology
(Ontario Tech University)

Oshawa, Ontario, Canada

August 2023

THESIS EXAMINATION INFORMATION

Submitted by: **Omar S. Hammad**

Master of Applied Science in Mechanical Engineering

Title: Effects of the Geometric Modifications on the Shear Layer Excitation Source in Co-Axial Side Branches

An oral defense of this thesis took place on August 18, 2023 in front of the following examining committee:

Examining Committee

Chair of Examining Committee	Dr. Amirkianoosh Kiani
Research Supervisor	Dr. Atef Mohany
Examining Committee Member	Dr. Moustafa El-Gindy
Thesis Examiner	Dr. Zeinab El-Sayegh

The above committee determined that the thesis is acceptable in form and content and that a satisfactory knowledge of the field covered by the thesis was demonstrated by the candidate during an oral examination. A signed copy of the Certificate of Approval is available from the School of Graduate and Postdoctoral Studies.

Abstract

This comprehensive study delves into the interaction between shear layer oscillations and the acoustic field within co-axial cavities, spotlighting the efficacy of the sound source model as a reliable semi-empirical modeling methodology. The focus is on how the downstream acoustic boundary conditions, when varied, markedly alter the acoustic field and the aeroacoustic sound source within deep co-axial cavities. Furthermore, it highlights how different upstream distances influence the aeroacoustic resonance of a coaxial side branch and the resultant peak acoustic pressure and the sound source term. Interestingly, edge geometry modification, specifically edge rounding and chamfering, plays a crucial role in the phasing of the shear layer with the acoustic field, thereby affecting the excitation and resonance behavior of the aeroacoustic system. These alterations significantly impact the aeroacoustic response, including peak pressure and lock-in range. These findings, derived from rigorous experimentation and predictive modeling, provide valuable insights into aeroacoustic modeling within coaxial cavities, contributing significantly to the design of industrial applications seeking to avoid and mitigate aeroacoustic resonance.

Keywords: Aeroacoustic sound source; Modeling; Flow-excited acoustic resonance; Cavity flow;Co-axial side branch; Shear layer excitation.

Acknowledgements

"Of all of Allah's servants, only the knowledgeable are truly in awe of Him. Allah is indeed Almighty, All-Forgiving." 35:28 Quran

First and foremost, I would like to extend my sincerest appreciation to Prof. Atef Mohany. His invaluable guidance, continuous support, and relentless encouragement have been the bedrock of my academic journey. His passion for knowledge, commitment to mentoring, and dedication to fostering intellectual growth have deeply inspired me and enriched my learning experience.

Next, I want to express my gratitude towards my esteemed colleagues Ahmed Shoukry, Abdelrahman Alsaka, Dr. Mohammad Alziadeh, Ali Saudi, Rasha Noufal, and Marc Hanna. Their relentless support and invaluable insights have been crucial in my development and have added depth to our intellectual discussions, enriching my learning journey. I owe a special thanks to my housemates, Ahmed Shoukry, Ahmed Abdelsattar, Abdelrahman Alsaqa, and Karim Monaem, who have provided a nurturing and supportive living environment throughout my academic pursuit. Their friendship, support, and companionship have lightened the rigors of academic life, turning a strenuous journey into an enjoyable adventure.

On a more personal note, I would like to express my deepest gratitude to my parents, Sameh and Safaa, for their unwavering love, steadfast support, and perpetual care. Your unyielding belief in me has been my pillar of strength, your sacrifices my

motivation, and your love my inspiration.

I must also mention the role of my dear grandmother, Zozo, whose unconditional love and wisdom have been a guiding light in my life. Her spiritual support and tender care have been a source of strength and inspiration throughout this journey.

Finally, I want to express my sincere thanks to my sisters, Rony, Mera, and Nana. Their constant care, emotional support, and undying faith in me have bolstered my spirits in times of stress and doubt, and have played a pivotal role in my academic success. As I look back on my journey, I am overwhelmed with gratitude for each of you. Alhamdulillah.

Author's Declaration

I hereby declare that this thesis consists of original work of which I have authored. This is a true copy of the thesis, including any required final revisions, as accepted by my examiners.

I authorize the University of Ontario Institute of Technology (Ontario Tech University) to lend this thesis to other institutions or individuals for the purpose of scholarly research. I further authorize University of Ontario Institute of Technology (Ontario Tech University) to reproduce this thesis by photocopying or by other means, in total or in part, at the request of other institutions or individuals for the purpose of scholarly research. I understand that my thesis will be made electronically available to the public.

Omar Hammad

Omar S. Hammad

Statement of Contributions

I hereby certify that I am the sole author of this thesis. I have used standard referencing practices to acknowledge ideas, research techniques, or other materials that belong to others. Furthermore, I hereby confirm that the creative contributions and innovative insights described within this thesis originate from my own endeavors with the aid of my supervisor Prof. Atef Mohany.

Contents

List of Tables

List of Figures

Nomenclature

Symbol	Definition
Latin letters:	
A	Side branch cross-sectional area
B	Total enthalpy
c	Chamfered distance
c_0	Speed of sound in air
D	Main Pipe Diameter
d	Side branch diameter
e	End correction factor
$\mathbf{F}_{\text{coriolis}}$	Coriolis force component $= -\rho(\omega \times U)$
fa	Acoustic mode frequency
f_s	Frequency of flow oscillation
He	Helmholtz number $= kD/2$
k	Wavenumber $= 2\pi/\lambda$
L	Upstream distance
M	Mach number
P	Acoustic pressure
$p(x,t)$	Spatiotemporal distribution of the acoustic pressure
$p^+(x,t)$	The spatiotemporal distribution of the incident acoustic pressure
$p^-(x,t)$	The spatiotemporal distribution of the reflected acoustic pressure
Pr	Prandtl number
q	Acoustic volume velocity

R	Reflection coefficient
r	Rounding radius
Re	Reynolds number
$s(x,t)$	Entropy fluctuations
Δs	Dimensionless acoustic source impedance
St	Strouhal number
U	Flow velocity
U_{con}	Vortex convection velocity
V	Normalized Acoustic Particle Velocity
v	Acoustic particle velocity
Z	Acoustic Impedance
ΔP	The pressure difference across the shear layer
Greek letters:	
α	Total attenuation constant
α_0	Viscothermal attenuation constant
Δ	Velocity ratio
γ	Specific heat ratio
λ	Wavelength
μ	Fluid dynamic viscosity
Π	Instantaneous Acoustic Power
Φ	Complex amplitude function
ψ	Complex stream function
ρ	Density of air
θ	Boundary layer momentum thickness
ω	Vorticity vector
ζ	Damping coefficient
$Y_\circ$	Characteristic acoustic Impedance

Chapter 1

Introduction

1.1 Problem Overview

Acoustic pulsations at a low frequency within pipe networks have been detected across a wide range of technical operations. Such pulsations present significant challenges, not solely due to the resultant noise, but also due to the potential for mechanical failures within the pipe infrastructure [75]. The elevated magnitude of these acoustic pressure variances can induce mechanical stress, potentially leading to fatigue-induced failure. Even at reduced pulsation levels, there can be interference with volume flow measurements [70], or it can activate vibration control apparatuses. In instances where the vibratory and pressure pulsation levels do not pose a direct threat to system safety and are deemed tolerable, they can nevertheless contribute to additional pressure losses and compromise overall system efficiency.

Predictable forced pulsations, such as those instigated by compressors, can be anticipated during the design phase through the implementation of numerical models. However, a distinct form of acoustic pulsations arises from aeroacoustic oscillations, induced by flow instability within the pipe systems. These oscillations are termed as

self-sustained or self-excited.

A key factor in the generation of aeroacoustic oscillations is the shear layer formed by the grazing flow inside a pipe when it passes over the aperture of a closed side branch. This shear layer acts as a significant source of sound, driving these oscillations within pipeline networks. The self-excited aeroacoustic pulsations in these unstable shear layers are the result of a feedback loop between the flow field, which is linked to the unstable shear layer, and the acoustic flow field.

Within this feedback excitation mechanism, the pivotal components are the oscillations of the shear layer and its interaction with the resonant acoustic mode. In such a context, the resonant acoustic mode acts as the feedback event, amplifying the system oscillations significantly. This complex interplay between hydrodynamic and acoustic phenomena is a central aspect of managing the performance and stability of pipe networks.

1.2 Motivations

This research is primarily driven by the susceptibility of various engineering equipment to flow-excited acoustic resonance, a phenomenon that arises at discrete flow velocities, thus endangering the integrity of the facility and exposing operations to the risks associated with acoustic resonance. There is a wealth of literature dedicated to investigating the aeroacoustic response of two-dimensional cavities for shallow and deep branches. However, cylindrical cavities, despite their omnipresence in industrial applications, have not received commensurate attention. The challenges associated with cylindrical cavities lie in their three-dimensionality and the complexity of their shear layer dynamics.

The design process of a pipeline system necessitates support from comprehen-

sive aeroacoustic experiments that accurately represent the acoustic system. The aeroacoustic response is determined by several factors, including damping, system pressure, boundary conditions, and the localized parameters of the acoustic and fluid fields. The immense variability of these parameters makes it practically impossible to encapsulate all potential combinations through experimental data alone. This underscores the need for an effective modelling technique capable of predicting the aeroacoustic response of resonating deep cavities. Traditional linear models have fallen short in predicting acoustic resonance due to the pronounced nonlinearity inherent in self-excited acoustic resonance. In response to this, Graf and Ziada [27] proposed a semi-empirical model capable of accurately predicting the aeroacoustic response, specifically applying it to coaxial cavities with sharp edges. Their results proved reliable and accurate, suggesting that their model can be utilized for predictions in geometrically similar setups that exhibit the same flow-sound interaction mechanisms. However, cavities in industrial applications vary significantly in terms of geometry, boundary conditions, and acoustic particle velocity distributions. Hence, there is an imperative need to extend this model to investigate its applicability to different geometric cavity modifications and to test its reliability in varied configurations.

1.3 Objectives

The objectives of this current research are as follows:

1. Ensuring the consistency of the aeroacoustic sound source modeling technique across different experimental setups, it's necessary to carry out experimental measurements of the aeroacoustic sound source term for the sharp-edged coaxial cavity by ensuring that the modeling technique's applicability relies only on the specific characteristics of the flow and acoustic fields, rather than being

influenced by the particulars of the experimental test section.

2. Investigate the impact of acoustic boundary conditions and the reflection coefficient at the pipe's acoustic boundary on the aeroacoustic sound source. This exploration necessitates a careful evaluation of how these elements may influence the aeroacoustic response, signifying that alterations in these parameters could lead to changes in the aeroacoustic system's behavior.

3. Investigate the influence of the upstream velocity profile, as it approaches the deep cavity, on the aeroacoustic sound source and its consequent effect on the aeroacoustic response. This will be achieved by adjusting the upstream distance to simulate developing flow conditions, enabling us to understand how variations in the initial flow conditions can impact the resulting aeroacoustic behavior.

4. Investigate the impact of rounding the edge of the co-axial cavity on the aeroacoustic sound source and its subsequent effect on the aeroacoustic response. This will be accomplished by testing various rounding values, aiming to understand how these geometric modifications can influence the cavity's aeroacoustic characteristics.

5. Evaluate the impact of chamfering the edge of the co-axial cavity on the aeroacoustic sound source and its ensuing influence on the aeroacoustic response. This is accomplished by testing various chamfer sizes and comparing their effect with that of the rounded edge, thus gaining a comprehensive understanding of how these specific geometrical adjustments can affect the aeroacoustic behavior of the cavity.

1.4 Thesis Outlines

This thesis is organized into 6 chapters. The arrangement of the chapters is as follows:

- Chapter 1: offers a broad overview of the problem at hand, outlining the challenges present, and highlighting the motivation behind this study. It further elucidates the objectives intended to be achieved through this research endeavor..

- Chapter 2: provides an extensive review of existing literature, focusing on topics such as self-excited acoustic resonance, self-sustained oscillations of the shear layer, and the acoustic coupling between the shear layer and the acoustic field. It also highlights the diverse experimental endeavors undertaken to investigate these phenomena. The review further elaborates on various attempts to model flow-acoustic coupling, whether it be through experimental means, analytical approaches, or numerical methods.

- Chapter 3: presents the experimental setup employed for the experimental component of the study, along with detailing the calibration procedures implemented for the various sensors and equipment. Additionally, it outlines the theoretical methodology utilized in computing the aeroacoustic sound source from the gathered experimental data.

- Chapter 4: This chapter delineates the modeling technique utilized to predict the aeroacoustic response, applying the aeroacoustic sound source map as input, and specifically applying it to the sharp-edge co-axial cavity case. Further, it discusses the effects of altering the downstream acoustic boundary condition and the upstream flow velocity on the aeroacoustic sound source term.

- Chapter 5: This chapter explicates the impact of rounding and chamfering on the aeroacoustic sound source. It presents a comparative analysis on how both

chamfering and rounding affect the aeroacoustic response. .

- Chapter 6:This chapter encapsulates the principal conclusions drawn from the study, elucidates the original contributions made, and proffers recommendations for future research.

Chapter 2

Literature Review

2.1 Industry Applications and Implications of Flow-Excited Acoustic Resonance

Flow-excited acoustic resonance has been the source of numerous technical challenges in the industrial sector, leading to considerable safety risks and financial losses. In 2002, the steam dryer of the boiling water reactor (BWR) at Quad Cities exhibited signs of high cycle fatigue failures. This unexpected issue arose following efforts to boost the unit's output power by 17%. Initial efforts to repair the dryer involving the utilization of thicker plates and stronger welds proved unsuccessful, as new cracks developed upon resumed operation [54].

These cracks materialized on the dryer's outer plates, confronting the main steam line inlet nozzles. To investigate the reasons of these cracks, the steam dryer was replaced with a thicker variant equipped with pressure transducers. This allowed for direct measurement of pressure fluctuations at numerous points.

Concurrent with these events, the safety relief valves placed along the main steam lines were subjected to elevated levels of vibration. Maintenance inspections per-

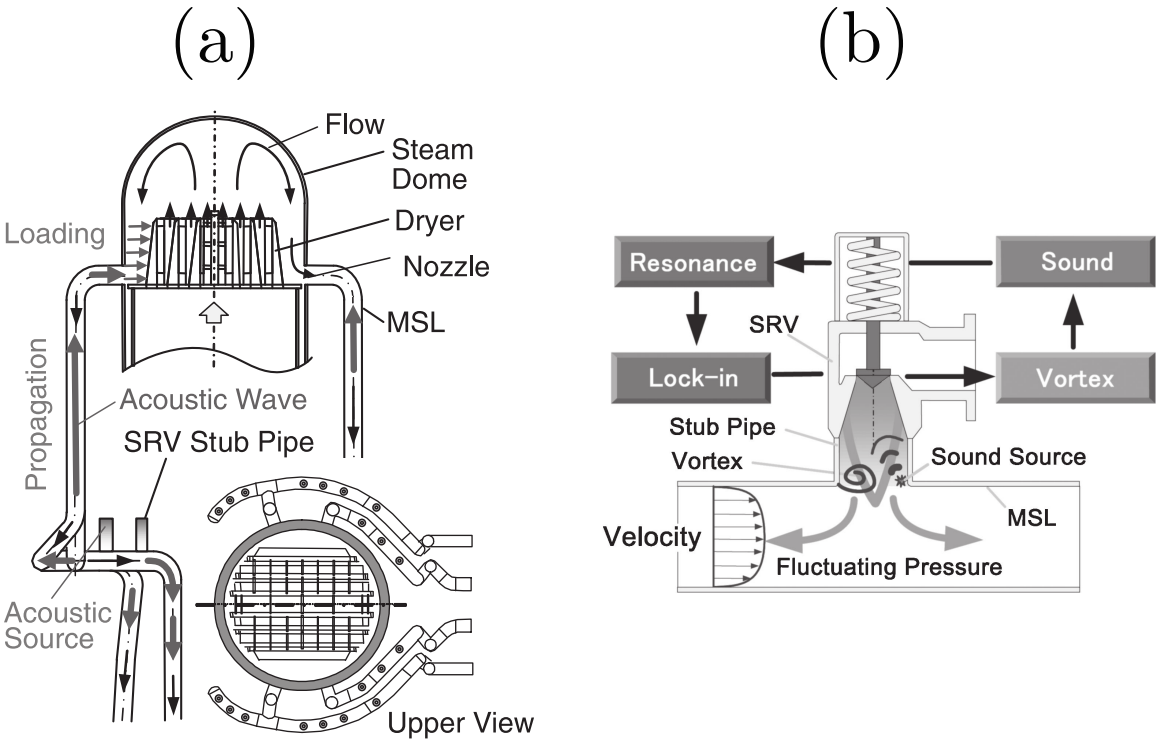

Figure 2.1: (a) Steam dryer assembly of quad cities unit 2, and (b) details of the acoustic excitation in the safety relief valve stub pipe. [49].

formed during a refueling outage revealed damage to some of the safety valves. The pressure measurements suggested that the increased steam velocity in the main steam lines, correlated with the elevated output power, stimulated the acoustic resonant modes in the standpipes of the safety valves installed along the main steam lines.

That produced tonal noise was of such intensity that it inflicted damage on some valves in addition to propagating upstream in the main steam lines, infiltrating the reactor dome and inflicting further damage on the steam dryer. This issue was ultimately resolved by modifying the geometry of the standpipe to circumvent the acoustic excitation during elevated output power [49].

In 1973, pronounced pulsations, an order of magnitude higher than the safe peak levels, were observed in a compressor station within the Dutch gas transport system in Ommen, The Netherlands. Remarkably, the ratio of the amplitude of the acoustic

velocity to the main flow velocity reached up to 0.4. Furthermore, the amplitude of the pressure pulsations achieved a substantial 1.5 bar in situations where static pressure was 60 brain a 42-inch pipes.

After investigation, the pressure oscillations were originated from the aeroacoustic coupling of the side branch with the separated shear layers [11]. Intriguingly, these pulsations only manifested when the flow velocity surpassed a certain critical threshold. This issue was consequently addressed by curtailing the local velocity of the flow at the shear layer mouth via the implementation of by-pass piping, a solution that effectively navigated the constraints of the situation while preserving the integrity and efficiency of the larger gas transport system.

The growing demand for energy has necessitated the escalation of flow velocity within components of power plants. As a result, this increase has induced vibration-related challenges and flow-excited acoustic resonance phenomena. These issues have been identified across a wide array of industrial systems and components, such as combustion chambers [60], pipe networks [10, 57, 66], flow over cylinders and square sections, as well as heat exchanger tube bundles [4, 6, 8, 69].

The heightened flow velocity within these structures intensifies the potential for aeroacoustic oscillations, which can lead to considerable mechanical stress and potential damage to the system's components. Therefore, it is imperative to continue the study and development of control strategies and design considerations that could mitigate these challenges [55, 68], enhance system stability, and ensure the safety and efficiency of power plants.

2.2 Acoustic Waves in Ducts

Flow duct systems form the critical infrastructure of various industrial applications, such as power generation facilities, petrochemical stations, and liquid and gas distribution pipelines. For practical implementations, these duct systems exhibit complex and intricate geometrical configurations, incorporating various fittings and discontinuities. These complexities often act as catalysts for noise generation and vibration within the piping system.

In circumstances where sound sources are present within the system, the design considerations become particularly challenging. The transmission and distribution of acoustic energy, along with fluctuating pressure throughout the system, emerge as significant areas of concern. These factors can impact the overall system performance, maintenance requirements, and long-term operational efficiency. Therefore, it is imperative to consider and address these issues in the design and operation of complex duct systems, ultimately to ensure reliable and safe operation of these critical infrastructures.

Sound propagation in open spaces constitutes a complex problem; nevertheless, wave propagation within ducts can be simplified through the assumption of plane wave acoustic theory. The emphasis here is on the plane acoustic wave, applying this theory to the propagation of pressure waves in ducts with moving bulk flows, inclusive of cavities, branches, and other forms of discontinuities.

The properties inherent in plane waves allow a simplification of the governing equations and contribute to a clearer understanding of how physical factors influence wave propagation. In addition, the uniform distribution of acoustic pressure and acoustic particle velocity across any duct cross-section in the plane wave condition allows for measurements to be taken at the pipe walls without disrupting the flow.

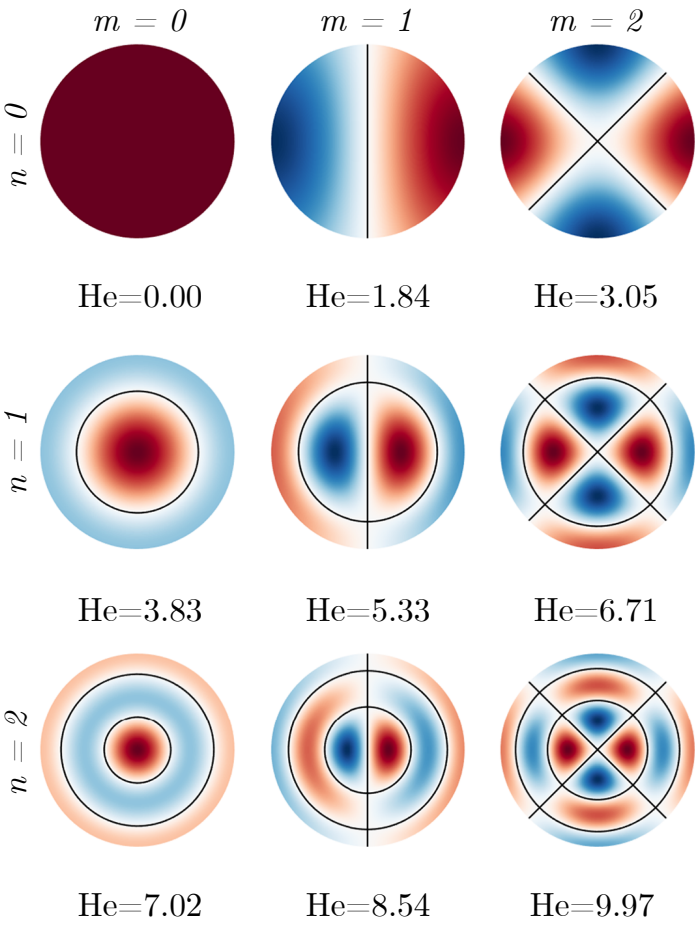

Figure 2.2: Mode shapes of different duct modes in circular pipes up to m=2, n=2, also showing the cut-on Helmholtz number for each mode. (adopted from Lympany and Ahuja (2020) [39])

However, to characterize the pressure wave propagation in a piping system as plane wave propagation, certain conditions have to be checked. These prerequisites ensure the accuracy of the plane wave model and its applicability to physical models.

A traveling wave within a duct can be assumed to be a plane wave when the wavelength (λ) surpasses the greatest dimension of the duct's cross-section. Regarding ducts with a circular profile with a diameter (D), and for stationary medium, the first transverse acoustic mode, characterized by a wavenumber ($k = 2\pi/\lambda$), materializes when the Helmholtz number ¿ 1.84 (He=$kD/2$). The second cross mode can be excited for pressure waves of the Helmholtz number slightly above 3. Regarding

the propagation of the first radial mode, Helmholtz number needs to surpass 3.83, as illustrated in Figure 2.2. It was suggested by Munjal (1987) [51] and Davies (1988) [16] that the moving bulk flow decreases the limiting values of the Helmholtz number by a factor of $(1 - M^2)$. Hence, the plane wave's limiting value of the Helmholtz number is approximately 1.84 or slightly less, a range that encapsulates many flow duct noise issues.

The amplitude of the pressure fluctuations is considered as another condition to assume the propagating wave as a planer wave. Davies (1987) [15] suggested that, for low amplitudes, the plane wave assumption holds valid which typically varies in the range of 0.01 to 0.001 bar, with the upper limit decreasing by increasing the frequency of the fluctuations.

A final limitation to the applicability of plane wave acoustic theory to flow ducts concerns the stiffness of the duct walls. When the walls of the duct are acoustically rigid and non-absorbent, this promotes a swift decay of the excited radial or transverse modes across the pipe diameter. In essence, the duct modes will be observable only around their source.

Much like structural resonance modes and frequencies, the acoustic modes of piping systems are contingent upon the boundary conditions at the pipe terminations. Reactive terminations can trigger the reflection of sound waves back into the pipe, subsequently resulting in the formation of standing waves, known as the system's acoustic modes. This set of conditions can lead to an accumulation of acoustic energy within the piping system, thereby making it easy for flow turbulence within the pipe to excite these acoustic modes. These resonant acoustic modes are identified as the system's eigen-modes [33]. Every mode is characterized by a complex resonance frequency (eigen-value) and a mode shape (eigen-vector). The frequency of the system's free oscillation at resonance conditions corresponds to the real part of

each complex frequency, while the quality factor of the resonance is gauged by the imaginary part [50].

The pipe system's resonance behavior is reliant on its geometric configuration and the boundary conditions of the domain. In real-world scenarios, the manifestation of sound radiation is a constant, thereby resulting in the eigen-values of acoustic modes being in the complex form. Global modes, that excite the entire system, can be defined based on the system's resonance modes. The responses of these modes are largely influenced by the boundary conditions. Conversely, trapped or localized modes encompass only a subset of the pipe system and exhibit relative insensitivity to the boundary conditions [21].

Resonance modes, when restricted to a specific section of the piping system and displaying nearly imperceptible radiation losses extending to other segments of the pipes, gain a degree of independence from the overall system. This detachment implies they remain uninfluenced by the boundary conditions defined at the termination points of the system. The energy pertaining to these modes is effectively trapped within a subsystem, leading to their characterization as 'trapped modes' within the literature. The pressure distribution representation of trapped acoustic modes can be illustrated via the example shown in Figure 2.3. This example delineates the configurations of three distinct side branches: single, tandem, and co-axial.

The pulsation amplitude within a side branch is profoundly affected by the acoustic radiation of the branch into the main pipe, an effect stemming from both viscothermal losses in the main pipe and radiation losses at the end conditions of the pipe. Nonetheless, significantly decreasing the branch to the main pipe diameter ratio (d/D), the acoustic radiation of the trapped mode into the main pipe diminishes, reflecting the behavior of acoustic radiation from a flanged open pipe into a semi-infinite volume. Consequently, the reflection coefficient of the branch comes close

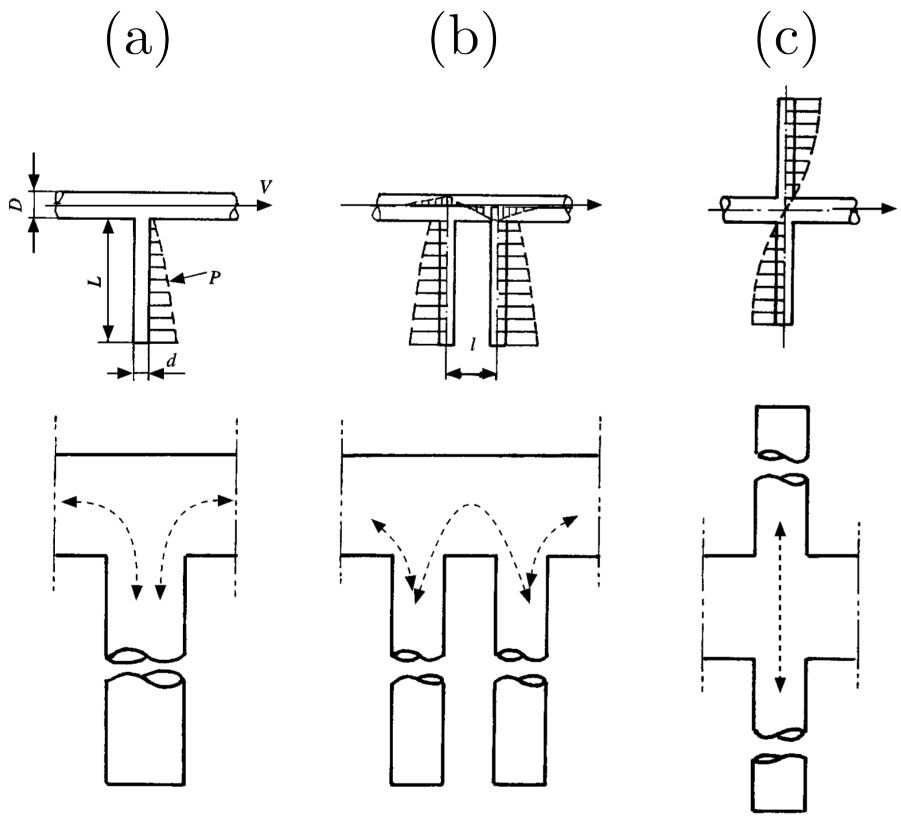

Figure 2.3: Different arrangements of side branches and their fundamental acoustic trapped mode (top figures). The arrows indicate the acoustic flux oscillation at each mode (bottom figures). (a) Single closed side branch, (b) tandem closed side branch, (c) co-axial side branch. [78]

to one [58]. In such a situation, intense acoustic resonance is excited and trapped within the branch, granted that the branch length corresponds to a low acoustic mode (for instance, $\lambda/4$); if not, the viscothermal losses within the branch could be large enough to suppress the resonance. Studies by Ziada and Shine [78] have illustrated that a decrease in the maximum pulsation pressure is accompanied by increasing the diameter ratio.

In situations involving two closely-located, equally-lengthed, and well-tuned branches, the acoustic particle velocity at the opening of one branch mirrors but opposes that at the opening of the other branch. For coaxial branches, the transmitted acoustic power

into the main pipe is rather negligible and it forms powerful acoustic coupling. As a result, the acoustic modes of the coaxial branches are identified as trapped acoustic modes with an vanishingly small imaginary component of the eigenvalue [21]. These conditions can lead to substantially increased pulsation amplitudes, surpassing those in a single branch scenario, especially for large d/D ratios, as corroborated by studies from Ziada and Bühlmann [76].

Regarding tandem side branches depicted in Figure 2.3 (b), the radiated acoustic power into the main pipe escalate with the increasing the center distance between the branches. The lower modes here are not considered fully trapped but are better referred to as "nearly trapped" modes due to the small yet non-zero imaginary components of their eigenvalues. A special case arises when the center distance between the side branches is about $\lambda/2$, creating a pressure node at the opening of each branch. Here, the excited modes become fully trapped once more as radiation losses become null. Another special configuration surfaces when a single side branch is well-tuned with either the upstream or downstream main pipe, thus forming an isolated subsystem of trapped modes.

Fundamentally, the acoustic energy in fluid conveying piping systems can be trapped within either a global mode or a localized mode, thereby creating a standing wave. Under certain circumstances, the radiation losses can be negligible, leading to pronounced generation of tonal noise. This can result in serious noise and vibration issues, as exemplified in Section 2.1. However, the triggering of these acoustic modes requires a sound source oscillating at the corresponding frequency. Therefore, the ensuing section will scrutinize the characteristics of flow instabilities serving as sound sources.

2.3 Flow-excited acoustic resonance

At higher Reynolds numbers, large flow structures like shear layers, wakes and jets created by flow instabilities become a significant source of unsteadiness within the flow field. This turbulence results in the generation of fluctuating forces on the pipe walls and the production of vortices. Since Powell's introduction of the edgetone theory [58], these oscillatory forces have been identified as a source of sound. Moreover, a correlation has been established between the vorticity field and sound generation. However, in Powell's theory, the pipe wall does not contribute to sound generation through vibration, and the theory doesn't provide any quantitative predictions for the sound generated from separated shear flows.

Later, Howe presented the vortex sound theory [30], which established a link between the flow field and the acoustic field. Utilizing Helmholtz's decomposition, Howe delineated the acoustic field as the fluctuating irrotational portion of the flow field. Substituting this definition into Crocco's formulation of the momentum equation, and assuming a low Mach number to dismiss the influence of convection on sound propagation, simplifies the wave equation to

$$\frac{1}{c_0^2}\frac{\partial^2 B}{\partial t^2} - \nabla^2 B = \nabla \cdot (\omega \times \mathbf{U}) \tag{2.1}$$

where c_0 is the speed of sound at no flow, $\mathbf{U}$ is the velocity vector, ω is the vorticity vector which is defined as the curl of the velocity, and B is the total enthalpy that is defined as $B = \frac{\mathbf{U}}{2} + \int \frac{dp}{\rho}$.

From Equation 2.1, it can be observed that the Coriolis force component $\mathbf{F}_{coriolis} = -\rho(\omega \times \mathbf{U})$ on the right-hand side acts as a sound source. Thus, Howe [30] proved that the instantaneous acoustic power, denoted by Π, generated through the convection of the vorticity field, denoted by ω, and acoustic particle velocity v, within a fluid

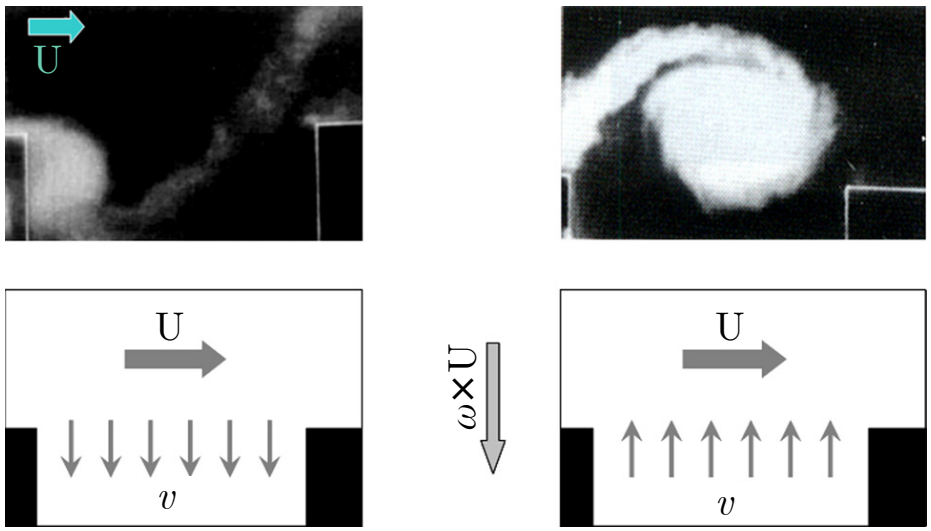

Figure 2.4: Visualization of the flow field during acoustic resonance of a deep cavity (upper figures) with the triple product illustration between the acoustic particle velocity, mean flow, and the vorticity (lower figures). [75]

volume $\forall$, can be described as follows:

$$\Pi = -\rho \int \omega \cdot (\mathbf{U} \times v) d\forall \tag{2.2}$$

The behavior of the vorticity as either an acoustic source or sink is dictated by the triple product in Equation 2.2. If the integration of the triple product over a complete acoustic cycle yields a positive result, the acoustic resonance will be self-excited. This necessitates precise timing between the formation of the shear layer and the acoustic cycle. As illustrated in Figure 2.4, the cross product of the mean velocity and the vorticity consistently points downwards. Therefore, during the vortex formation, negative acoustic power, denoted by Π, is transferred to the vortex. However, as the vortex is conveyed away from the leading edge, the direction of the acoustic particle velocity reverses, which corresponds to generated acoustic power Π. The integration of this process over an entire acoustic cycle will be positive, as the magnitude of the vorticity is larger when the vortex is carried along by the flow. This implies that there

is a net generation of acoustic power per cycle, which signifies the manifestation of acoustic resonance.

Given that vorticity is recognized as the sound source in fluid-resonant scenarios, as demonstrated by Howe, it is crucial to investigate the generation of the vorticity field within side branches and the instability of the shear layers. Understanding these factors is essential for comprehending the underlying mechanisms of sound generation in fluid-resonant systems.

2.4 Coupling between the acoustic and shear layer modes

As delineated in the preceding section, the shear layer's instability conveys energy into the acoustic field, thereby producing velocity-dependent tones. This instigates a two-way interaction between the flow field and the acoustic field. For specific circumstances, acoustic modes are shown at discrete frequencies in cavity geometries, which align with the range of oscillation frequencies for the set operational flow velocities. In such a scenario, there are pivotal flow velocities where the oscillation frequency corresponds with the system's acoustic mode [45]. Hence, the oscillations in the shear layer trigger the system's acoustic mode, resulting in a unique flow-acoustic coupling [47]. This occurs due to the advantageous positioning of the velocity fluctuations in relation to the acoustic particle velocity. Pressure variations in this situation support the generation of a standing acoustic wave [1].

The frequency of the oscillations in the flow field are in direct proportion to the flow velocity with the proportionality constant Strouhal Number. Stouhal Number is a direct correlation that can be observed between the frequency of the flow oscillations, denoted as f_s, the side branch opening represented by d, and the unrestricted flow

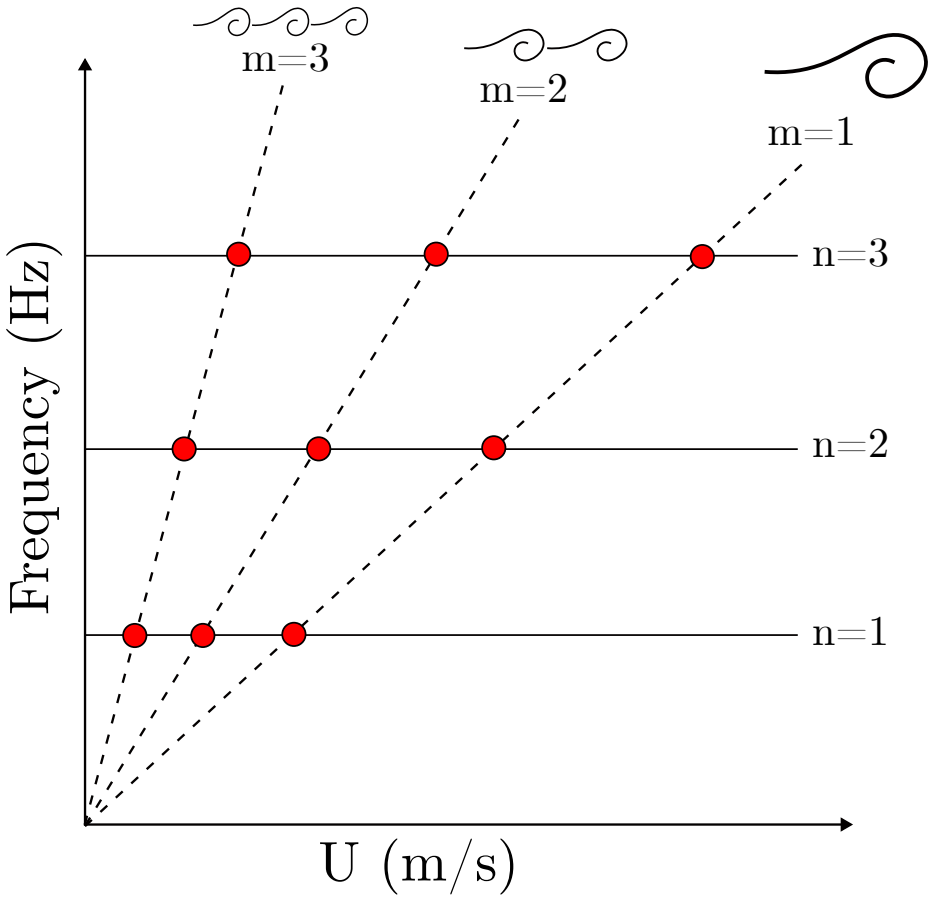

Figure 2.5: Schematic of the coincidence of the hydrodynamic and acoustic modes. The dashed lines represent different Strouhal numbers.

velocity, labeled as U, as evidenced in Eq. 2.3.

$$St = \frac{f_s d}{U} \tag{2.3}$$

While the acoustic mode is primarily determined by the geometry of the system. Thus, a potent coupling between the flow field and the acoustic field occurs when both frequencies match, as displayed in Fig. 2.5. During this overlap, the flow oscillations and the resonance frequency enter a lock-in state. Consequently, the aeroacoustic resonance begins at a specific frequency and continues over a limited range of flow velocities [3].

Hence, this interactive mechanism is overseen by a process of energy swapping, where energy is periodically moved between the flow field and the acoustic field. Some researchers has indicated that this energy transition process is related to a pressure variation across the source region, resulting from the instability of the shear layer that synchronizes with the acoustic particle velocity [46, 47]. Thus, the presence of an excitable acoustic mode offers affirmative feedback to the flow oscillations as long as these oscillations can surpass the system's acoustic damping.

The intertwined interaction during resonance is notably accentuated, leading to an enhancement of both the flow oscillations and the resonance tone [7]. As a result, the intensity of the acoustic field is responsible for controlling and structuring the vortices within the shear layer [74]. Furthermore, the expansion of flow instabilities results in a considerable rise in flow drag, which adversely affects the effectiveness of the respective system.

As stated, two primary factors contribute to the creation of flow-acoustic coupling: the flow field and the acoustic field. Consequently, the system's resonance frequency determines the lock-in regions for flow-induced resonance, contingent on the geometry of the cavity and its boundaries. Typically, the flow-induced acoustic resonance mechanism is widespread in many engineering applications, referring to such instabilities. However, even though the mechanisms in play fall under the same umbrella, i.e., fluid resonance, the interaction details between the flow field and acoustic field can vary. In fact, since the system's geometry directs the resonance acoustic mode, various geometric shapes yield unique acoustic mode shapes, subsequently influencing the flow-excited acoustic resonance mechanism. Aiming to gain a deeper understanding of flow-induced acoustic resonance in different side branch geometries, substantial research in recent decades has dedicated itself to investigating applications subjected to similar effects due to the presence of large flow structures.

Such applications encompass instances where multiple cavities exist in a duct with different configurations, side branches in pipeline systems, cross-flow over cylinders and tube arrays, as well as circular axisymmetric cavities [2, 46, 64, 78]. The feedback mechanism outlined in this section depends on the side branch geometry, and couples with the self-sustaining flow oscillations, producing notably high acoustic pressure amplitudes. Consequently, the coupling showcases a more reciprocal energy exchange between the flow and acoustic field, as evidenced by the improved organization and modulation of the shear layer [5].

This emphasizes the significance of gaining a more profound comprehension of the shear layer instability embodying the fluctuating flow field in deep cavity scenarios. The reason is that the amplification of shear layer fluctuations at a particular frequency excites the acoustic mode, serving as the initiation for flow-excited acoustic resonance.

2.5 The instability of shear layer flow and saturation

Flow is deemed unstable if it can amplify minor disruptions into significant ones. In contrast, stable flow is characterized by its resistance to the magnification of minor disturbances, whether self-generated or driven by external sources. Instability in the flow field is a typical occurrence in various flow regimes, for example the flow of the unstable shear layer formed due to the separation over cavities or side branches, flow within valves and orifices, jet flows. These instances of unstable flow regimes all share a characteristic: the blending of flow streams with diverse flow velocities. For instance, in the scenario of confined flow over cavities, two zones of flow exist. The first is almost stationary fluid inside the cavity, while the second is the grazing

main pipe flow that is convected with the average flow velocity in the pipe. At the interface, a mixing layer region forms at the mouth of the cavity, as depicted in Figure 2.6. Typically, the velocity distribution at the interface comprises an inflection point, which is deemed an adequate condition for instability, as illustrated by Rayleigh's inflection point theorem [61]. The theorem states that for an equilibrium flow to be unstable, the equilibrium velocity profile must contain an inflection point.

This indicates that the inflection point is an essential precondition for the enhancement of any disruption, yet the stability theory for inviscid flows fails to clarify why certain velocity profiles, which lack inflection points, are unstable. An example of this is the instability of fluid in straight pipes leading to the transition from laminar to turbulent flow, without the presence of an inflection point. Conversely, the viscous theory reveals the existence of a critical Reynolds number, beyond which some perturbations in the flow may become unstable.

Lord Rayleigh's hydrodynamic stability theory leverages the incompressible, two-dimensional, and perturbed linearized Navier-Stokes equations to address stable and unstable frequency domains of the flow field. These equations are inviscid and two-dimensional, which simplifies them into an ordinary differential equation, with solutions assumed to be in exponential form.

$$\Psi(\mathrm{x},\mathrm{y},\mathrm{t}) = \Phi(\mathrm{y})\mathrm{e}^{\mathrm{i}\alpha_i(\mathrm{x}-\mathrm{ct})} \tag{2.4}$$

Here, Ψ represents the complex stream function, Φ is the complex amplitude function, α_i indicates the wave number and c symbolizes the wave speed. Through the application of the stream function definition, the perturbed Navier-Stokes equations can be simplified to a fourth-order differential equation only functioning on the amplitude phi, also known as the Orr-Sommerfeld equation.

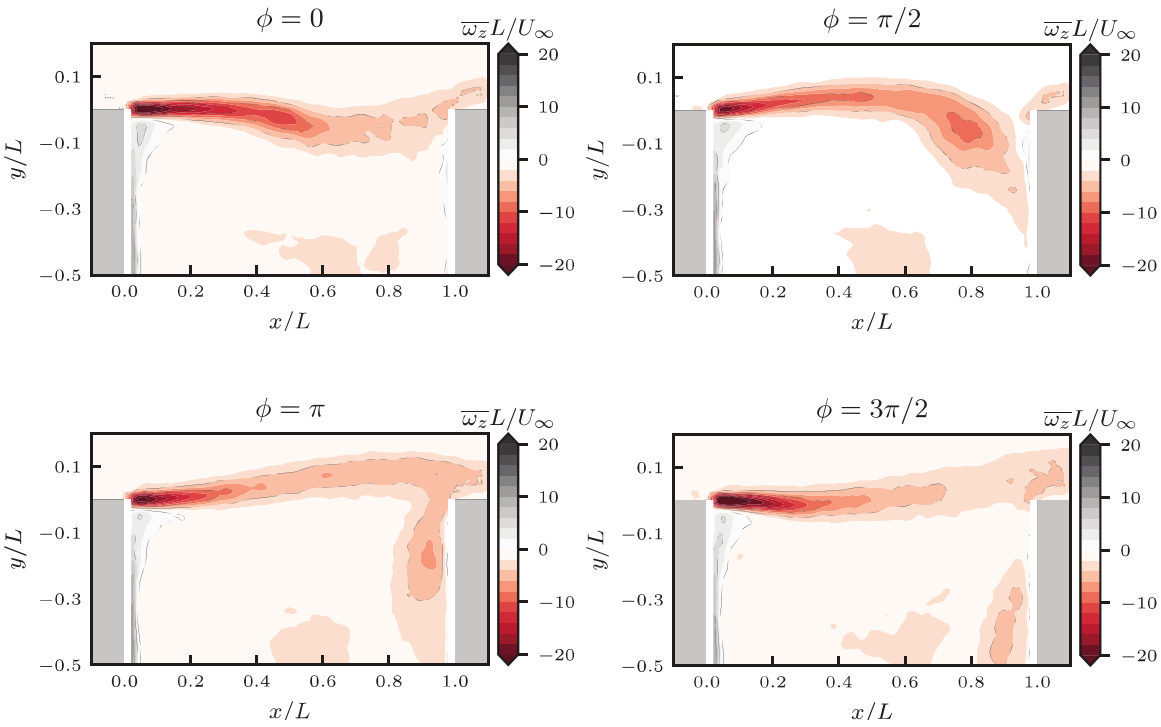

Figure 2.6: Instantaneous normalized vorticity contour of the flow over a 2-D cavity showing the mixing between the shear layer and the stationary flow inside the cavity. [1]

$$(\bar{U} - c)\left(\Phi'' - \alpha_i^2 \Phi\right) - \bar{U}''\Phi = -\frac{1}{\alpha_i \,\mathrm{Re}}\left(\Phi'''' - 2\alpha_i^2 \Phi'' + \alpha_i{}^4 \Phi\right), \tag{2.5}$$

where the characteristic length of Reynolds number is the momentum thickness θ. In industrial scenarios, high Reynolds numbers are anticipated, making the equation's right-hand side negligible since 1/Re is relatively small. This simplification turns the Orr-Sommerfeld equation into the Rayleigh equation—a simplified second-order ordinary differential equation.

$$\Phi'' = \left(\frac{\overline{\mathrm{U}''}}{\overline{U} - \mathrm{c}} + \alpha_i^2\right)\Phi \tag{2.6}$$

Solving Equation 2.6 requires the definition of the mean velocity profile and appropriate boundary conditions, as it's an eigenvalue problem.

The growth pattern of perturbation is also essential to define, determining whether it's a function of time or space. This necessitates that c be complex and α_i real when disturbance growth is a function of time. Conversely, α_i is complex and c real when the disturbance growth is a function of space. Importantly, Φ, α_i, and c are all functions of the disturbance frequency. Gaster [24] compared spatial and temporal perspectives, concluding they aren't identical, and establishing spatial stability theory as a better representation for large disturbance amplification in the flow. Miksad [42] studied the nonlinear growth of a mixing layer, discovering that nonlinear effects become significant when the ratio between the fluctuation of the disturbance velocity to the mean flow velocity reaches 3.5

The linear stability theory's key findings involve predicting the instability frequency range and the frequency of the peak instability, i.e., the frequency with the highest amplification factor. As an example, Figure 2.7 illustrates the exponential growth of the fundamental frequency β, which is defined as $\beta = 4\pi f\theta/\bar{U}$, along the thin shear layer's spatial extension, which forms from two parallel flow streams with unequal velocities. The linear disturbance increases rapidly until it deviates from linear progression, entering a highly nonlinear transition region. This region features vortex coalescence and energy exchange between the fundamental frequency and its harmonics, eventually leading to fully turbulent flow and a decrease in disturbance amplification.

Lucas et al. [38] highlighted some inviscid stability theory applications for analyzing various velocity profiles, including hyperbolic-tangent, piecewise linear, discontinuous, wake velocity profiles, and axisymmetric jet and planar jet mixing layer. The hyperbolic tangent velocity profile exemplifies the thin layer mixing of two parallel flow streams with differing velocities. The velocity ratio Δ influences the difference between the two flow streams and follows the $U(y)$ distribution, as shown in Equation

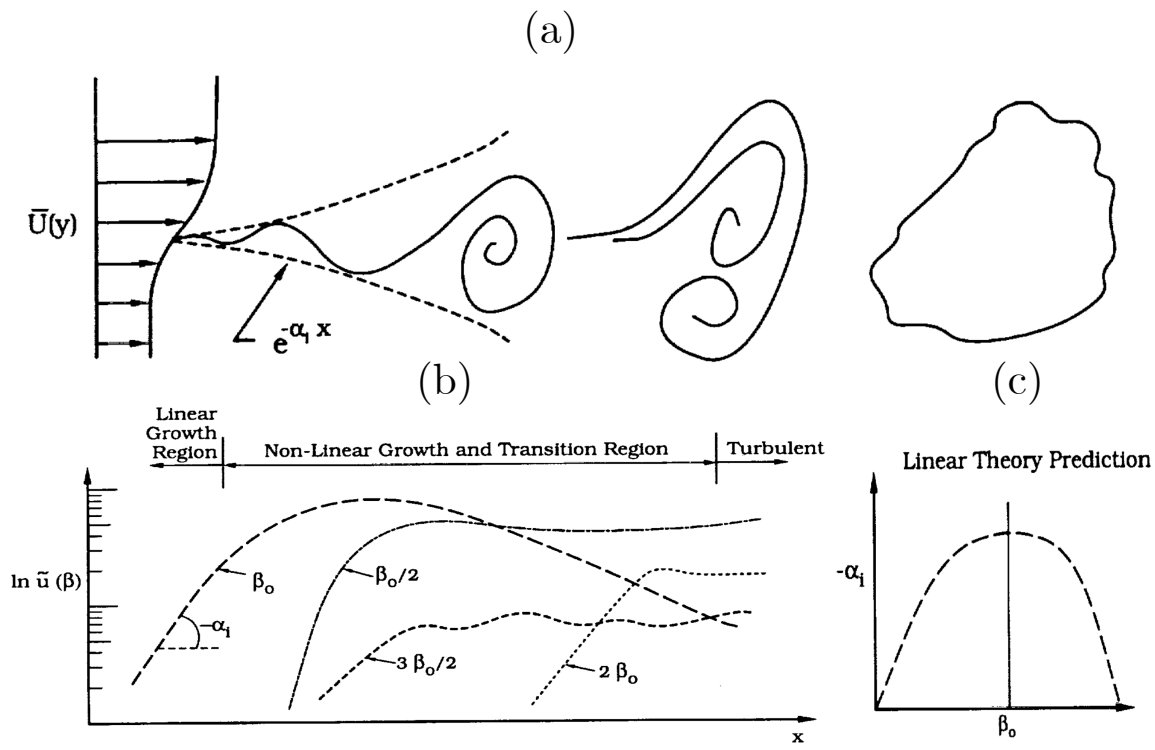

Figure 2.7: The predictions of the linear stability theory for the case of a thin shear layer. (a) A schematic of the transition from the linear growth of perturbations to the small-scale, fully turbulent flow. (b) The logarithmic progression of the perturbations in the thin shear layer for the fundamental frequency $\beta_\circ$ and its harmonics. (c) The amplification factor vs the normalized frequency showing a peak amplification at normalized frequency od $\beta_\circ$. [38]

2.7 and Figure 2.8.

$$\begin{aligned} \Delta &= \frac{U_1 - U_2}{U_1 + U_2} \\ U\,(y, \Delta) &= 1 + \Delta \tanh(y/2) \end{aligned} \tag{2.7}$$

A unique case, where delta equals one, leads to a stationary lower stream, similar to flow over deep cavities. Monewitz and Huerre [48] solved the Rayleigh equation at various velocity ratios, as shown in Figure 2.8b, where the non-dimensional frequency beta is approximately 0.21, equivalent to a Strouhal number of 0.017. This finding aligns with DeMetz and Farabee's experimental data [18], who identified a Strouhal

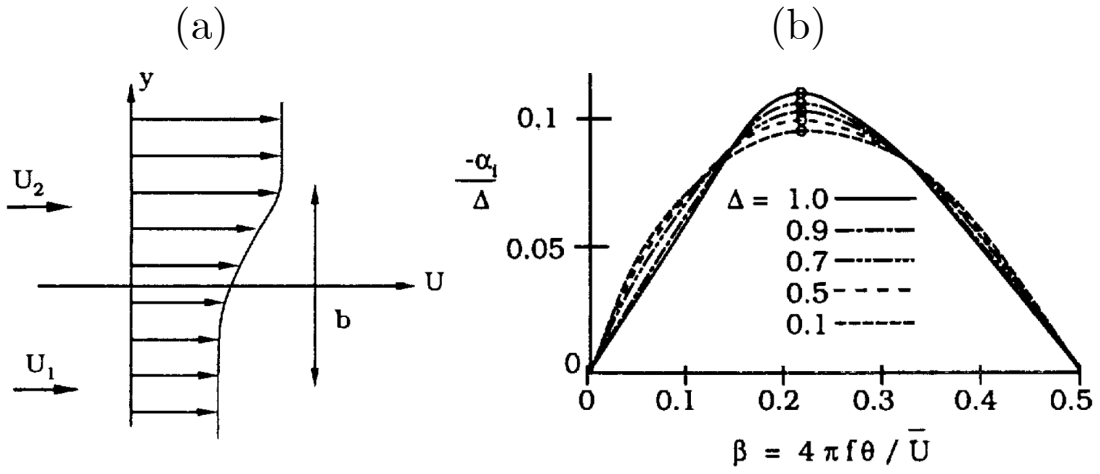

Figure 2.8: (a) The velocity distribution of the hyperbolic-tangent velocity profile. (b) The amplification factor vs the normalized frequency at various velocity ratios. [48]

number of 0.022 for the resonance frequency of a laminar boundary layer passing over a cavity, validating this number for circular and rectangular openings.

In conclusion, the shear layer can amplify and propagate disturbances within the flow field. Yet, under certain feedback conditions, these disturbances can be forced. Potential feedback disturbances include pressure fluctuations arising from shear layer impingement, acoustic field oscillations, flow field oscillations due to structural vibrations.

2.6 Shear Layer Forced Perturbations and the Feedback Mechanism

Stimulating free shear layers through external disturbances provides key insights into the reaction of the shear layer to various perturbations that could instigate self-perpetuating oscillations. One notable finding regarding the impact of enforced excitations was proposed by Blevins [9], who noted the concentration of the shear layer's broad-range fluctuations into a high-Q factor, single-frequency response. This sug-

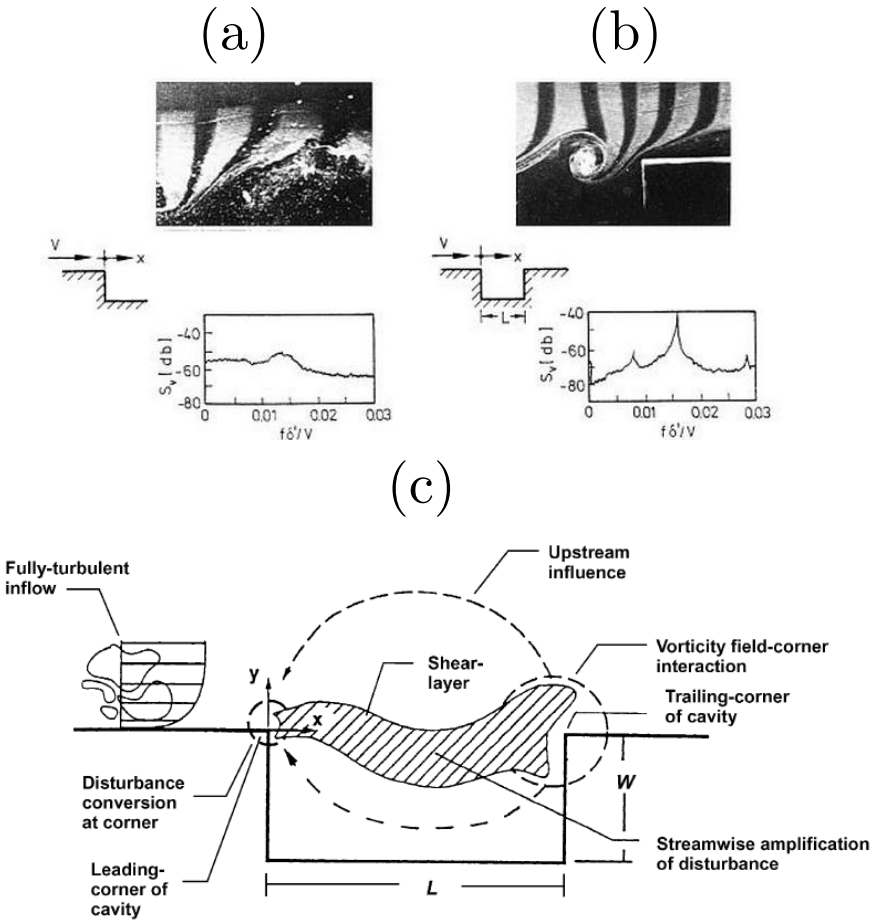

Figure 2.9: Organization of the vertical structures in the shear layer due to the pressure feedback from the impingement downstream edge. [63] [64]

gests a feedback mechanism can reorganize and influence flow instability. As observed by Rockwell and Knisely [63], the presence of a downstream edge, as demonstrated in Figure 1, enhances the coherence of vortical structures, suppresses wide-ranging velocity fluctuations, and reorganizes flow. Numerous past studies have explored the influence of different geometric and hydrodynamic parameters on shear layer flows.

Rockwell [62] proposed the possibility of creating self-perpetuating oscillations through the impact of the shear flow. He outlined a sequence of events leading to a self-sustained oscillation: the impacted shear flow on the downstream edge creates a pressure pulse that is generated and propagated upstream, providing a feedback

signal that disrupts the recently separated shear flow and induces an oscillation at the feedback signal frequency. This newly disturbed shear flow then forms a new, more structured vortex that travels downstream, repeating the feedback cycle.

Rockwell and Naudascher [65], in their review on cavities as oscillators, divided cavity oscillators into three fundamental types. The first type, fluid dynamic oscillations, are best exemplified by self-perpetuating oscillations due to a feedback signal, where the cavity oscillations are solely driven by the feedback signal arising from the inherent instability of the shear layer. The second type, fluid resonant oscillations, is where the cavity oscillations are organized by the intrinsic coupling between the shear layer instability and one or more acoustic modes of the duct or cavity, with deep side branches as an example. The third category, fluid elastic oscillations, is where the cavity oscillations are organized due to the coupling of the inherent stability of the shear layer with an elastic motion of an element in the cavity walls. Examples include a cavity with a vibrating end, bellows, or flap.

2.7 Aeroacoustic Interaction Patterns

Numerous scholars have delved into the interplay between flow and acoustic fields, reflecting its paramount significance. The criticality of acoustic resonance within pipeline systems has drawn significant attention towards the study of deep [74, 78] and shallow cavities [2, 28]. The interaction of longitudinal acoustic modes of pipes and shallow cavities has been the focal point for many researchers, whereas others have concentrated on the shear layer exciting the transverse acoustic modes of the deep cavity. Notwithstanding the fact that the instability of flow remains constant in both instances, i.e., shear layer instability, these studies underscore the considerable impact of the flow-acoustic field interaction which can entirely alter the excited acoustic mode.

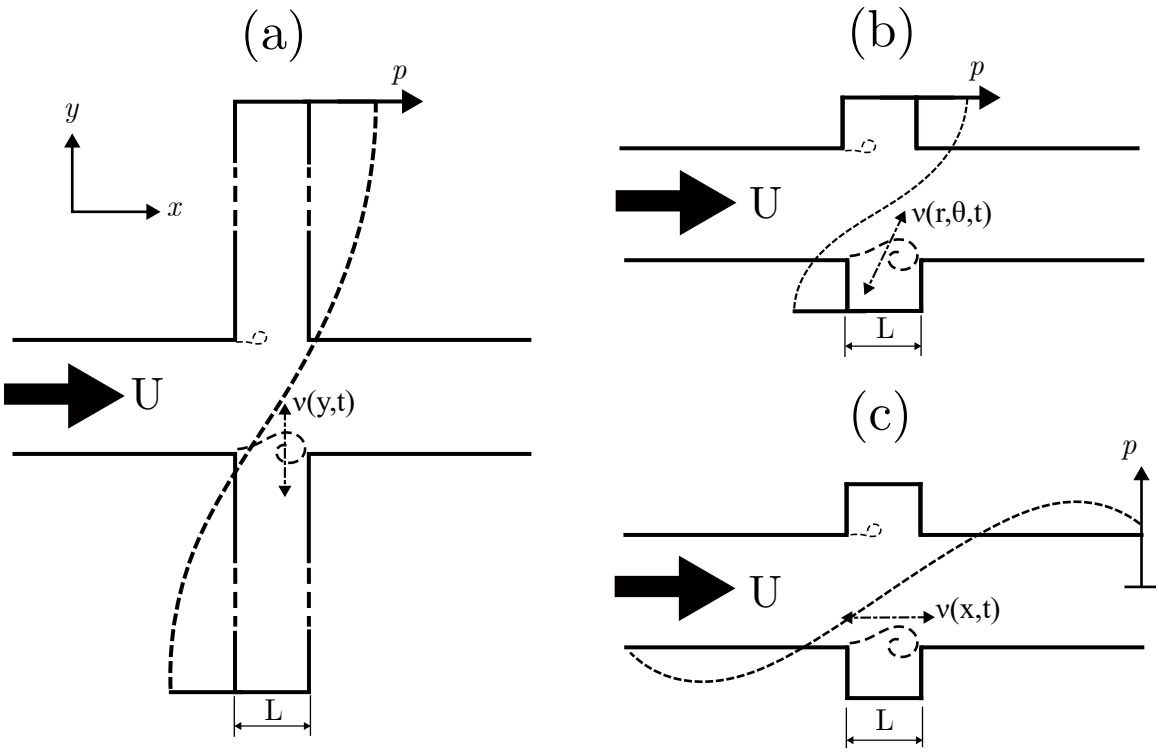

Figure 2.10: Different possible acoustic excitations and the acoustic particle velocity direction for (a) deep co-axial cavity, (b) shallow cavity, (c) axisymmetric cavity.

The mechanism of flow-sound interaction that may result in aeroacoustic resonance is predominantly contingent on the localized variables within both the sound and flow fields. Certain specific aspects, such as the vorticity distribution along with the amplitude and phase angle of the acoustic particle velocity, play a crucial role, as demonstrated by Howe [31] in equation 2.1. However, given the established premise that flow instability serves as the origin of aeroacoustic excitation, it is imperative to delve into the variety of excitable acoustic modes consequential to this flow instability.

Regarding coaxial side branches, the existence of a deep cavity with an impeccably reflective end will confine the acoustic wave within the branch, leading to acoustic particle velocity propagation in the y-direction, orthogonal to the convection direction of vorticity, as depicted in Figure 2.4. This orthogonality enhances the $\mathbf{U} \times v$ term in Howe's triple product, engendering a potent acoustic source. The acoustic

resonance-generated tone possesses a significantly larger wavelength compared to the side branch opening, facilitating solely planar wave propagation in the side branch. The sound source resultant from fluid-acoustic interaction was experimentally quantified for circular side benches with sharp edges and fully developed flow by Graf and Ziada [27], underscoring the importance of the acoustic particle velocity distribution on the resultant aeroacoustic source.

As the cavity depth diminishes to a magnitude comparable to the cavity opening, the sound field becomes intricate, with the acoustic particle velocity distribution dependent on both radial and angular directions, as illustrated in Figure 2.10. The complex nature of the acoustic and vorticity fields makes it challenging to measure the sound source for this scenario. Nonetheless, Aly and Ziada [2] explored the self-excitation mechanism inherent to this situation.

The third possible scenario involves an exceptionally long wavelength compared to the cavity opening. Here, flow instability would stimulate the main pipe's acoustic mode if the cavity is positioned at a pressure node, resulting in a particle velocity distribution paralleling the flow mean field. The sound source derived from this excitation was examined by Mohamed and Ziada [44], revealing different implications of the sound source on acoustic resonance.

Design considerations aiming to circumvent flow-excited acoustic resonance should distinctly determine the critical Strouhal number, marking the onset of resonance, and the aeroacoustic source of strength, directly influencing the amplitude of the acoustic pulsation. Numerous prior studies define the onset of acoustic resonance in various applications and geometries [25, 29, 64, 77]. The subsequent section will examine various proposed methodologies to model and measure the aeroacoustic power source and the resultant acoustic energy.

2.8 Analytical and Numerical Methods of Acoustic Source Determination

The acoustic phenomena occurring in a flute showcase notable similarities with the pulsations present in pipelines with deep side branches. In the case of a flute, the produced sound production is attributed to the unstable free jet that is created when air is blown across the instrument's mouth. The subsequent oscillations of the jet coupled with the acoustic mode within the flute, establishing a closed feedback loop that parallels the one observed in closed-branch pipe systems. Early predictive models of a flute's aeroacoustic behavior, premised on the notion that the emerging jet and the excitable acoustic mode constitute a closed feedback cycle, employ linear theory to predict oscillation conditions. These models are formulated by matching the impedance of the resonator and the source impedance.

Early attempts to predict self-sustained oscillations in flow-induced cavity noise used Michalke's stability theory [41] with a Kutta-like condition for the shear layer perturbation due to acoustic oscillation. However, these models did not account for certain observed effects, such as the effect of the upstream edge geometry on pulsation behavior, and presumed the criticality of the shear layer impingement for sound production.

Elder's alternative linear model [22] proposed the shear layer as an oscillating "membrane" driving cavity oscillations. Howe's formulation, which amalgamates Elder's concept with the Kutta condition, indicates that the downstream edge singularity is not effective in the sound production process, and predicts limited Strouhal ranges for sound production.

Experimental results [34], though, revealed a significant dependence of Strouhal ranges and the acoustic amplitude on the boundary layer's structure and the cavity

edges' shape. Finally, Karlsson and Abom [32] introduced the vortex-sound interaction effect in linear multi-port models to ina an attempt to predict the self-sustained oscillations, splitting the problem into a scattering matrix indicating the passive part and sound sources which indicate the active part, thereby suggesting that vortex-sound interaction could cause sound's linear amplification or damping.

Another approach to model the aeroacoustic source utilizes Howe's model for the aeroacoustics of a flute. Howe's model [31] primarily emphasized on the effect of vortex shedding from the labium, the flute's sharp downstream edge. This presumes that the produced vortices could be condensed into a line vortex, with imposing the Kutta condition at the labium's edge to calculate the circulation. Although Howe [31] postulated that this vortex generates acoustic energy, empirical observations indicate it absorbs sound instead [141, 142]. Bruggeman et al. [10] adapted Howe's concept [31] to a single side branch with sharp edges, intending to characterize the formation of the vorticies from the upstream edge. However, this model falls short as both the circulation and the vortex convective velocity tend to infinity as the vortex nears the downstream wall of the T-junction. Nevertheless, the model can be utilized to forecast the absorption of sound energy at high amplitude due to the shed vortices from the downstream edge of the single-side branch.

Drawing on comprehensive measurements within the aperture of a Helmholtz resonator, the streamlined vortex model was proposed by Nelson et al. [52]. This model presupposes the formation of a line vortex separating the upstream edge of the side branch each time the acoustic particle velocity diverts into the branch. The vortex is further postulated to move downstream towards the other edge at a constant convective speed, U_{con}, following a straight trajectory. This model assumes the circulation of the vortices as independent of oscillation amplitude, thereby categorizing it as a moderate amplitude model. By integrating Nelson's vortex model with the vortex

sound theory, the model did explain the sound generation in a Helmholtz resonator qualitatively.

Kook and Mongeau [35] introduced a refined version of the model proposed by Nelson et al. [52, 53], where a vortex concentration parameter is incorporated to accommodate the diffusivity of the vortices traveling downstream. The concentration parameter is then estimated from experimental data for the Helmholtz resonator and incorporated into a feedback model to roughly predict the aeroacoustic response.

A significant restriction of single vortex models is their inability to sufficiently characterize situations where the Strouhal number limit is less than 1. Consequently, numerical models have been devised to provide a more detailed view of the flow field. These insights, when integrated with the acoustic field as boundary conditions, allow for predictions concerning sound sources across various configurations.

Several methods for flow simulation have been embraced in previous studies, such as the vortex blob method [12,36], laminar and incompressible simulations [40], turbulent and unsteady simulations [59], Large Eddy Simulations (LES) [23], compressible Euler simulations [19, 37], and Direct Numerical Simulations (DNS) [26]. Enhancing the precision of flow modeling leads to improved predictions of the aeroacoustic response, given that non-reflective acoustic boundaries are appropriately imposed on the domain boundaries.

However, Dequand et al. [19] found that their pulsation amplitude predictions, obtained using a compressible Euler solver, were over-predicting experimental observations by 40 % in ducts with square cross-sections. This discrepancy is partly suspected to stem from the impact of the dissipated energy from the wall vibration during experiments.

It is also worth noting that the increased computational cost linked with precise numerical simulations restricts the modeled resonators to specific sizes. Tonon et

al. [71] provide a comprehensive review of the various numerical techniques utilized for modeling aeroacoustic sources.

2.9 The Experimental Approach in Determining the Sound Source

Initial models that studied the aeroacoustic behavior of a flute operated under the presumption that a feedback loop is formed by the jet and the resonating acoustic field. These models aimed to forecast the conditions for oscillations using linear theory. These models were developed through matching the impedance of the resonator and the source impedance.

Coltman (1968) [13] pioneered the process of measuring the sound power produced by an instrument. His focus was on the generated sound arising from the shear layer instability over a flute's mouth. This methodology hinged on the balance between the measured sound generation, quantified as source impedance, and the difference in the linear acoustic system impedance calculated around the mouth of the flute. Coltman's experimental procedure [13] involved using a loudspeaker to externally excite the system with a harmonic stimulus at a particular frequency and amplitude. Following this, he assessed the source impedance by dividing the pressure-induced across the flute's mouth by the acoustic volume flux passing through the mouth.

Being inspired by Coltman's method [13], Graf and Ziada [27] conducted experimental measurements to measure the acoustic source impedance in coaxial side branch systems configured in both cross and tandem [27] arrangements with sharp edges. From these experiments, the source impedance was ascertained for coaxial side branches with sharp edges and a diameter ratio of 1.75 subjected to fully developed turbulent flow in the primary pipe. During the experiments, a loudspeaker was

utilized to stimulate the branch at its acoustic mode, with each measurement series performed at a fixed normalized acoustic pressure, while changing the flow velocity in the main pipe changes the Strouhal number.

A significant attribute of the introduced method by Graf and Ziada [27] was the quantitative analysis of the nonlinear saturation of the shear layer disturbances. Moreover, the results indicated that in the moderate amplitude regime, the power of the acoustic source depends on the square root of the pulsation amplitude, contrary to the linear dependence proposed by Bruggeman et al. [11]. The experimental data from Graf and Ziada [27] is valuable in modeling the generated sound level of side branch systems, across varying lengths of the side branches and static pressures.

Given that the measurements by Graf and Ziada [27] were conducted exclusively for junctions with sharp edges and fully developed flow, and considering the precision in the prediction of pulsation amplitudes, there is a compelling need for a systematic repetition of these measurements for single side branches and coaxial side branches with different geometrical modifications similar to what are frequently encountered in industrial applications.

2.10 Summary and Focus of the Work

In summary, the instability of the flow field, prompted by the creation of a separated shear layer, can amplify specific frequencies leading to the development of self-sustained oscillations. The enhancement of these oscillations and the formation of coherent vortical structures are triggered by the presence of a downstream impingement edge [56]. The interaction between an excitable acoustic field and the vorticity field establishes a feedback loop accountable for the emergence of flow-excited acoustic resonance. Such vigorous oscillations can induce acoustic fatigue in various pip-

ing components, leading to unplanned maintenance and consequential revenue loss. Moreover, the acoustic resonance elevates the dynamic head loss within the piping system. Therefore, the design process for piping systems against acoustic resonance must consider the critical Strouhal number at which the acoustic resonance locks-in, the range of the lock-in region, and the amplitude of acoustic pulsations during acoustic resonance. While the literature provides comprehensive definitions for the onset of acoustic resonance across various geometries, many of the methods proposed for modeling the acoustic source and predicting acoustic power are either computationally burdensome or lack precision. Yet, consensus indicates that the acoustic source is reliant on the local variables of the vorticity and acoustic fields, necessitating some geometry and flow topology simplifications. Graf and Ziada [27] circumvented these simplifications, however, offering accurate predictions of the acoustic amplitude of a co-axial side branch with sharp edges and fully developed flow using a semi-empirical model.

This study expands upon the methodology proposed by Graf and Ziada [27] to delineate the acoustic source of excitation for co-axial cavities. The refinement includes features such as rounded and chamfered edges, variations in the upstream distance before the cavity, and variations in the acoustic boundary conditions. Experiments are executed at high Reynolds numbers within three-dimensional turbulent flow regime in pipes, replicating the conditions commonly found in industrial piping systems. Despite its utility, this approach does not delve into the complexities of unsteady flow topology or the interaction mechanism between flow and sound. However, the methodology's simplicity in tackling such a multifaceted issue establishes it as superior compared to other suggested models.

Chapter 3

Methodology

3.1 Experimental Set-up

An in-depth analysis of aeroacoustic sources associated with side branches of varying geometrical configurations is presented in this chapter. The investigation involves two distinct types of excitation; self-excitation and forced excitation, with a specific focus on the transverse acoustic mode inside the side branch. The experiments were conducted in the fluid-structure interaction and noise control laboratory at Ontario Tech University. The research methodology adopted for this study is referred to as the "sound source method" [27]. This technique necessitates the utilization of a comprehensive array of pressure microphones strategically placed upstream, downstream, and throughout the length of the side branch. Data collected from these multiple locations contribute to a detailed mapping of the aeroacoustic sources in question. Subsequent to this data compilation, a rigorous post-processing step is executed. In this phase, the data are applied to a semi-empirical, highly adaptable model. This model, due to its versatility, is capable of predicting self-excitation in side branches in a more generalized fashion. Therefore, the study essentially extends the bound-

aries of knowledge in this particular field by providing predictive capabilities for side branches' aeroacoustic behavior across varied geometrical circumstances.

3.1.1 Anechoic airloop

In order to facilitate the experiments, an anechoic airloop is meticulously constructed as shown in figure 3.1. This airloop is powered by a Denver screw compressor, linked via a belt-pulley connection to a 25 HP White-Westinghouse electric motor, responsible for providing the requisite power to the compressor. Control of the motor's frequency is ensured through the use of a Westinghouse variable frequency drive, offering a precise resolution of 0.01 Hz. This level of precision permits fine-tuning of the air velocity within the test section. To mimic an anechoic termination condition, the test section is attached to an acoustically isolated, anechoic enclosure, herein referred to as the 'suction box'. The box houses a horizontally positioned baffle plate, designed to create partial isolation between the box's inlet and outlet. This isolation plays a crucial role in reducing the likelihood of large-scale structure formation within the suction box. So, a more streamlined flow will be present between the inlet and the outlet with less recirculation. A flexible hose connects the suction box to the suction end of the screw compressor, thereby serving as a damper to isolate any vibrations originating from the compressor, which could otherwise translate to the test section and negatively influence the measurements. On the delivery side, the compressor's outlet is linked via a flexible, insulated hose to the 'delivery box'. This box is designed to dampen any acoustic reflections that could potentially travel back to the suction side and, consequently, to the test section. The comprehensive design of this experimental setup is meticulously planned to ensure accurate and consistent measurements while reducing potential interference from various sources.

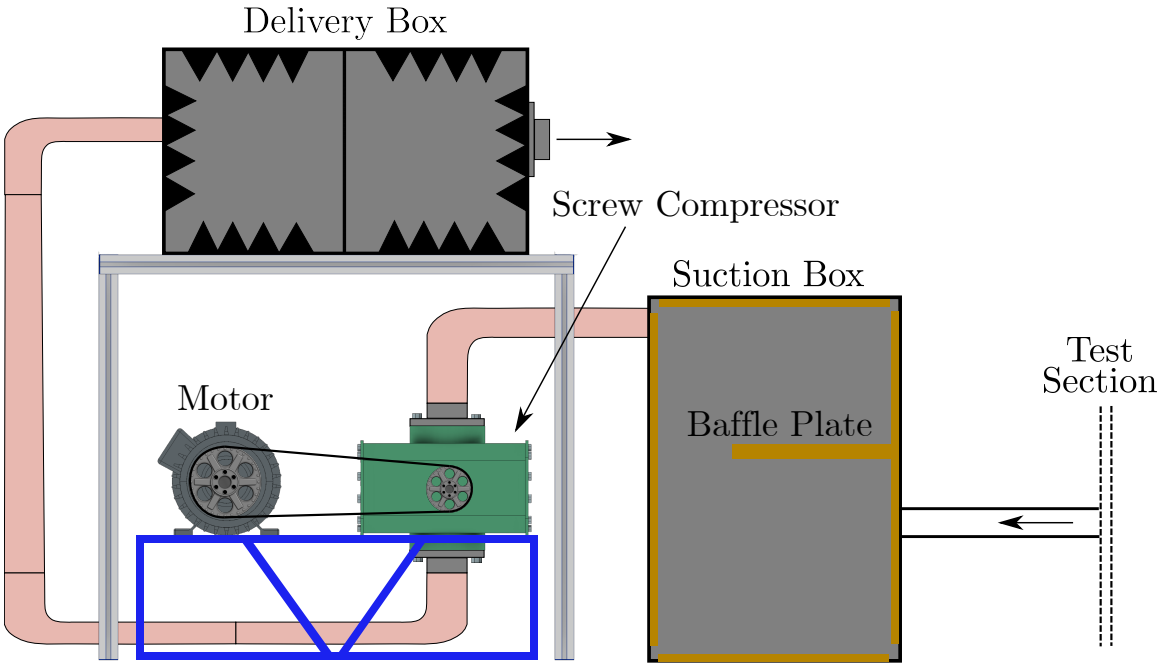

Figure 3.1: Anechoic airloop testing facility

3.1.2 Test section

The test section of the experiment is constructed using a 4-inch PVC main pipe, fitted with a bellmouth at its open end. Figure 3.2 gives a detailed schematic of the test section. The bellmouth is designed to enable a smooth, streamlined flow into the pipe, thereby minimizing turbulence intensity. Situated 1.75 λ from the entrance of the pipe, there is a co-axial 2-inch side branch, the first fundamental acoustic transverse mode of which is measured to be $f_a = 115Hz$. The distance from this branch downstream to the suction box is set to be 0.75 λ. These two distances guarantee that the cavity is strategically positioned at a pressure antinode within the main pipe's acoustic distribution. As a result, the trapped mode experiences maximal acoustic excitation, while radiation into the main pipe is minimized due to the heightened acoustic impedance of the pipes both upstream and downstream. One end of the side branch is fitted with an adaptable cap, allowing for the attachment

of an excitation source. This setup is utilized to force-excite resonance at specific acoustic particle velocities. For low acoustic particle velocities, a high-sensitivity loudspeaker is used to induce pulsations. Conversely, for higher acoustic particle velocities, a mechanical shaker assembly is employed. This shaker is connected to the branch via a custom-built assembly, incorporating a bellow with an aluminum sleeve at its center, facilitating the connection between the shaker's thread and the bellow. Either excitation sources allows us to vary the acoustic wave frequency and amplitude independently by applying a white noise at the desired parameters. It's noteworthy to mention that the loudspeaker is favored for low acoustic particle velocities due to its enhanced accuracy. However, the loudspeaker's range is relatively limited. In situations where the acoustic particle velocities exceed the loudspeaker's range, the mechanical shaker becomes a more suitable alternative due to its capability to handle higher ranges effectively.

3.1.3 Pressure measurement

An array of eight PCB model 377A12 pressure microphones is used to gauge the acoustic pressure at diverse locations within the setup. The factory nominal calibration value for all the microphones are approximately $25mV/kPa$ and a resonant frequency around $50kHz$. However, the microphones are pre-calibrated before all the measurements to ensure pressure accusation accuracy. Two of these microphones are situated upstream, with another two downstream of the side branch. Additionally, two microphones are located on the side of the branch where the excitation source is installed. There's also a microphone positioned on the main pipe in the cross-stream plane, where the side branch is attached. Lastly, the eighth microphone is set at the opposite end of the side branch. It's crucial to highlight that all these microphones are flush-mounted to minimize their interference with the fluid flow, thereby ensuring

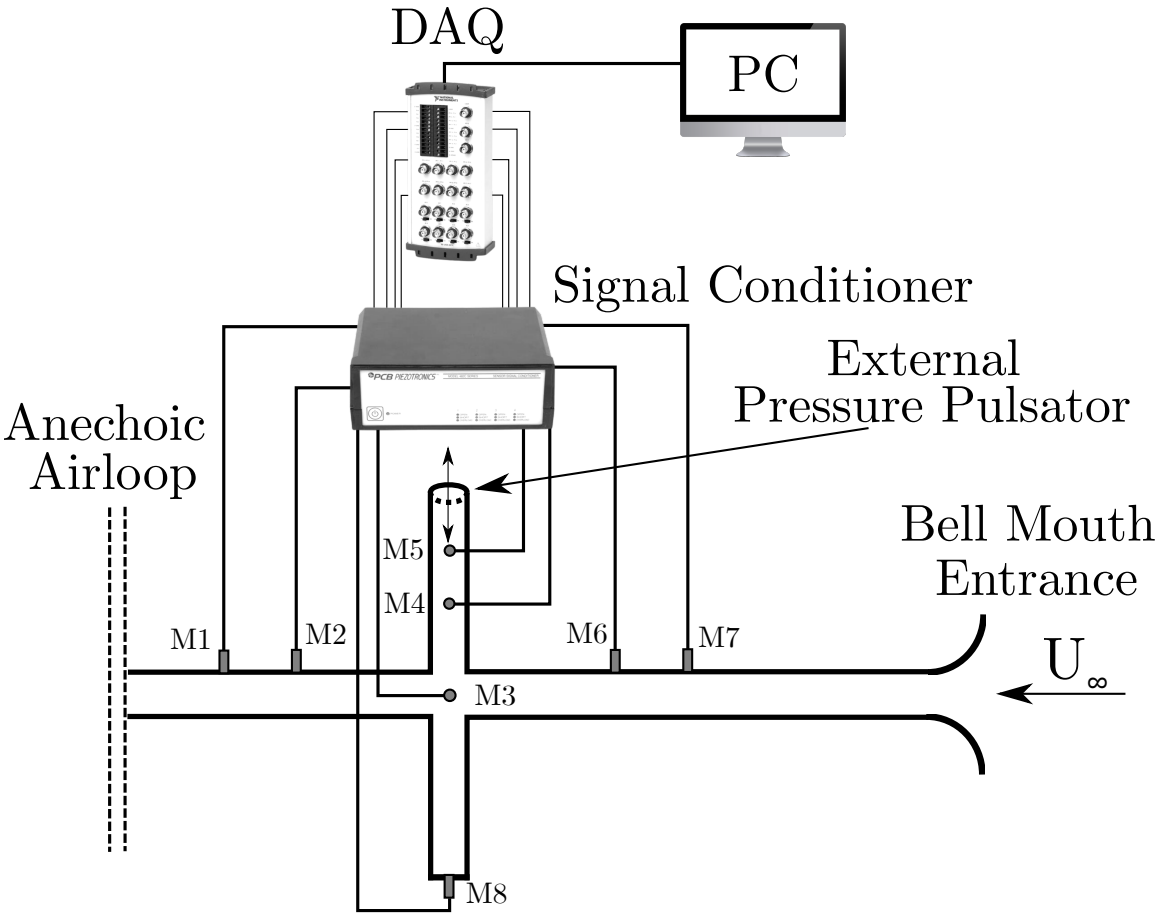

Figure 3.2: Test section schematic

the integrity of the measurements. Further enhancing the validity of the readings, each microphone is individually calibrated against its output voltage, providing reliable and consistent acoustic pressure measurements across the experimental setup. All these microphones are then connected to a PCB signal conditioner which is then connected to a NI data acquisition card (DAQ). The microphones data are then stored on a computer for processing.

To effectively employ the source method computation, it is essential to measure the acoustic pressure wave both upstream and downstream of the side branch. This is why a pair of microphones are strategically placed in each of these locations. Furthermore, the precise positioning of these microphones is key to satisfying a set of conditions

crucial to the accuracy of the measurements.

Firstly, to minimize noise interference in the recorded signal, it has been empirically determined that positioning the microphone approximately $\lambda/8$ distance from the pressure node yields the lowest noise-to-signal ratio. This optimal placement ensures that the signal captured is predominantly representative of the acoustic wave of interest, rather than ambient noise. Secondly, to avoid signal redundancy, the microphones are placed at specified distances apart to ensure that each one records a unique portion of the acoustic wave rather than duplicating readings. Lastly, all measurements are carried out at relatively low frequencies, corresponding to a Helmholtz number less than 0.2. This constraint is maintained to satisfy the assumption of plane wave propagation, a condition that simplifies the mathematical analysis and is generally valid for systems with small geometrical dimensions relative to the wavelength. By ensuring these conditions, the accuracy and relevance of the data captured by the microphones are significantly enhanced, providing a robust foundation for subsequent analytical processes.

Post-processing of the collected time signals from all the microphones is performed using MATLAB. The signals are processed in both the time and complex frequency domains to provide comprehensive insights into the acoustic characteristics of the system. Fast Fourier Transform (FFT) is employed to obtain the frequency spectra of the signals. This method allows for the identification of the peak frequency within the test section, providing valuable information about the dominant acoustic behaviors in the system. However, frequency transformations can sometimes result in spectral leakage, a phenomenon where energy from one frequency bin leaks into another, distorting the true spectral representation. To mitigate this issue, a windowing technique known as the Hamming method is applied. This method tapers the signal at its ends, reducing the discontinuities at the boundaries and thus minimizing the

spectral leakage problem.

3.1.4 Microphones calibration

A GRAS pistonphone is employed to perform the microphone calibration before each measurement. Figure 3.3 shows the calibration setup. The GRAS is a calibration device specifically designed for pressure-sensitive microphones. It operates by creating a known and precise sound pressure level inside a sealed chamber, a function facilitated by a piston moving rhythmically within a cylinder. Each one of the eight microphones is inserted into the chamber and exposed to this sound wave. The pistonphone's output wave frequency and amplitude are predetermined as a part of the pistonphone factory calibration process. The microphone is connected to a signal conditioner, which is subsequently linked to a Data Acquisition (DAQ) system and a computer for data acquisition. The output voltage from each microphone is logged, and this value is then divided by the predetermined amplitude of the pistonphone to dynamically ascertain the sensitivity of the microphone. This process ensures a consistent and accurate conversion of the voltage signal to an equivalent acoustic pressure measurement. This critical calibration step enables precise data collection, forming the basis for the analysis and conclusions drawn from the experimental data.

3.1.5 Velocity calibration

As previously discussed, the electric motor's frequency is regulated through a variable frequency drive. To establish a correlation between the motor frequency and the free-stream velocity, a pitot tube is utilized. The pitot tube is meticulously aligned with the pipe and positioned precisely at the pipe's centerline as shown in figure 3.4. White and Corfield (1991) [72] found that the flow becomes fully turbulent after the pipe

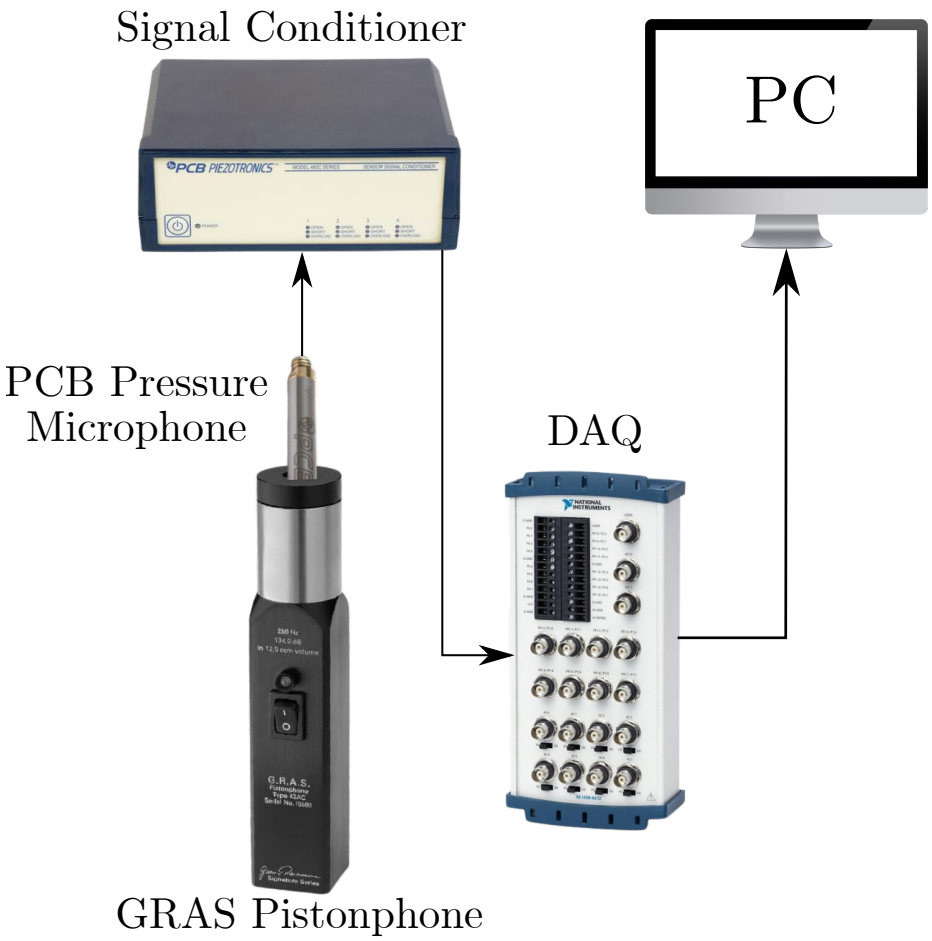

Figure 3.3: Mic calibration setup

entrance at approximately $40D$. So, the pitot was placed at the middle core of the developing region at a distance $10D$ from the entrance. At this region, even if the pitot is shifted from the pipe centreline, the variation in the measured velocity will still be negligible. White and Corfield (1991) [72] investigated the relation between the mean flow velocity for fully turbulent developed pipe flow and the centreline velocity. They found that $U = 0.84U_{centreline}$. Later, Doherty (2007) [20] came up with a relation between the centreline velocity at the developing region ($\approx 10D$) and the centreline velocity at the fully developed turbulent ($\approx 40D$). He found that $U_{Centreline(10D)} = 0.87U_{Centreline(40D)}$. So combining those findings it can be deduced

that the actual flow velocity can be calculated as follows:

$$\begin{aligned} U_\infty &= \tfrac{0.84}{0.87} \cdot U_{Pitot} \\ U_\infty &= 0.965 \cdot U_{Pitot} \end{aligned} \tag{3.1}$$

The pitot is then connected to a digital manometer, which measures the pressure differential between the stagnation pressure $P_{Stagnation}$ (the pressure measured when the air is brought to rest) and the static pressure P_{Static} (the pressure at a point in the moving air stream). This differential equates to the dynamic pressure of the air, which can be used to derive the free-stream velocity. Applying the following equation at frequency steps allows us to obtain a linear relationship between the motor frequency and the free-stream velocity as measured by the Pitot tube:

$$U_\infty = \sqrt{\frac{2(P_{Stagnation} - P_{Static})}{\rho}} \tag{3.2}$$

By measuring the dynamic pressure at various motor frequencies and applying the above equation, a linear correlation between the motor frequency f_{Motor} and the pitot tube reading was established as shown in figure 3.5. The relationship is defined as follows:

$$U_\infty = 1.1883 * f_{Motor} \tag{3.3}$$

In this way, the free-stream velocity can be predictably controlled and measured in the system by adjusting the motor frequency, providing an essential tool for the experimental analysis.

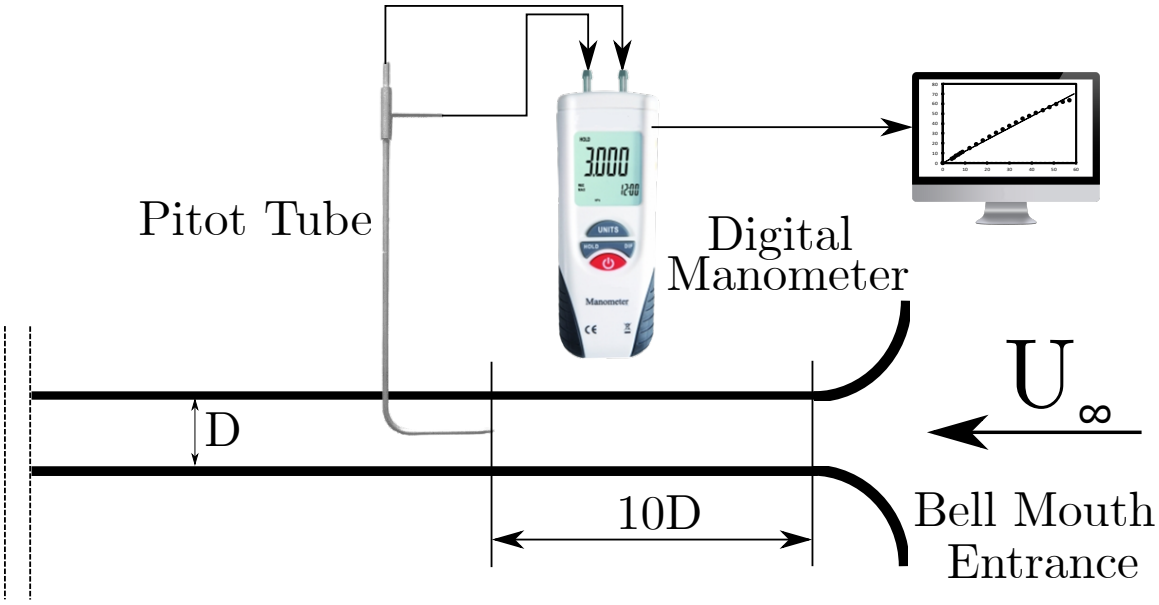

Figure 3.4: Velocity calibration using a configuration of a pitot tube and a digital manometer

3.2 Sound Source Characterization and Predicting the Acoustic Pressure

3.2.1 Planar wave travel inside a duct duct

In an enclosure such as a pipe or a closed side branch, a planar wave is likely to propagate in a standing wave pattern along the streamwise direction. The formation of these standing waves is an outcome of the interference occurring between the incident wave and the reflected wave. The incident wave, a traveling wave, originates from the source of the sound generation. Therefore, the spatiotemporal distribution of the standing wave, resultant of the interfering waves, can be described as follows:

$$\mathbf{p}(\mathrm{x},\mathrm{t}) = \mathbf{p}^{+}(\mathrm{x},\mathrm{t}) + \mathbf{p}^{-}(\mathrm{x},\mathrm{t}) \tag{3.4}$$

$p(x,t)$ represents the spatiotemporal distribution of the acoustic pressure, $p^{+}(x,t)$

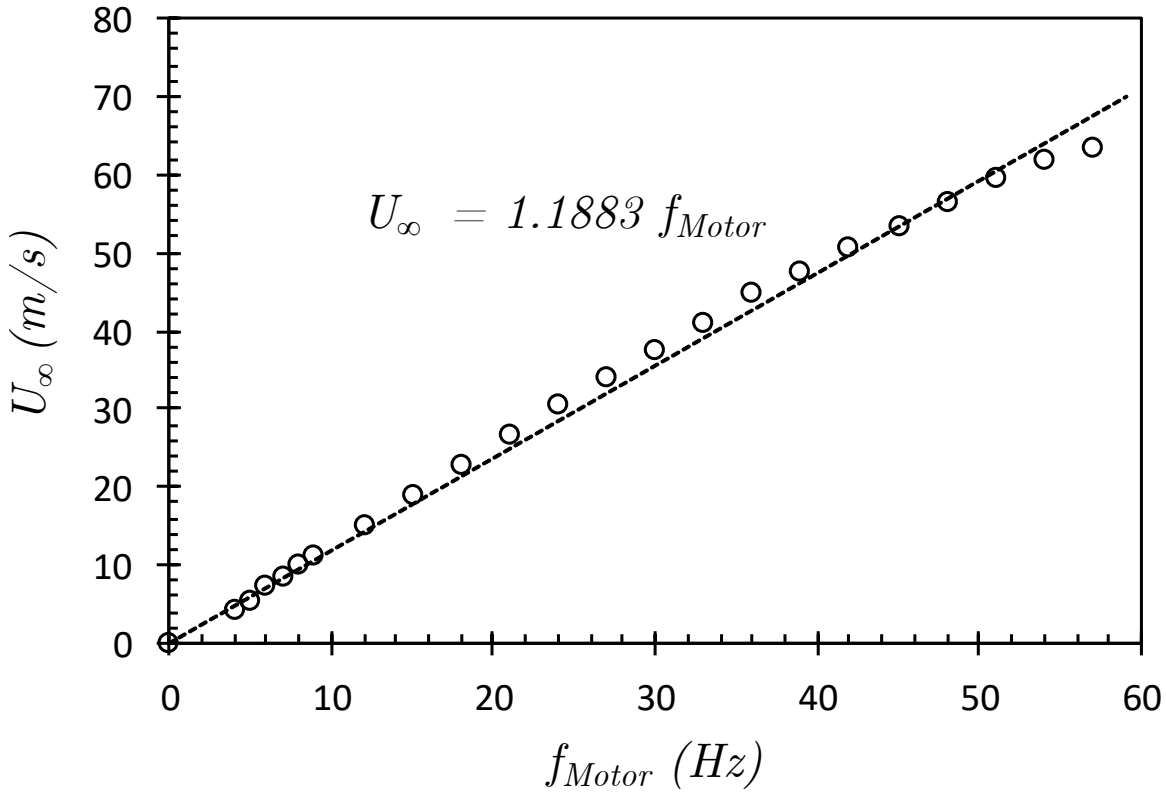

Figure 3.5: Velocity calibration curve

is the spatiotemporal distribution of the incident acoustic pressure, $p^{-}(x,t)$ is the spatiotemporal distribution of the reflected acoustic pressure. The relative phasing between the two waves alternates periodically.

It can be considered theoretically the planar sound wave in a straight uniform pipe as an isentropic work done by a piston doing compression and rarefaction inducing the wave peaks and troughs. The density can be defined as a function of streamwise location and time as $\rho(x,t)$ and the local fluid particle velocity as a function of streamwise location and time as $v(x,t)$. As it is a standing wave, it can be assumed that the wave is traveling at the speed c_0 can be calculated as follows:

$$\mathrm{c_0^2} = (\mathrm{p}/\rho)_\mathrm{s} = \gamma \mathrm{R} \mathrm{T_0}, \tag{3.5}$$

where $T_\circ$ is the average air temperature, R is the gas constant which is equal to $R = 287 J/kgK$ is case of air at normal conditions, γ is the specific heat ratio, and $s(x,t)$ is the entropy fluctuations. The flow Mach number is considered to be $M = \frac{U}{C_\circ}$. With the flow velocity denoted as U, the wave speed in the flow direction is computed as $c_0(1+M)$, and the wave speed in the opposite direction is computed as $c_0(1-M)$.

The propagation of the actual wave is subject to certain losses attributable to the viscothermal effects of the pipe walls. These losses arise primarily due to the friction between the air and the pipe walls, as well as the inherent heat transfer involved. As a consequence, the amplitude along the streamwise length of the pipe experiences an exponential decay. Additionally, there are other forms of losses, such as those caused by free shear layer heat conduction. This phenomenon is an offshoot of the transitional region associated with turbulent mixing. Given these losses, the assumption of the flow being isentropic becomes untenable. In the ensuing section, this real-world scenario will be addressed. However, a simplified case will be initially examined to facilitate easier modeling.

Isentropic planar wave travel inside a duct with no flow

If a duct with no flow is considered and no pressure variations, the conservation equations can be formulated based on the spatiotemporal fluctuations of the pressure $p(x,t)$ and particle velocity $v(x,t)$.

The wave equation reduced to one dimension of the v is as follows:

$$\frac{\partial^2 v}{\partial \mathrm{x}^2} = \frac{1}{\mathrm{c}_0^2}\frac{\partial^2 v}{\partial \mathrm{t}^2} \tag{3.6}$$

It can be assumed that the fluctuations of the acoustic particle velocity exhibit a

simple harmonic motion function. The pressure fluctuations inside a pipe or a side branch are as follows:

$$\mathbf{p}_{(x,t)} = \left(p^{+}e^{-ikx} + p^{-}e^{ikx}\right) e^{i\omega t} \tag{3.7}$$

Where,

$$\omega = 2\pi f, k = \frac{2\pi}{\lambda} \tag{3.8}$$

Where $e^{i\omega t}$, and e^{ikx} is the imaginary representation of the particle velocity harmonic motion as it is progessing in time and streamwise direction respectively. ω is the wave angular velocity, k is the acoustic wave number and equal, and λ is the wavelength.

A formula for the spatiotemporal distribution of acoustic particle velocity within a duct can be formulated, assuming zero flow and ignoring the losses for an isentropic condition. The computation can be undertaken as follows:

$$v_{(x,t)} = \frac{1}{Y_0}\left(p^{+}e^{-ikx} - p^{-}e^{ikx}\right) e^{i\omega t} \tag{3.9}$$

The previous equation assumes that an ideal case for the acoustic impedance as $(Y_\circ = \rho_\circ c_0)$.

Employing the viscothermal losses of a planar wave traveling inside a duct

As mentioned before, the flow speed is a direct function of the forward (in the flow direction) and backward wave (against the flow direction). As a result, each wave will have a different wave number which can be calculated as follows:

$$\begin{aligned} \mathrm{k_f} &= \omega/\left(\mathrm{c_0} + \mathrm{U}\right) = \mathrm{k}/(1 + \mathrm{M}) \\ \mathrm{k_r} &= \omega/\left(\mathrm{c_0} - \mathrm{U}\right) = \mathrm{k}/(1 - \mathrm{M}) \end{aligned} \tag{3.10}$$

So, equation 3.10 can be implemented into the spatiotemporal pressure fluctuation equation 3.7 and will have it in a modified form as:

$$p_{(x,t)} = \left(p^{+} e^{\frac{ikx}{(1+M)}} + p^{-} e^{\frac{ikx}{(1-M)}}\right) e^{i\omega t} \tag{3.11}$$

The wave number k, in this case, takes the viscothermal losses into account, and it is replaced with a complex wave number denoted as β. β can be calculated as follows ([51], [14]):

$$\boldsymbol{\beta} = \omega/\mathrm{c}_0 + \alpha(1 - \mathrm{i}) \approx \mathrm{k} - \mathrm{i}\alpha \tag{3.12}$$

The α which is the total attenuation consists of the sum of two components. Firstly, the flow friction coefficient ζM. Secondly, the viscothermal attenuation coefficient $\alpha_\circ$. So, the total attenuation can be calculated as follows:

$$\alpha = \alpha_0 + \zeta \mathrm{M} \tag{3.13}$$

The damping coefficient ζ is a direct function of the Froude friction factor and the pipe diameter in the case of a circular pipe and is calculated as follows:

$$\zeta = F/2D \tag{3.14}$$

The viscothermal attenuation coefficient $\alpha_\circ$ is a function of the Prandtl number P_r and fluid dynamic viscocity μ and other factors maentioned before in this section. It can be calculated as follows:

$$\alpha_o = \frac{2}{\mathrm{Dc}_0} \sqrt{\frac{\mu\omega}{2\rho_\mathrm{o}}} \left(1 + \left(\sqrt{\gamma} - \frac{1}{\sqrt{\gamma}}\right) \sqrt{\frac{1}{\mathrm{P_r}}}\right) \tag{3.15}$$

So, the later stated losses can be implemented into the spatiotemporal equations of the pressure and acoustic particle viscosity after calculating the characteristic impedance which is calculated as $\mathrm{Y} = \rho_\mathrm{o}\mathrm{c}_0 \left(1 - \frac{\alpha}{\mathrm{k}} + \mathrm{i}\frac{\alpha}{\mathrm{k}}\right)$ and the pressure and acoustic

particle as follows:

$$p_{(x,t)} = \left(p^{+}e^{-\frac{i\beta x}{(1+M)}} + p^{-}e^{\frac{i\beta x}{(1-M)}}\right)e^{i\omega t} = \left(p_x^{+} + p_x^{-}\right)e^{i\omega t} \tag{3.16}$$

$$v_{(x,t)} = \frac{1}{Y}\left(p^{+}e^{-\frac{i\beta x}{(1+M)}} - p^{-}e^{\frac{i\beta x}{(1-M)}}\right)e^{i\omega t} \tag{3.17}$$

The two microphone method first introduced by Davies et al. (1980) [17] can is used to determine the value of the $\mathrm{p_x^+}$ and $\mathrm{p_x^-}$. The used microphones has to measure the pressure at a consistent point with is usually a flush mounted point to the inner surface of the pipe distant with a predetermined length.

A crucial parameter in the context of acoustic standing waves is the reflection coefficient, denoted as R_x. Given that it is the ratio of two complex quantities, namely, the complex amplitudes of the incident and reflected waves, R_x is itself a complex ratio. If the reflection occurs from an entirely rigid surface, the value of this ratio equates to one. The R_x can be calculated using the following equation:

$$\mathbf{R_x} = \frac{\mathbf{p_x^-}}{\mathbf{p_x^+}} = |\mathrm{R}|\mathrm{e}^{-\mathrm{i}\theta} \tag{3.18}$$

The reflected wave can be quantified using the acoustic impedance, denoted as Z_x. This is computed by dividing the pressure fluctuation function by the acoustic particle velocity. It is critical to observe that acoustic impedance is defined locally, implying that its computation needs to be performed at a specific streamwise location [67]. The calculation can be simplified and performed as follows:

$$\mathbf{Z_X} = \mathbf{Y}\frac{(1+\mathrm{R_x})}{(1-\mathrm{R_x})} \tag{3.19}$$

Experimental Characterization of the Sound Source Impedance

The developed method by Graf and Ziada [27] to characterize the acoustic sound source impedance is further extended in this study to cover the effect of different geometrical modifications of the co-axial cavity on the sound source term. The method used in this study is based on three assumptions:

1. The excitation of the acoustic resonance is prompted by a periodic pressure differential across the shear layer. The pressure difference is generated by the convection of vortex structures within the shear layer extension, as well as their interaction with geometric singularities. However, in modeling the source term, the pulsating pressure difference along the cavity opening is averaged, and treated as a 'lumped' variable which is represented by the term ΔP, as depicted in Figure 3.6. It's crucial to underline that, for this suggested source model, an exhaustive understanding of the excitation mechanism of the flow topology in the shear layer isn't necessary. This is because the experimentally determined parameters of the source term already account for it.

2. The pressure differential across the shear layer is delineated as $\Delta P = P_1 - P_j$, which solely depends on the local variables surrounding the shear layer. These include the Strouhal number, the acoustic particle velocity in the vicinity of the cavity mouth, the velocity profile at the cavity's upstream edge, and the geometry of the pipe junction. However, Graf and Ziada [27] have substantiated that ΔP is not a direct function of either the length of the side branch or the acoustic impedance present in the main pipe.

3. The generated acoustic power equals the pressure difference across the shear layer multiplied by the acoustic volume velocity at the cavity mouth, as depicted in Figure 3.6. For the system to maintain steady-state oscillation, the power

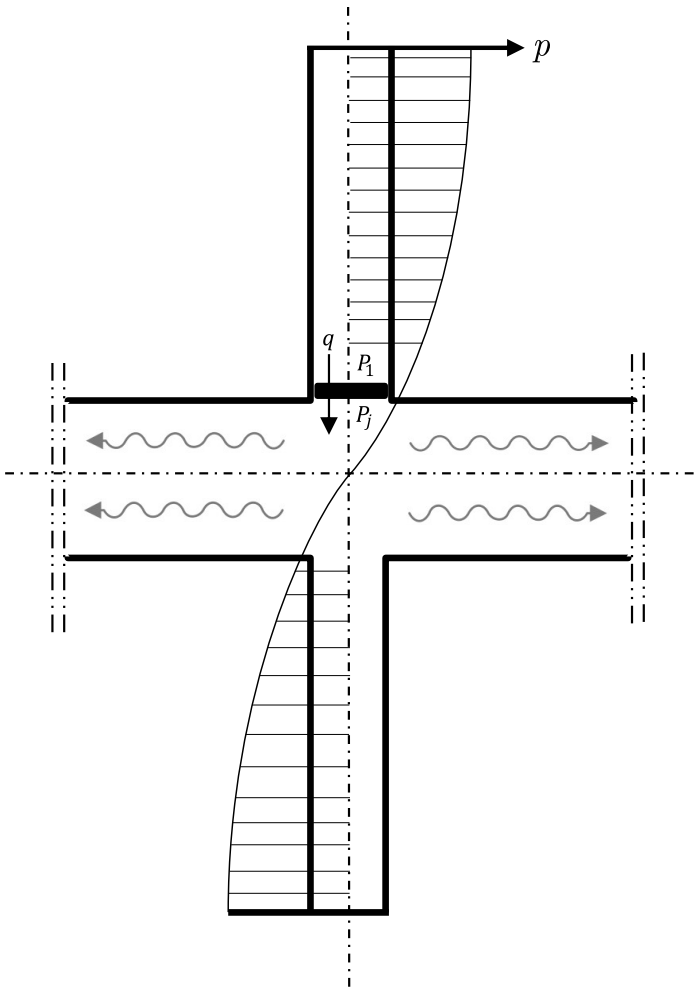

Figure 3.6: Model of the shear layer pressure difference term.

generated by the unsteady shear layer must be counterbalanced by the visco-thermal dissipation and radiated acoustic energy losses.

In line with these postulations, the phenomenon of self-excited acoustic resonance is conceptualized as a harmonic oscillator, driven by the pressure difference ΔP. The power transfer from the fluid field to the acoustic field is only contemplated at the fundamental frequency of oscillations, though higher harmonics are assumed to correspond to large amplitude non-linear effects. Despite this, their contribution to the total acoustic power is generally deemed to be insignificant.

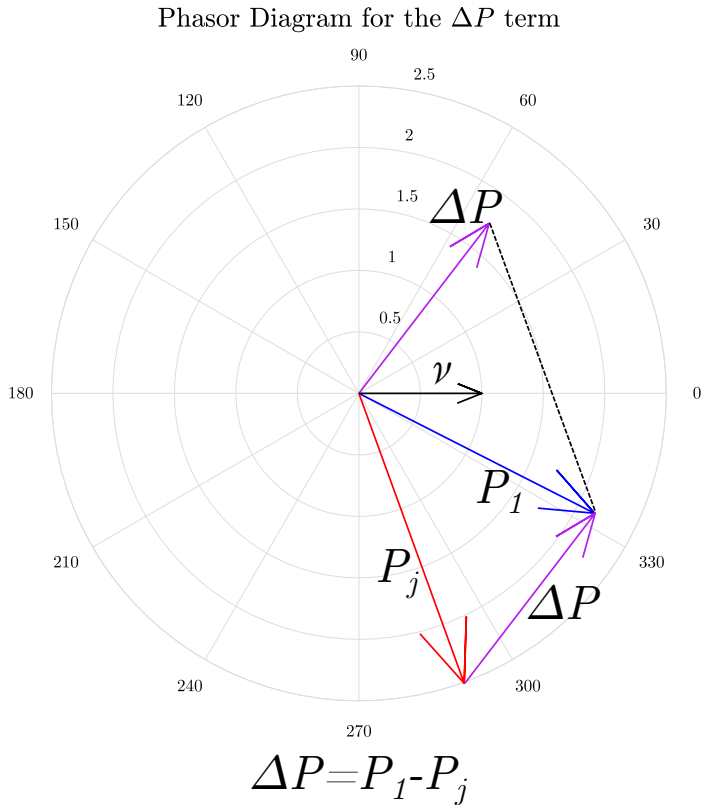

Figure 3.7: Phasor Diagram of the ΔP term.

The fundamental frequency of the pressure differential ΔP across the shear layer is presented as a complex value. The real component of ΔP aligns in phase with the acoustic particle velocity at the junction. When the real part of ΔP is positive, it signifies a beneficial energy transfer from the flow field, represented in the pressure difference, to the acoustic field. This transfer results in the generation of acoustic power and the excitation of acoustic resonance. In contrast, a negative real component of ΔP represents the transfer of acoustic energy from the acoustic field to the flow field, which suggests the absorption of the acoustic energy by the flow field.

Conversely, the imaginary component of the pressure difference synchronizes in phase with the acoustic acceleration, which governs the exchange of reactive power. When the imaginary component is positive, the pressure differential ΔP functions

as an additional stiffness to the system, thereby tending to increase the oscillation frequency. However, a negative imaginary component behaves as an added mass, which tends to reduce the oscillation frequency.

For a clearer understanding of the pressure difference calculation methodology, consider the case depicted in Figure 3.7. The pressure values P_1 and P_j across the cavity mouth are determined using the two-microphone method for the standing wave in both the side branch and the main pipe. Subsequently, the phase of each pressure is normalized in relation to the acoustic particle velocity at the cavity mouth, denoted as ν. Following this, the pressure difference is computed as $\Delta P = P_1 - P_j$. This sequence of steps is represented in the phasor diagram shown in Figure 3.7. The pressure difference ΔP has a positive real component, implying a potential for acoustic resonance. The positive imaginary component indicates that the excitation frequency will be slightly higher frequency.

To generate a non-dimensional source term that corresponds to the unsteady shear layer characteristics, the pressure difference is normalized by the dynamic head in the main pipe $\frac{1}{2}\rho U_\infty^2$, but since the sound source corresponds to the acoustic standing wave produced in the pipe as well, it is divided by the normalized acoustic particle velocuty at the branch opening $V = \nu/U_\infty$. Thus, the dimensionless acoustic source impedance is

$$\Delta s = \frac{\Delta P}{\frac{1}{2}\rho U_\infty^2 V}. \tag{3.20}$$

The characterization of the sound source term for the co-axial side branch with a sharp edge and fully developed flow was conducted by Graf and Ziada [27]. However, a multitude of industrial applications have to deal with the complexities of rounded and chamfered edges of the cavities. These geometric modifications can influence

the distribution of acoustic particle velocity at the edge as well as the overall flow topology. Furthermore, variations in upstream distances could significantly impact the flow distribution and consequently, the mechanisms of flow-sound interaction. It's also important to note that the acoustic standing wave formed in the side branch is typically considered to be a trapped mode with minimal radiation into the main pipe. However, the radiated waves are not completely dissipated outside of the system which might alter the aeroacoustic response. Therefore, it becomes imperative to investigate the effects of edge roundings, chamfers, upstream distance, and acoustic boundaries of the main pipe on the sound source term, which will be addressed in the subsequent chapters.

Chapter 4

Effect of the Upstream Distance on the Aeroacoustic Sound Source

In the present chapter, an experimental investigation of the aeroacoustic sound source in coaxial cavities, originating from the shear layer excitation at the cavity mouth coupled with the transverse acoustic mode, is undertaken. The research employs a circular pipe accompanied by circular side branches, the latter characterized by sharp edges.

The initial step involves developing a source term for a three-dimensional fully-developed turbulent upstream flow, with the purpose of validating the experimental setup against the prior work of Graf and Ziada [27]. The source term encapsulates the interaction between the flow and acoustic fields at the side branch junction. Given that the shear layer region is small relative to the acoustic mode's wavelength, the source term is treated as a lumped acoustic dipole term. Chapter 2 elucidates the experimental determination of the magnitude and phase of this complex aeroacoustic source term.

Subsequent sections introduce and apply a modeling technique for the aeroacous-

tic response, followed by a validation method based on comparing the aeroacoustic response with model predictions derived from the complex aeroacoustic sound source.

Additionally, the chapter scrutinizes the influence of alterations to the acoustic boundary conditions of the main pipe. This analysis underscores the effect of the reflection coefficient on one side of the main pipe in modifying the aeroacoustic response, and confirms the efficacy of the sound source method in modeling disparate operating conditions.

The chapter concludes by assessing the impact of varying upstream distances of the main pipe before the cavity on the aeroacoustic response and source term. The underlying objective is to demonstrate that non-developed flow yields diminished acoustic pulsations, a smaller critical Strouhal number, and an expanded lock-in range.

4.1 Features of the Aeroacoustic Sound Source and Model Validation

In the following sections, the unique characteristics of the aeroacoustic sound source resulting from shear layer separation and impingement at the juncture between a circular pipe and a co-axial side branch with a sharp transition are explored. The analysis is comprehensive and delves into how various physical phenomena impact the overall aeroacoustic performance of such systems. In addition to the quantitative analysis, a semi-empirical model is also proposed, capable of predicting the frequency and amplitude of pressure pulsations. This model aims to predict the occurrence of self-excited acoustic resonance due to fluid-resonant modes in pipelines of varying configurations. Through these two approaches – detailed analysis and empirical modeling – a comprehensive understanding of the acoustic behavior in these systems is aimed

to be provided. Such understanding is vital for preventing undesirable acoustic resonance in various applications, including industrial systems and pipelines, where such resonances could potentially lead to structural damage or other efficiency limitations.

4.1.1 Features of the Aeroacoustic Sound Source in Sharp Co-axial Side Branch

Figure 4.1 illustrates the relationship between the Strouhal number St, the aeroacoustic complex sound source term S, and the forced normalized acoustic particle velocity V. The source term S possessing both real and imaginary components is a primary feature, and its implications will be explored in depth in subsequent sections and chapters of this thesis. The real part of S, or its modulus, represents the acoustic power sources and sinks in the system. Conversely, the imaginary part of S, represented by its phase angle, indicates the added mass and stiffness effect, also known as the reactive acoustic power. As deduced from the figure, the Strouhal number shifts the source term on the imaginary axis. This shift signifies its effect on the phase, and, consequently, on the formation and downstream convection of the shear layer. Conversely, the applied pulsations, represented by different normalized acoustic particle velocities, shift the source term on the real axis. This suggests that these pulsations primarily affect the absolute value of the source term. In summary, this figure clearly illustrates the interplay between the Strouhal number, the acoustic source term, and the forced acoustic particle velocity, highlighting their combined impact on the aeroacoustic behavior in the system.

Figure 4.2 provides an in-depth look at the relationship between the aeroacoustic source term S and the normalized acoustic particle velocity V, presented at various Strouhal numbers St_t, each depicted in a unique color. For $V < 0.2$, the real compo-

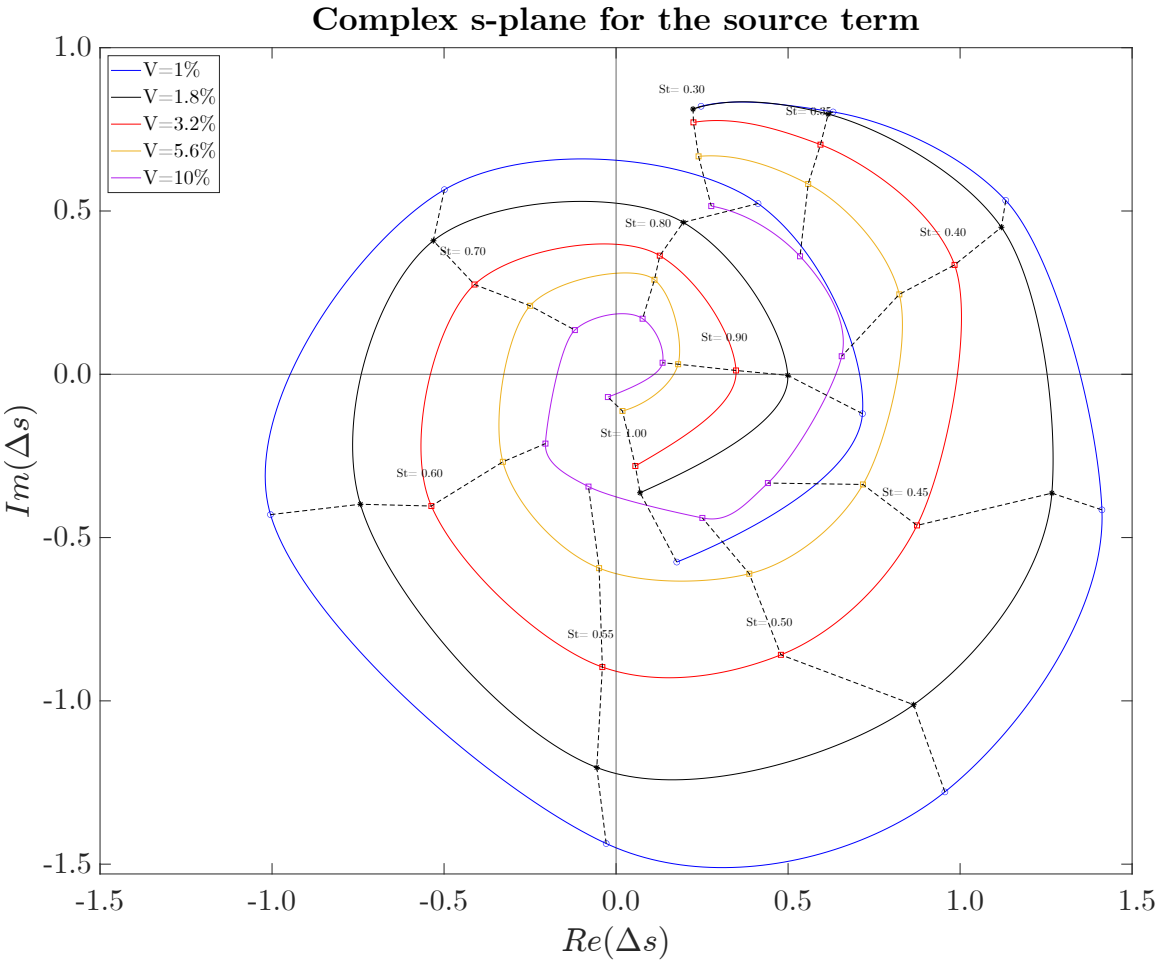

Figure 4.1: The aeroacoustic complex sound source term S at different normalized acoustic particle velocities ($V = v/U$). The Strouhal number is outlined with a step equal 0.25

nent of the source term S exhibits a significant decrease as V increases. This trend implies that, in this range, the aeroacoustic source is heavily reliant on the amplitude of the applied pulsation. This trend is primarily attributed to the externally applied excitation far surpassing the pressure drop, suggesting a discrepancy in their respective intensities. Moreover, these findings suggest that there exists a threshold for the amplitude of the shear layer oscillations. This threshold can be associated with the shortening of the vortex formation length at the upstream edge as the level of applied excitation rises. For $V > 0.2$, the aeroacoustic source term S plateaus across

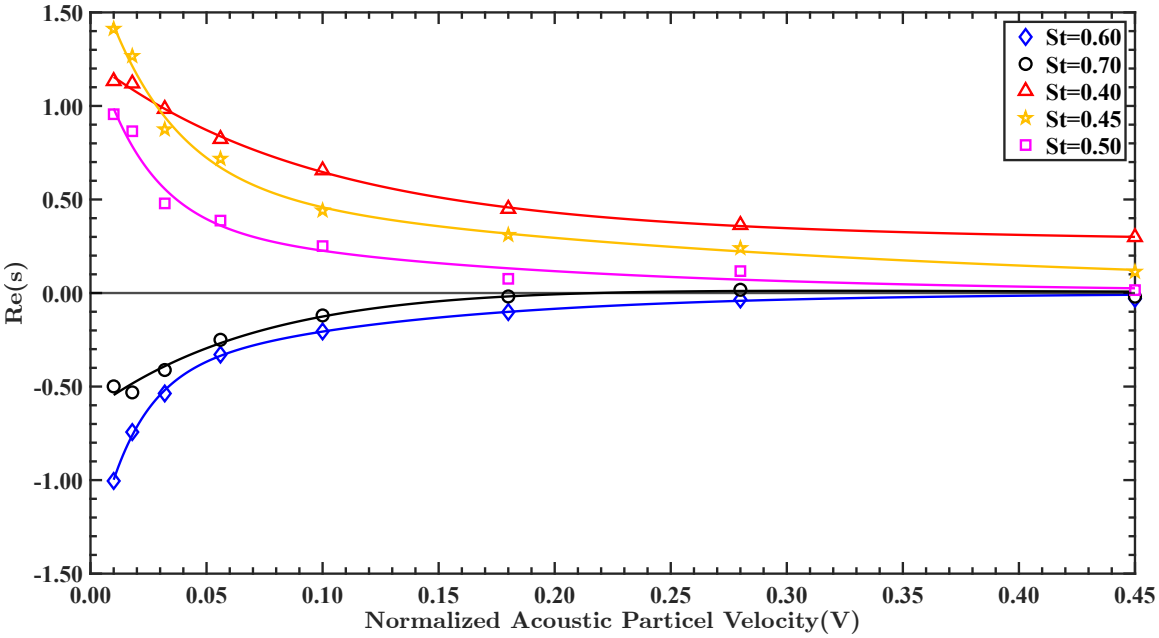

Figure 4.2: Aeroacoustic sound source S real component vs. the normalized acoustic particle velocity V at Strouhal numbers S_t ranging from 0.4 to 0.7

all Strouhal numbers, indicating a linear relationship between the applied excitation and the pressure drop across the shear layer. An intriguing aspect can be observed for high Strouhal numbers $S_t > 0.6$, where the aeroacoustic source term is negative in the low excitation range. However, it asymptotically approaches zero as the excitation level increases. This indicates that the acoustic power is being absorbed by the system, a phenomenon that could be attributed to vortex damping as discussed by Ziada (1994) [74].

In Figure 4.3, it is observed that the real component of the source term, which represents acoustic power, is positive (indicating it acts as an acoustic power source) between two Strouhal ranges: $0.3 < St_t < 0.55$ and $0.75 < St_t < 1$. These ranges correspond to the single and double vortex modes, respectively. In the single vortex mode, a single vortex propagates over the branch streamwise length during one excitation cycle, while in the double vortex mode, two vortices convect over the branch

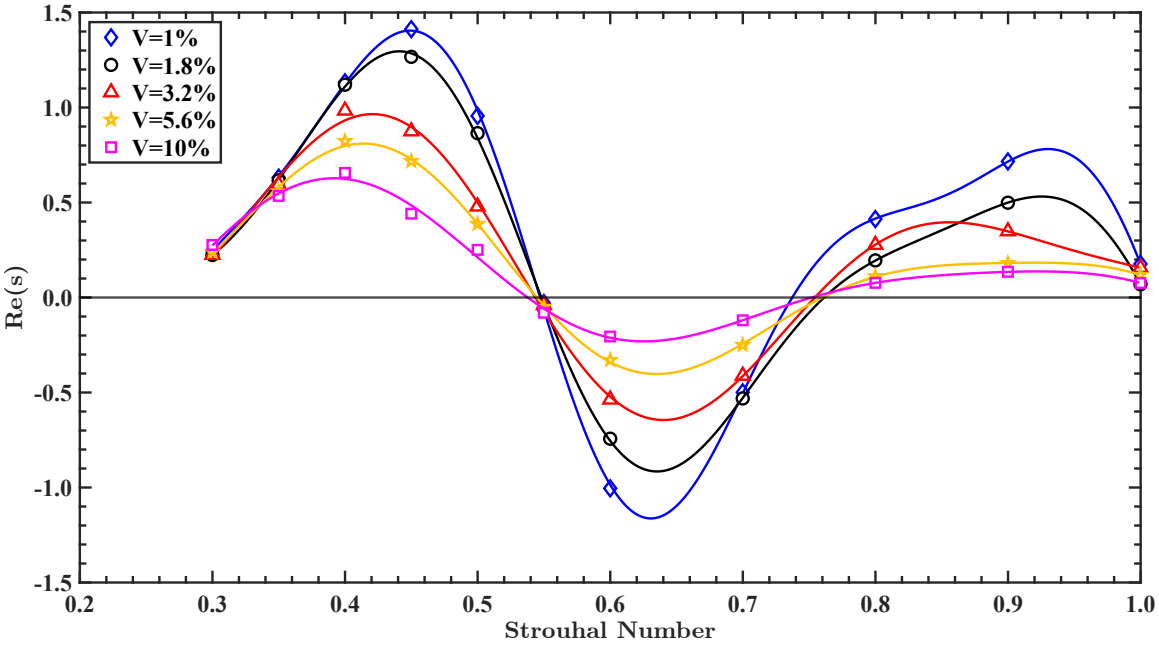

Figure 4.3: Aeroacoustic sound source S real component vs. the Strouhal number S_t at different normalized acoustic particle velocity V ranging from 1% to 10% with an uneven step.

length. The trend in the figure suggests that the Strouhal number alternates between acting as an acoustic power source and a sink across different Strouhal number ranges. A noteworthy feature is that the peak of acoustic power occurs at slightly lower Strouhal numbers as the excitation level increases. This suggests a strong influence of the excitation level on the phasing of the shear layer vortices and their distance from the upstream edge. Specifically, as the excitation level increases, the vortex forms closer to the upstream edge and the curvature of the shear layer becomes more pronounced. This allows the vortex to form further inside the branch. These observations provide crucial insights into the dynamics of aeroacoustic power sources under various conditions, highlighting the role of the Strouhal number and excitation level in shaping the behavior of the system.

4.1.2 Modeling Technique and Validation

Modeling Technique

In this section, the previously derived experimental aeroacoustic sound source is merged with an analytical portrayal of the side branch, thereby forming a semi-empirical model. This model is equipped to predict both the amplitude of pressure pulsations and the excitation frequency when interacting with the co-axial side branch.

After illustrating the simulation procedure, the experimental results of the aeroacoustic response are compared with the simulation outcomes, highlighting the precision of the modeling technique. The modeling methodology proposed by Graf and Ziada demonstrates accuracy in predicting the aeroacoustic response across a variety of parameters, including the mean flow velocity within the main pipe, the branch length, the piping system's static pressure, and visco-thermal and radiation losses.

Given that the power produced by the aeroacoustic sound source must be offset by the acoustic impedance of the piping system due to visco-thermal and radiation losses, the acoustic impedance across the shear layer at the junction (ΔZ) must adhere to the relation $\Delta Z = s$.

The acoustic impedance across the shear layer exhibits direct proportionality to the acoustic pressure across the shear layer. To differentiate between the acoustic pressure arising from the acoustic field and the measured pressure across the shear layer - used to determine the aeroacoustic source term - an 'a' subscript will be appended to the acoustic variables. Consequently, the acoustic pressure difference across the shear layer is given by

$$\Delta P_a = P_{1a} - P_{ja}. \tag{4.1}$$

However, due to the symmetry of the coaxial cavity about the junction where the acoustic particle velocity peaks, $P_{ja} = 0$, and hence $\Delta P_a = P_{1a}$. Thus, ΔZ is solely a function of the acoustic impedance of the side branch and remains unaffected by the acoustics of the main pipe. However, this assumption does not hold when the length of both branches is not equal.

Taking into consideration the visco-thermal losses, the characteristic impedance is determined by:

$$Y = \rho_\circ c_\circ (1 - \frac{\alpha}{k_\circ} + j\frac{\alpha}{k_\circ}). \tag{4.2}$$

Therefore, one can calculate the acoustic impedance of a single side branch with a length L and correction length e using:

$$Z_{branch} = \frac{P_{1a}}{q_{1a}}, \tag{4.3}$$

Here, q_{1a} refers to the acoustic volume velocity, defined as $q_{1a} = v * A$, with A symbolizing the cross-sectional area of the branch. Consequently, the acoustic impedance of a side branch with a perfectly reflective end can be expressed as:

$$Z_{branch} = \frac{P_{1a}}{q_{1a}} = \frac{Y}{jtan(k(L+e))} \tag{4.4}$$

Given that ΔZ is solely a function of the acoustic impedance of the side branch, it's feasible to normalize the acoustic impedance to dimensionally align with the aeroacoustic sound source, as detailed below:

$$\Delta Z = \frac{Z_{branch}}{\frac{1}{2}\rho U^2 \frac{v}{U}} = \frac{2}{Mjtan(k(L+e))}(1 - \frac{\alpha}{k_\circ} + j\frac{\alpha}{k_\circ}) \tag{4.5}$$

As elucidated by Equation 4.5, the acoustic impedance across the shear layer zone

can be readily calculated, given known parameters such as cavity geometry, upstream flow velocity, and the anticipated excitation frequency of the branch. It's noteworthy that the value of ΔZ fluctuates with varying the excitation frequency for a specific flow velocity. Matching the shear layer acoustic impedance (by changing the frequency) with the aeroacoustic source term at a particular flow velocity (i.e., along a defined Strouhal number line) results in a singular point on the complex plane, corresponding to a specific normalized acoustic particle velocity $V = v/U$. This process is iteratively applied for each successive flow velocity.

The significance of the total aeroacoustic attenuation constant $\alpha = \alpha_\circ + \zeta M$ under dynamic flow conditions should be underscored. This parameter serves as a pivotal element of the model, with the impact of the pipeline's static pressure accounted for within the visco-thermal attenuation coefficient, $\alpha_\circ$. Concurrently, the turbulent flow friction term, ζM, dictates the system's damping. Careful consideration should be given to the measurement technique employed for ζ, and its consequential effect on both the aeroacoustic response and the aeroacoustic sound source modeling technique.

Mohamed (2015) [43] applied another methodology to precisely evaluate the acoustic impedance of the shear layer for axis-symmetrical cavities, namely, the two-microphone method. He performed comparative analyses between acoustic impedance measurements made with this method during external loudspeaker excitation at zero mean flow conditions, and those conducted during the cavity's self-excitation at resonance. Furthermore, these empirical results were juxtaposed with theoretical calculations. This exercise revealed that the most accurate measurements were procured during self-excitation. Nevertheless, analytical computations overestimated the peak acoustic amplitude by only 15%, while the lock-in range was accurately predicted relative to the self-excited aeroacoustic case.

This discrepancy between the analytical results and self-excited case likely stems

from the assumption of a perfect open end on both sides for the longitudinal acoustic wave prompted by the axisymmetric cavity. The flexible connection at the test section's outlet could potentially have mitigated the reflected wave, thereby leading to weaker self-excitation.

The influence of the end conditions of both the upstream and downstream pipes forms a critical factor in discerning the acoustic properties of the system. Mohamed (2015) [43] illustrated the significant influence these end conditions exert on global excitation modes. However, it is worth noting that these end conditions also impact the aeroacoustic response and the aeroacoustic sound source of trapped modes, such as those within co-axial cavities.

Model Validation

The self-excited aeroacoustic response of the system, as depicted in Figure 4.4, shows an impressive correlation with the superimposed model prediction. Notably, the model is capable of accurately predicting the excitation frequency, range, and amplitude with only minor discrepancies. Two distinct Strouhal periodicities, which correspond to the single and double vortex modes (the first and second hydrodynamic modes), are observed to couple with the first, second, and third acoustic modes at each frequency coincidence. A significant observation is that the peak amplitude of the normalized acoustic particle velocity and the lock-in range is considerably lower in comparison to the excitation resulting from the coincidence with the single vortex mode. This can primarily be attributed to the lower availability of acoustic power in the shear layer in the case of the double vortex mode. When comparing the amplitude peaks during the first and second acoustic mode excitation from the single vortex mode, it's noticeable that the peak during the second mode reaches a value of 0.35%, while it's only 0.15% during the first mode excitation. This can be attributed to the

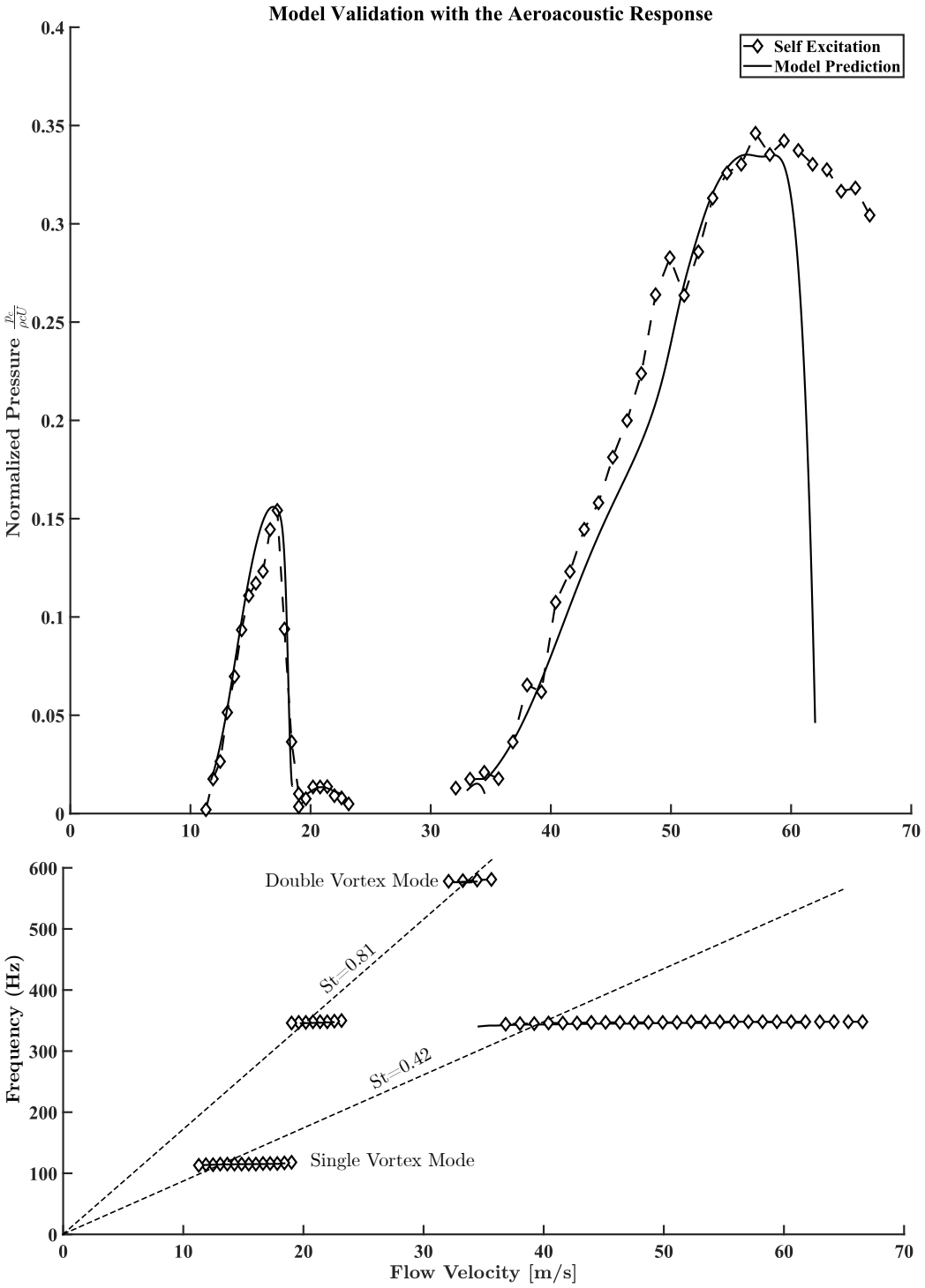

Figure 4.4: Self-excited aeroacoustic response at a range of flow velocities with the model prediction super imposed

substantially higher flow velocity at which the second mode excitation takes place. As the flow velocity increases, the available energy in the fluid also increases, thus allowing a higher energy exchange between the sound and flow fields under acoustic resonant conditions.

4.2 Effect of End Conditions on the Aeroacoustic Sound Source

In examining trapped modes, it should be observed that the acoustic terminations of the main pipes may not necessarily influence the excited acoustic mode within the coaxial cavity. This observation contrasts with the case of T-junctions global excitation modes, where the cavity experiences coupling with either the upstream or downstream cavity [74]. Mohamed (2015) also explored the impact of downstream acoustic boundary termination on the acoustic impedance of the pipe, revealing that the simulation approach to aeroacoustic resonance, utilizing the aeroacoustic sound source method, would vary by up to 20 percent in terms of peak acoustic pressure. Notably, this variation did not influence the extension of the lock-in range when compared to the self-excited aeroacoustic data.

In this subsection, the influence of downstream acoustic boundary termination on both self-excited acoustic resonance and the aeroacoustic sound source will be investigated. Two distinct acoustic boundary terminations are employed within the same test section as outlined in section 2.2. Instead of attaching an anechoic box to the downstream pipe, a muffler is installed to simulate an open-end condition. The two test scenarios under examination within this section are: (1) an open-anechoic configuration, where an actual open end is present on the upstream end of the test section, coupled with an anechoic box designed to minimize acoustic reflections, and

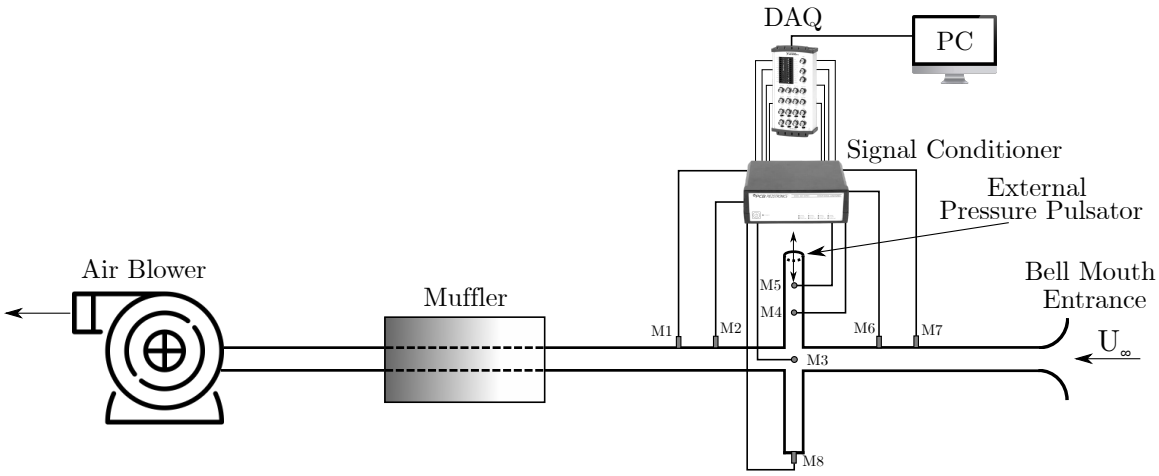

Figure 4.5: Test section with open-open acoustic boundary conditions.

(2) an open-open configuration, which maintains the same open end on the upstream pipe but replaces the anechoic box with a muffler to model an open end on the downstream side. It should be noted that in both configurations, the coaxial cavity installed on the main pipe possesses sharp edges, and the length of the upstream and downstream pipes remains consistent.

The upstream pipe's length is tailored to correspond to 1.75λ of the first excited acoustic mode inside the cavity, a configuration aimed at decoupling the pipe from the cavity's excitation by maximizing the acoustic impedance of the upstream pipe at this frequency. The length of the upstream pipe is set at 5.25 meters, equating to 52 diameters of the main pipe, a requirement for ensuring fully developed turbulent flow. In contrast, the downstream pipe's length is adjusted to correlate with 0.75λ, further decoupling the downstream pipe from the cavity's excitation. The downstream pipe is then linked to a muffler, which is, in turn, connected to an air blower, as depicted in Figure 4.5.

Figure 4.6 illustrates the impact of varying the downstream acoustic boundary condition on the aeroacoustic response of the coaxial side branch. The inclusion of the muffler induced modifications in the maximum normalized pressure pulsation, the

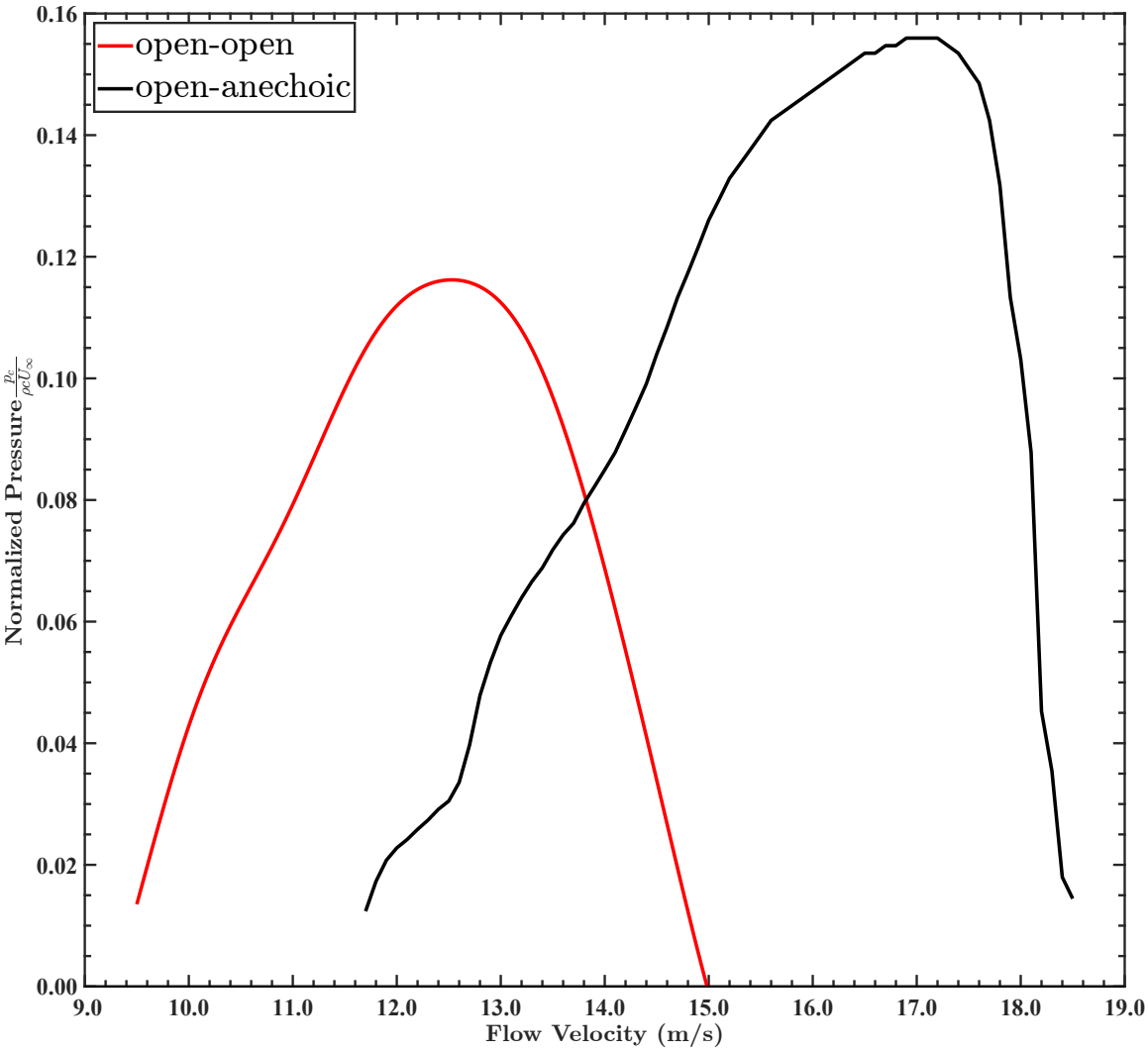

Figure 4.6: Comparison between the aeroacoustic response for co-axial side branch at two different downstream acoustic terminations.

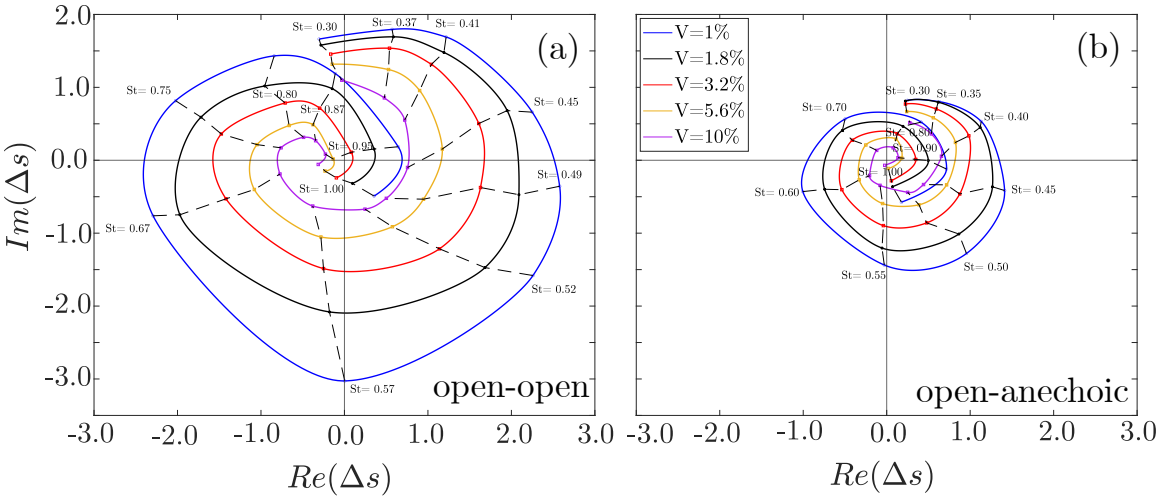

Figure 4.7: The tested configurations for varying the upstream distance with decoupled cavity mode for an open-open acoustic boundary condition.

critical Strouhal number initiating the aeroacoustic resonance, and the extension of the lock-in range. As delineated in Figure 4.6, the peak normalized pressure experienced a reduction of approximately 25%, descending from 0.16 in the open-anechoic scenario to roughly 0.12 in the open-open configuration. Furthermore, the onset of aeroacoustic resonance in the open-open situation occurred at 10 m/s, correlating to a Strouhal number (St) of 0.57. Conversely, the open-anechoic case exhibited a postponed onset of resonance at 12 m/s, aligning with a Strouhal number (St) of 0.49.

Regarding the lock-in range, the open-open configuration demonstrated an extension from 10 to 14.5 m/s, corresponding to a Strouhal range of St=0.57-0.38. This differs from the open-anechoic configuration, where the lock-in range spanned from 12 to 18 m/s, aligning with a Strouhal range of St=0.49-0.32. These results indicate that end conditions indeed influence the aeroacoustic response. Nevertheless, with only a 25% reduction in peak acoustic pressure, this adjustment does not qualify as a suppression technique. Despite this, its potential to cause premature excitation of aeroacoustic resonance, particularly within an open-open configuration, necessitates consideration in the design process.

The alteration in aeroacoustic response arising from changes in the downstream acoustic boundary condition highlights the potential influence of acoustic energy radiated from the side branch on the acoustic waves within the downstream pipe. Upon reconstruction of the acoustic waves in the downstream pipe using the two-microphone method, a standing wave with a frequency of approximately 87 Hz was noted, corresponding to the half-wavelength excitation mode. Consequently, the reflection coefficient at this frequency was studied to evaluate the performance of the muffler and the anechoic box in transmitting radiated acoustic waves outside the piping system.

For the open-open configuration, the reflection coefficient at the muffler—calculated as the ratio between the reflected pressure amplitude (p^-) and the incident pressure amplitude (p^+)—was found to be 0.87. Contrastingly, the reflection coefficient for the anechoic box configuration was 0.8. This decrease in the reflection coefficient corresponds to a reduction in the spectral amplitude of this mode by a factor of 5.

Given the demonstrated influence of the downstream acoustic boundary condition on the acoustic field within the pipeline—consequently affecting the flow field due to feedback mechanisms—it is essential to examine the effect of altering the downstream acoustic boundary condition on the aeroacoustic sound source. Figure 4.8 depicts the complex s-plane for both the open-open and open-anechoic configurations. Despite the maintenance of the spiral geometry in both maps, two major differences were observed: a shift in the open-open configuration in the negative real direction relative to the open-anechoic s-plane map centered about the origin point; and an increased amplitude of the source term at each point for the open-open configuration, given the same Strouhal number and normalized acoustic particle velocity (V).

The modeling technique relies on matching the acoustic impedance of the shear layer zone with the aeroacoustic source term for each flow velocity, frequency, and damping constant. As an analytically calculated parameter, the acoustic impedance

remains independent of the downstream boundary condition. Thus, discrepancies between the two source maps suggest changes in the aeroacoustic response. The more "compact" nature of the source map for the open-anechoic configuration implies greater nonlinearity in the excitation mechanism, correlating to sharp variations in the simulated acoustic pressure pulsation for small changes in acoustic impedance. This nonlinearity is less pronounced in the open-open configuration. Furthermore, the negative shift in the open-open configuration's source map, coupled with reduced system non-linearity, results in larger acoustic particle velocities with negative real components at all Strouhal numbers, thereby limiting the maximum possible pressure pulsation excited inside the cavity due to self-excitation.

In conclusion, changing the downstream acoustic boundary condition for the main pipe containing a coaxial side branch does influence the aeroacoustic response and consequently, the aeroacoustic sound source. However, the effect of the downstream boundary condition on the coaxial branch excitation is less pronounced compared to a T-junction, where pressure pulsation can vary by an order of magnitude due to minor changes in the acoustic boundary conditions of the main pipe, as reported by Hofmans (1998)[74].

4.3 Effect of Changing the Upstream Distance on the Aeroacoustic Sound Source

Prior research has established that the vortex convection velocity at the cavity mouth is a crucial determinant of acoustic resonance initiation, activated upon reaching a critical value. At this critical convection velocity, the net acoustic power generated over an entire acoustic cycle is positive as per Howe's integral (Eq. 2.2). This suggests that the aeroacoustic response in the side branch owing to the shear layer excitation

is contingent upon the local flow velocity at the separation edge of the side branch, as delineated by Ziada and Shine (1999) [78]. They examined the impact of an upstream elbow on the aeroacoustic response of a single side branch and the subsequent positioning of the side branch in relation to the elbow. Their research indicated an amplification in peak acoustic resonance when the side branch was placed on the outer side (higher velocity) of the elbow compared to the base case without the elbow. Conversely, positioning the side branch on the inner side of the elbow mitigated peak acoustic pressure and postponed the onset of acoustic resonance. This underscores that velocity distribution approaching the side branch does influence the aeroacoustic response. However, accurate quantification of the velocity distribution approaching the side branch may not be beneficial in industrial scenarios. Furthermore, Ziada and Buhlmann (1992) [76] studied the effect of turbulence intensity on the aeroacoustic response of coaxial and tandem side branches and concluded that increasing the turbulence intensity negligibly impacts the extension of the lock-in range, suggesting that geometrical parameters of the pipeline systems are sufficient for characterizing the cavity type and the excitation mechanism.

In this section, the influence of the upstream distance on the aeroacoustic resonance of the coaxial side branch and, consequently, the aeroacoustic sound source is investigated. If the upstream pipe length is adjusted to correspond to an odd number of quarter wavelengths of the first excited acoustic mode within the cavity for a trapped acoustic mode inside the side branch, the pipe can be decoupled from the cavity's excitation by maximizing the acoustic impedance of the upstream pipe at this frequency. This implies that the upstream distance can be adjusted to discrete lengths to ensure the cavity's maximum acoustic pressure and to inhibit any excitation of duct modes or global modes.

Four distances were tested, as illustrated in Figure 4.8 and Table 4.1. Cases (a)

Table 4.1: The tested configurations for varying the upstream distances.

Upstream Distance L (m)	L/D	L/λ
2.24	22.4	3/4
3.73	37.3	5/4
5.22	52.2	7/4
6.71	67.1	9/4

and (b) represent a non-fully developed flow, while cases (c) and (d) denote a fully developed flow (at $40D$ from the bell-mouth). Instead of the anechoic airloop, a muffler was utilized for these measurements as displayed in Figure 4.5. The rationale behind this approach is the intent to simulate conditions prevalent in industrial applications, where downstream pipes are typically not long enough to be considered anechoic ends. This real-world approach reflects a practical understanding of the behavior of such systems within their typical environments and offers insights directly applicable to industrial settings.

As the upstream distance is extended, the velocity distribution over the flow approaching the coaxial cavity increasingly resembles the fully developed turbulent flow, which can be approximated by a power-law velocity profile. Additionally, elongating the upstream distance moves the open acoustic boundary condition further from the cavity, thereby reducing reflections from the open end due to attenuation and viscothermal losses. Figure 4.9 illustrates the influence of adjusting the upstream distance on the complex sound source term. The primary observation on the sound source term is the reduced amplitude of the source term for the same Strouhal number and normalized acoustic particle velocity in the 3/4 λ configuration. However, beginning from the 5/4 λ configuration, the source term values appear to be roughly equivalent when compared with the 7/4 and 9/4 λ configurations.

This observation can be confirmed by examining the real component of the source term versus the Strouhal number, as portrayed in Figure 4.10, and the same nor-

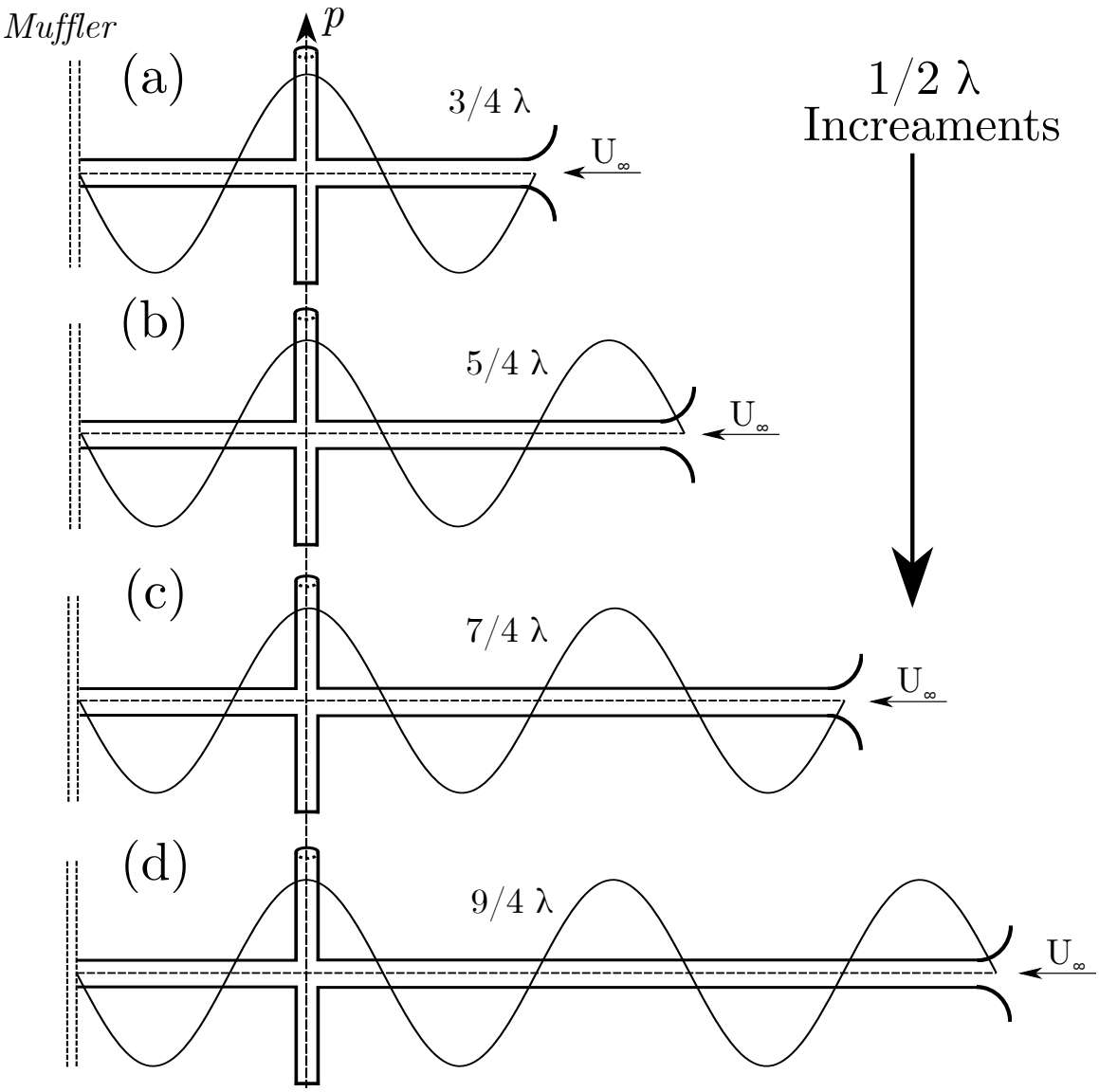

Figure 4.8: The tested configurations for varying the upstream distance with decoupled cavity mode for an open-open acoustic boundary condition.

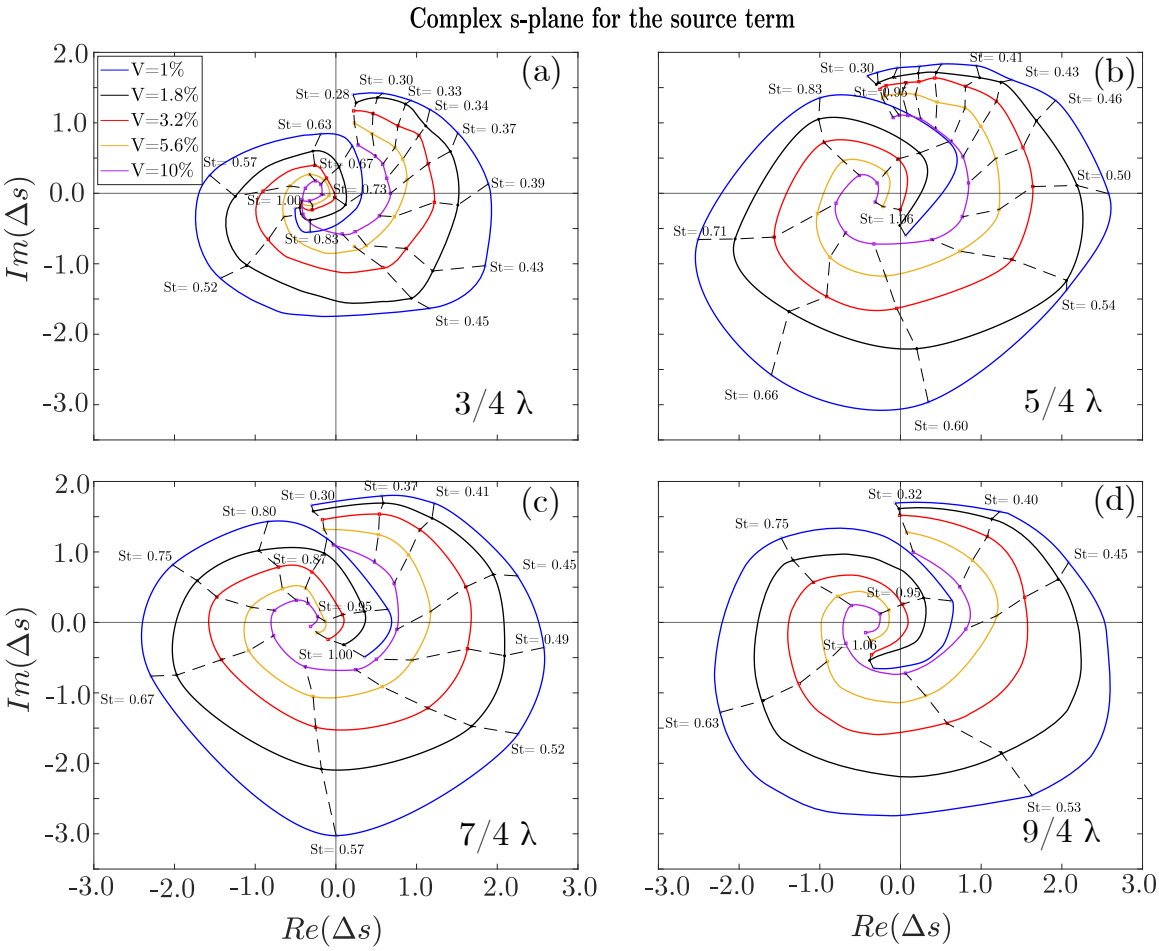

Figure 4.9: The aeroacoustic sound source maps for different upstream distances.

malized acoustic particle velocity for all cases $V = 1\%$. It can be noticed that the peak of the real component in the first positive range of the Strouhal number at the 3/4 λ configuration is shifted to around St=0.4 instead of St=0.5 for the other configurations. This suggests that the peak acoustic pressure will be excited at higher flow velocity (lower Strouhal number) in the 3/4 λ configuration due to the different upstream velocity distribution. It should be noted that the model does not predict the peak acoustic pressure for each case at the Strouhal numbers where the real component is maximized according to Figure 4.10 since this figure only presents the real component for normalized acoustic particle velocity $V = 1\%$. This does not entirely

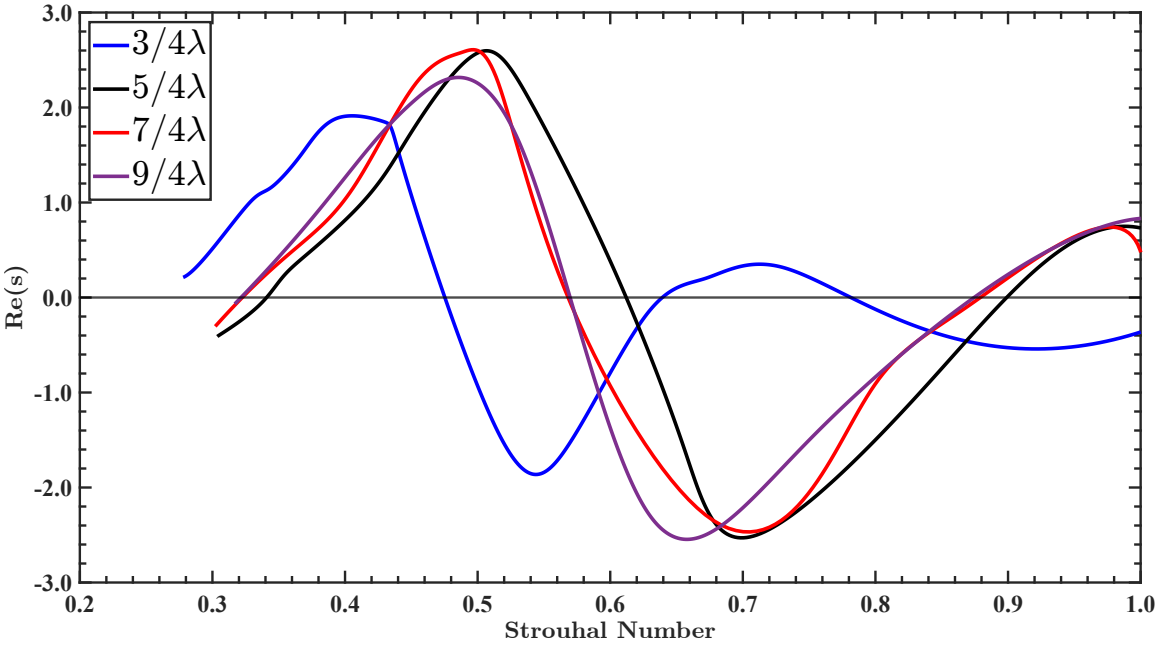

Figure 4.10: Variation of the real component of the aeroacoustic sound source with Strouhal number at different upstream distances for V=1%.

reflect the entire simulation technique but serves as a useful illustration.

The simulation technique elucidated in section 4.1.2 is employed to predict the aeroacoustic response for each of the four studied configurations, which is then validated against the self-excited experimental data for the first hydrodynamic mode coupling with the first acoustic mode. The validation was not performed for higher acoustic modes due to the flow velocity limitation of the used blower, which does not contradict the model's capability to predict the excitation of higher acoustic modes. The model prediction matched the aeroacoustic response for the lock-in range and the peak acoustic pressure within 10% for every case, but for brevity, the validation of the 9/4 λ is presented here, as shown in Figure 4.11.

Upon comparing the aeroacoustic responses of different upstream distances, it becomes clear that reducing the upstream distance below the $40D$ threshold that demarcates the fully developed flow, results in a decrease in both the peak acoustic

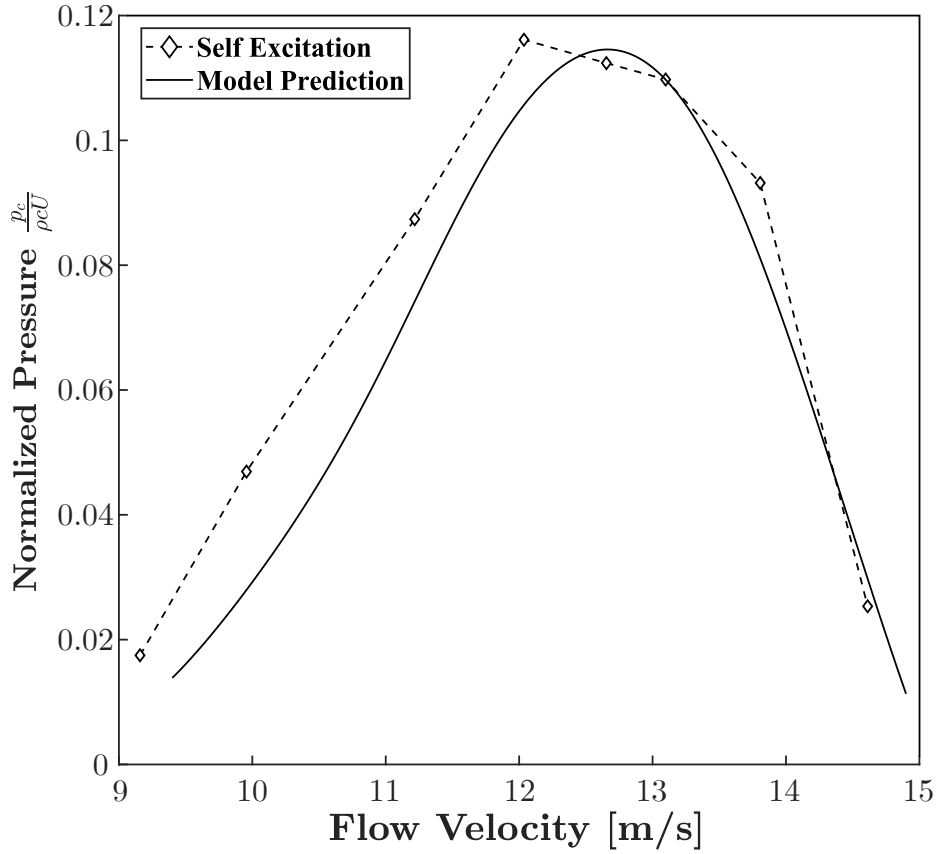

Figure 4.11: Validation results of the 9/4 λ configuration for the first hydrodynamic mode coincidence with the first acoustic mode of the co-axial cavity.

pressure and the critical Strouhal number, as demonstrated in Figure 4.12. For the fully developed flow configurations (7/4 and 9/4 λ), the acoustic response is virtually identical in terms of peak acoustic pressure, critical Strouhal number, and the lock-in range. However, an almost fully developed flow (5/4 λ) is characterized by a slight reduction in peak acoustic pressure and a smaller critical Strouhal number (i.e., higher velocity for the onset of resonance). This effect becomes more pronounced in the non-developed velocity profile configuration (3/4 λ), where the peak acoustic pressure is reduced by a third of its value for the fully developed flow configurations. Also, this peak pressure is observed at a higher flow velocity, indicating that the non-developed flow reaches the "local velocity" that excites the acoustic resonance at the cavity

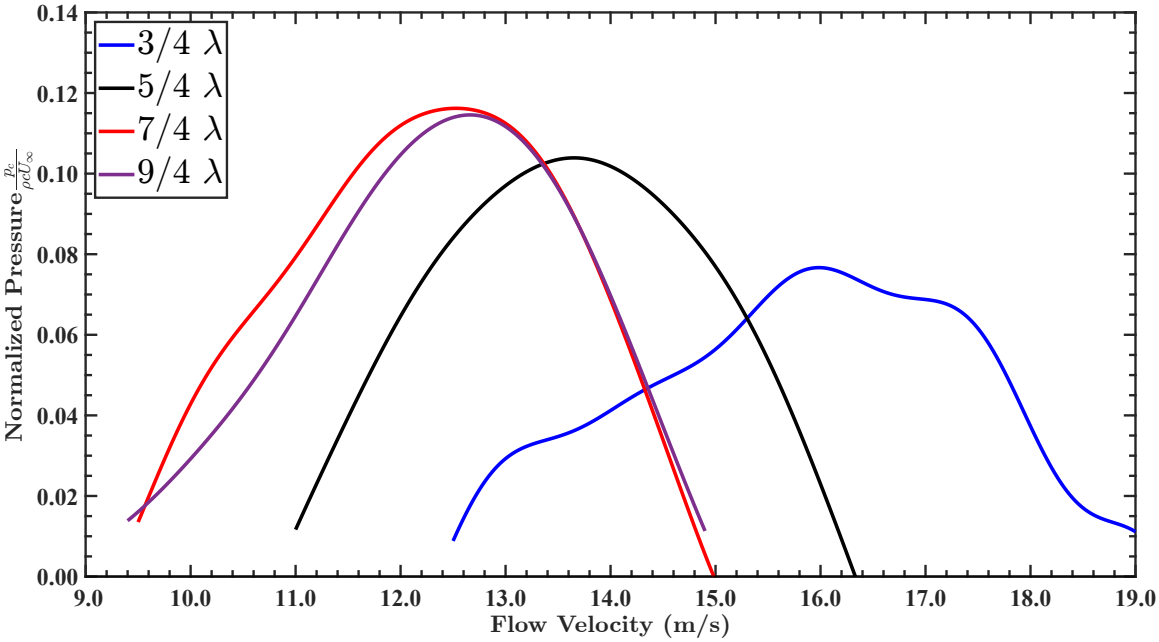

Figure 4.12: The aeroacoustic response as predicted by the model for varying the upstream distances.

mouth at higher flow velocities. Furthermore, the lock-in range of the acoustic resonance is extended over a larger velocity range when compared to the fully developed velocity profile configurations. Hence, it is evident that the non-developed velocity distribution impacts the self-excitation mechanism of the aeroacoustic resonance in deep coaxial cavities. This aligns with the observed effects of the elbow on the aeroacoustic resonance of the single side branch when positioned on the elbow's inner side. This implies that, as the fully developed flow has a larger momentum thickness (θ) and a larger velocity gradient at the wall, the local velocity at the cavity mouth is higher for the same mean flow velocity, which excites the acoustic resonance at a higher Strouhal number (lower mean flow velocity). Table 4.2 presents a summary of the lock-in range, the optimal Strouhal number (at which the peak acoustic pressure is observed), and the peak normalized acoustic pressure for each configuration.

In Summary, the influence of acoustic terminations on acoustic modes within

Table 4.2: Summary of the aeroacoustic response as predicted by the model for varying the upstream distances.

Upstream Distance L (m)	L/D	L/λ	Critical Strouhal number $St_{crticial}$	Lock-in range	Peak Normalized Pressure
2.24	22.4	3/4	0.46	St=0.3-0.46	0.077
3.73	37.3	5/4	0.53	St=0.36-0.53	0.103
5.22	52.2	7/4	0.62	St=0.39-0.62	0.115
6.71	67.1	9/4	0.62	St=0.39-0.62	0.115

coaxial cavities is explored, demonstrating that the acoustic terminations of main pipes may not have a significant impact on these modes. Two acoustic boundary conditions were examined: an open-anechoic configuration, and an open-open configuration. The impact of these different configurations on the aeroacoustic response and the aeroacoustic sound source were studied. Results showed that the inclusion of a muffler, simulating an open-end condition, altered the maximum normalized pressure pulsation, the critical Strouhal number initiating the aeroacoustic resonance, and the extension of the lock-in range.

The peak normalized pressure was reduced by 25% with the inclusion of a muffler. The onset of aeroacoustic resonance was also affected, occurring at 10 m/s in the open-open configuration and 12 m/s in the open-anechoic configuration. The lock-in range extended from 10 to 14.5 m/s for the open-open configuration and 12 to 18 m/s for the open-anechoic one. These results indicate the importance of considering the effect of end conditions on the aeroacoustic response during the design process, even though the variation in peak acoustic pressure does not qualify as a suppression technique.

The investigation also revealed that changes in the downstream acoustic boundary condition influence the acoustic field within the pipeline and the aeroacoustic sound

source. The open-open configuration, compared to the open-anechoic one, showed a negative shift and increased amplitude in the s-plane map. The open-open configuration demonstrated less nonlinearity and larger acoustic particle velocities, thereby limiting the maximum possible pressure pulsation excited inside the cavity due to self-excitation.

When contemplating the upstream pipe, it is vital to note that if its length is tuned to an odd number of quarter wavelengths of the cavity's first excited acoustic mode, it can decouple the pipe from the cavity's excitation, maximizing acoustic impedance. Four different upstream distances were examined under conditions mimicking industrial environments. As the upstream distance lengthens, the flow approaching the coaxial cavity resembles fully developed turbulent flow. The study revealed that extending the upstream distance reduced the amplitude of the source term for the same Strouhal number and normalized acoustic particle velocity in the 3/4 λ configuration. But from the 5/4 λ configuration onwards, the source term values appeared equivalent. The peak of the real component shifted to around St=0.4 in the 3/4 λ configuration, suggesting peak acoustic pressure is excited at higher flow velocity due to different upstream velocity distribution. Predictive simulations were performed for each configuration and validated against self-excited experimental data for the first hydrodynamic mode coupling with the first acoustic mode. These demonstrated that reducing upstream distance below the 40D threshold (that demarcates fully developed flow) resulted in a decrease in both peak acoustic pressure and the critical Strouhal number. For fully developed flow configurations, the acoustic response was similar. However, a non-developed velocity profile configuration had a third of the peak acoustic pressure of fully developed flows, with peak pressure at higher flow velocity. This indicates that the non-developed flow reaches the local velocity exciting the acoustic resonance at the cavity mouth at higher flow velocities. The lock-in

range of the acoustic resonance was also extended over a larger velocity range. Therefore, the non-developed velocity distribution affects the self-excitation mechanism of aeroacoustic resonance in deep coaxial branches, consequently the aeroacoustic sound source.

Chapter 5

Effect of Edge Geometry on the Aeroacoustic Sound Source and Response

In this chapter, an experimental investigation of the aeroacoustic sound source and response in coaxial cavities with various edge modifications is carried out. This step naturally follows the investigation of the sound source for sharp edge cases, given the significant role edge geometry plays in the separation of the shear layer from the upstream edge and its impingement on the downstream edge. By modifying the edge geometry, the aim is to further understand how the shear layer's response and sound source alter in response to different parameters. Four different junction edge rounding radii and four different edge chamfers are tested, as depicted in Figure 5.1. In the following sections, a modeling technique for the aeroacoustic response is introduced and applied. This is followed by a validation method based on comparing the observed aeroacoustic response with model predictions derived from the complex aeroacoustic sound source. Finally, the impact of different degrees of edge chamfering

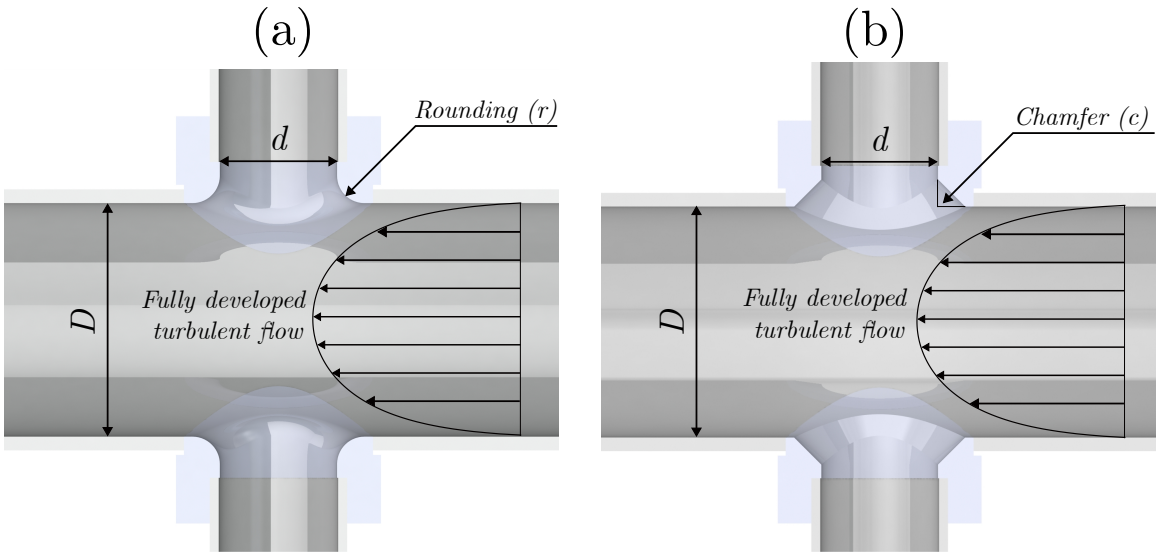

Figure 5.1: Co-axial branch junction edges (a)rounding; (b) chamfering

and rounding on the aeroacoustic response and source term is assessed. The ultimate aim is to demonstrate how the edge geometry influences the critical Strouhal number, sound source, and lock-in ranges.

5.1 Features of the Aeroacoustic Sound Source for Co-axial Cavities with Rounded Edges

In a multitude of applications, rounding and chamfering features can be found due to their practical advantages and because it is often a byproduct of manufacturing considerations. Consequently, rounding frequently appears at junctions within various pipeline systems. An extensive body of research exists that investigates the implications of rounding on both internal and external flows, providing valuable insights into its effects. It has been observed that rounding can enhance vortex shedding and formation, thereby influencing the aerodynamic or hydrodynamic characteristics of a system. To elucidate the effects of rounding more systematically and in greater

depth, a study featuring four different rounding radii is proposed. This experiment will be carried out on a side branch with a diameter of 50 mm, and installed on a main pipe with a diameter of 100 mm. The selected rounding radii for this investigation are 6 mm, 8 mm, 10 mm, and 12 mm. When these measurements are converted into non-dimensional rounding values, they correspond to 0.12, 0.16, 0.20, and 0.24, respectively. These specific radius and diameter ratios have been chosen not merely by happenstance; they bear practical relevance as they are frequently encountered in industrial applications. By focusing on these particular measurements, the findings of this research will hold direct applicability to real-world scenarios, thereby contributing valuable knowledge for the design and understanding of similar industrial systems. The results from this study are expected to shed more light on how rounding, a seemingly minor geometric detail, can have significant implications for the behavior of fluid flow within a piping system.

5.1.1 The Effect of Different Edge Rounding Radii on the Aeroacoustic Sound Source

As discussed in previous chapters, the aeroacoustic sound source serves as a quantitative representation of the flow-acoustic coupling mechanism. This source term, which can be empirically measured, offers a valuable means to examine the myriad factors influencing aeroacoustic resonance. Furthermore, it facilitates the prediction of the aeroacoustic response for scenarios with similar coupling properties, even when the geometrical attributes vary. Consequently, the importance of understanding and leveraging the source term extends beyond its theoretical significance. It provides a practical tool to predict and potentially control the aeroacoustic behavior in a wide array of configurations, thus enhancing the design and optimization processes in rel-

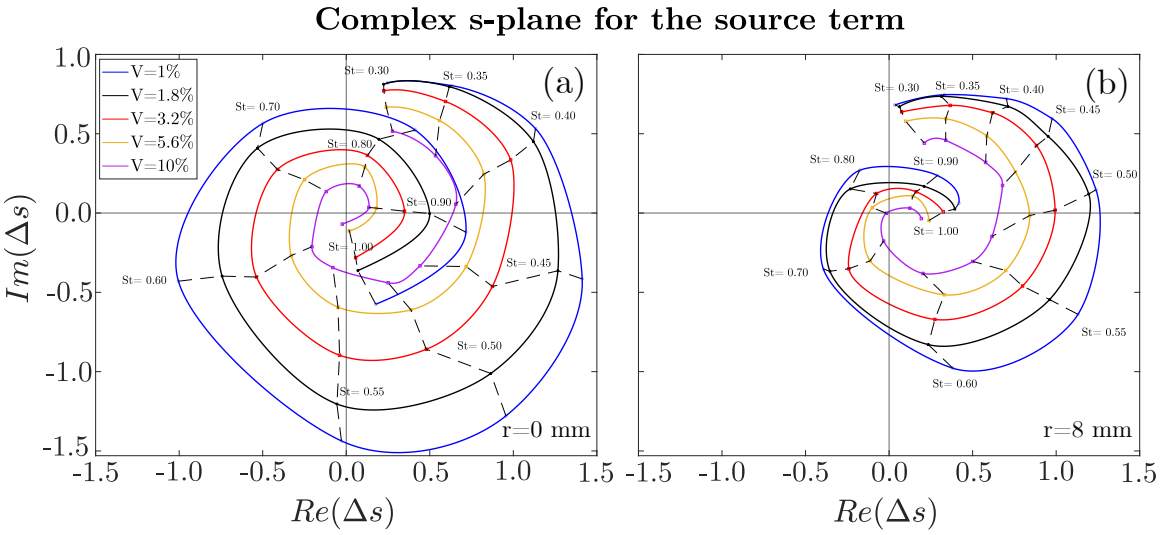

Figure 5.2: The aeroacoustic sound source maps for the sharp edge and r=8 mm configurations for the low and moderate excitation amplitudes.

evant applications.

Upon examining the aeroacoustic source term for the sharp edge case in comparison with the 8 mm rounded case, while keeping all other variables constant, a distinct difference in their amplitudes is observed, as depicted in Figure 5.2. Specifically, the source term in the rounded case exhibits a smaller amplitude for the same Strouhal number, defined as St=$\frac{f_{excitation}(d+2r)}{U}$, and normalized acoustic particle velocity compared to the sharp edge case. This observation echoes the findings reported when comparing the aeroacoustic source term for anechoic and open end terminations. The reduced amplitude and the condensed nature of the source map in these cases have led to heightened non-linearity in the excitation mechanism, which in turn correlates to abrupt variations in the simulated acoustic pressure pulsation in response to minor changes in the acoustic impedance of the branch. Another differential aspect between the two source maps is the specific Strouhal number at which the spiral intersects the positive real axis, which corresponds to the optimal Strouhal number where peak acoustic resonance occurs. For the rounded case, this happens at approximately

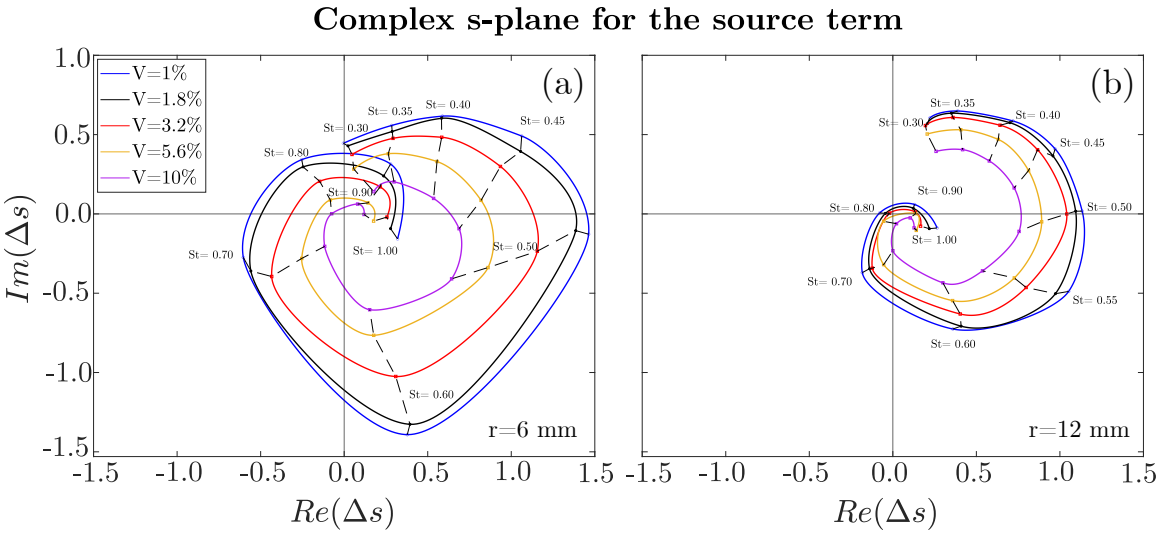

Figure 5.3: The aeroacoustic sound source maps for the 6 mm and 12 mm rounding configurations for the low and moderate excitation amplitudes.

St=0.5, whereas for the sharp edge case, it occurs around St=0.42 . This further illustrates the influence of the geometric attributes on the excitation and resonance behavior of the aeroacoustic system.

The disparities between the aeroacoustic sources of the sharp edge case and the rounded cases become more noticeable with an increase in the rounding radius. This is evidenced when comparing the source maps for the configurations with rounding radii of 6 mm and 12 mm. The source map associated with a larger rounding radius is more compact; however, the amplitudes are not uniformly smaller for all points with corresponding Strouhal numbers and normalized acoustic particle velocities. For instance, the amplitude of the spiral at V=1% is markedly smaller for the larger rounding radius compared to that with the smaller radius. Contrarily, the spiral at V=10% exhibits larger amplitudes for the larger rounding radius, indicating that a smaller acoustic impedance is required to excite the V=10% excitation level compared to the smaller rounding radius. These differences in the aeroacoustic sound source hint at potential disparities in the aeroacoustic response due to changes in the

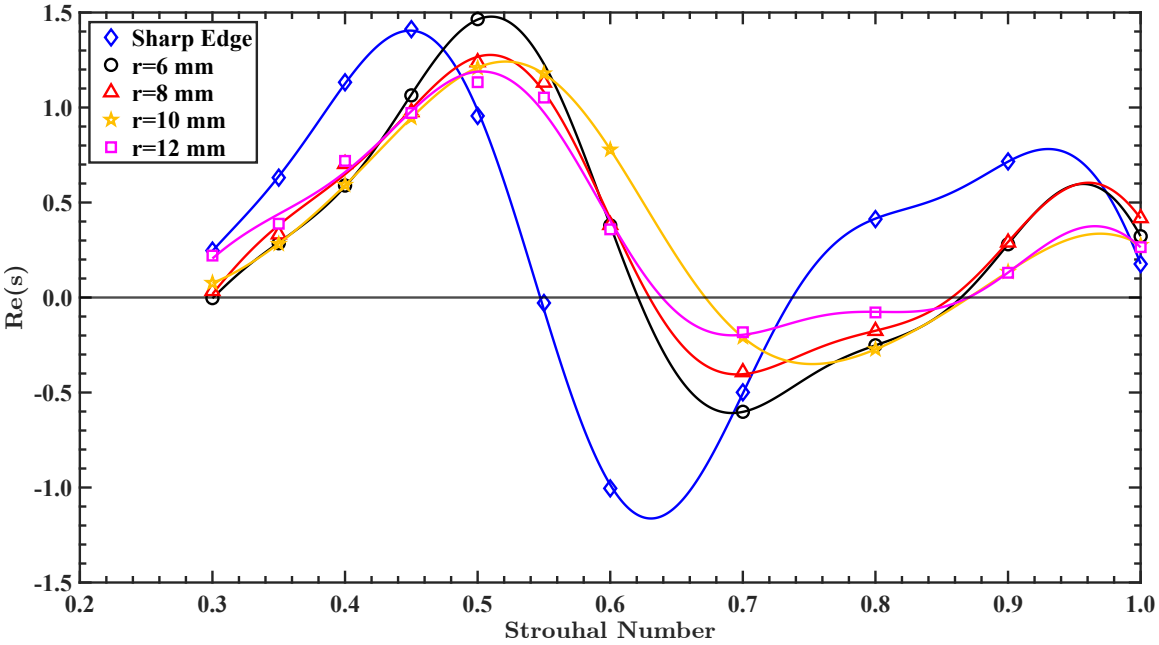

Figure 5.4: The real component of the aeroacoustic sound source for the sharp edge configuration and 6, 8, 10, and 12 mm rounding configurations at excitation level of 1%.

phasing between the fluctuating pressure difference across the shear layer and the acoustic particle velocity at the cavity mouth. Such variations bear implications on the amplitude of the pressure pulsation and the extent of the lock-in range.

The lock-in range of a given configuration is contingent upon two key elements. Firstly, the amplitude of the real component of the aeroacoustic sound source must coincide with the acoustic impedance of the cavity. Secondly, the Strouhal numbers with potential for excitation need to be considered, those being the ones where the real part of the sound source is positive.

When comparing sharp and rounded cases, as demonstrated in Figure 5.4, it is found that the real components for all rounding radii are shifted positively. This allows for a larger span of Strouhal numbers to exist within the positive range, thereby increasing the possibility of these Strouhal numbers being excited, given that the acoustic impedance of the cavity aligns with them. This suggests that the lock-in

range is broader for the rounded cases.

Moreover, as the rounding radius increases, the real amplitude becomes smaller, which highlights the compactness of the source. An additional observation is the potential for the second hydrodynamic excitation in the sharp case, which lies in the range of St=0.75-1, as the $Re(s)$ turns positive again. Conversely, for the rounded cases, this range is located at St=0.9-1, indicating that the second hydrodynamic mode could be excited at lower flow velocities, and that the flow will possess lower energy. Another factor that reduces the likelihood of exciting the second hydrodynamic mode is the diminished real amplitude of the aeroacoustic source term for the rounded configurations compared to the sharp cases.

5.1.2 Rounded Edges Model Validation

The computational methodology delineated in section 4.1.2 has been utilized to model the aeroacoustic response for each of the four considered rounded cases. These predictions are subsequently cross-validated against the self-excited experimental data, focusing on the coupling of the first hydrodynamic mode with the first and third acoustic modes. The model's predictions align well with the experimental aeroacoustic response, accurately capturing the lock-in range and peak acoustic pressure across all rounding radii. For conciseness, the validation of the r=10 mm configuration is presented in Figure 5.5.

The excitation of the second hydrodynamic mode is absent in both the aeroacoustic response and the model. This can be attributed to the large system impedance at corresponding flow velocities and the minimal amplitude of the aeroacoustic source term at Strouhal numbers related to the two-vortex mode excitation. To enable self-excitation of this second hydrodynamic mode, the system's impedance should be lowered to allow for more significant pressure pulsation excitations. This can be

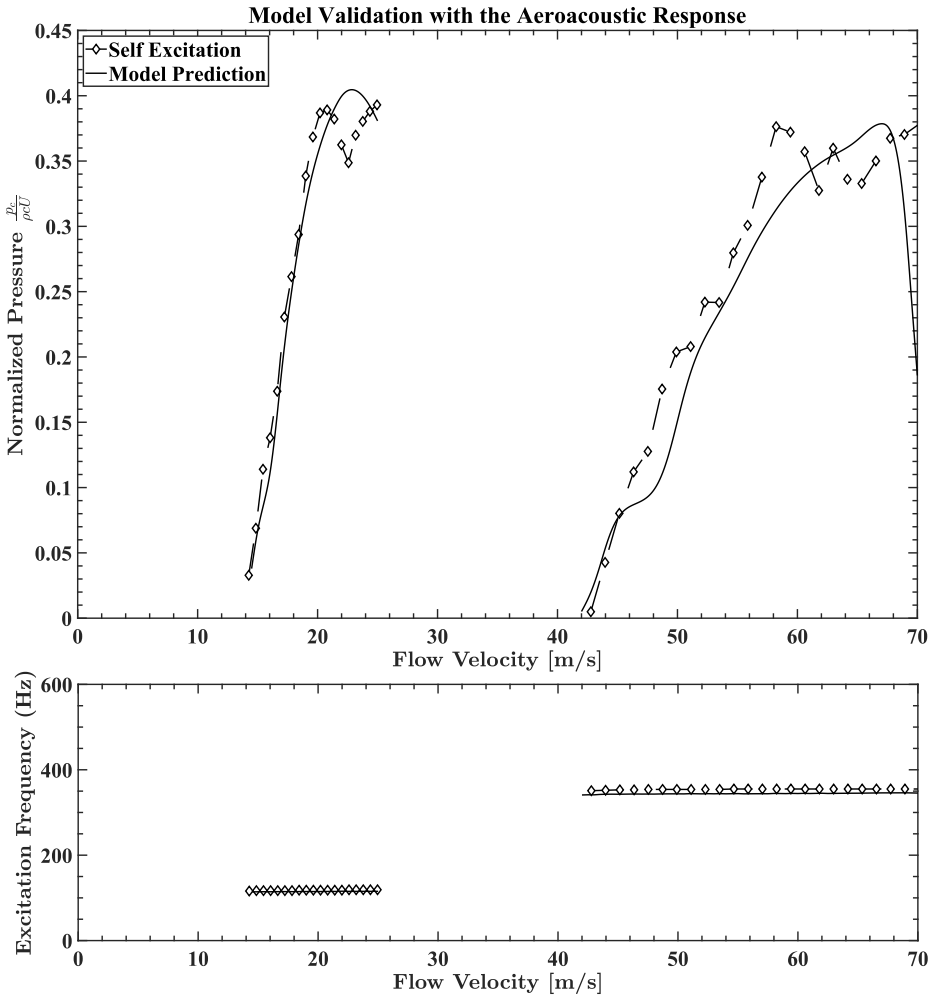

Figure 5.5: Validation results of the r = 10 mm configuration for the first hydrodynamic mode coincidence with the first and third acoustic modes of the co-axial cavity.

achieved by decreasing the absorption coefficient, either by enhancing the system's static pressure or by reducing the branch length. Diminishing the system's damping could also aid in the excitation of the second hydrodynamic mode.

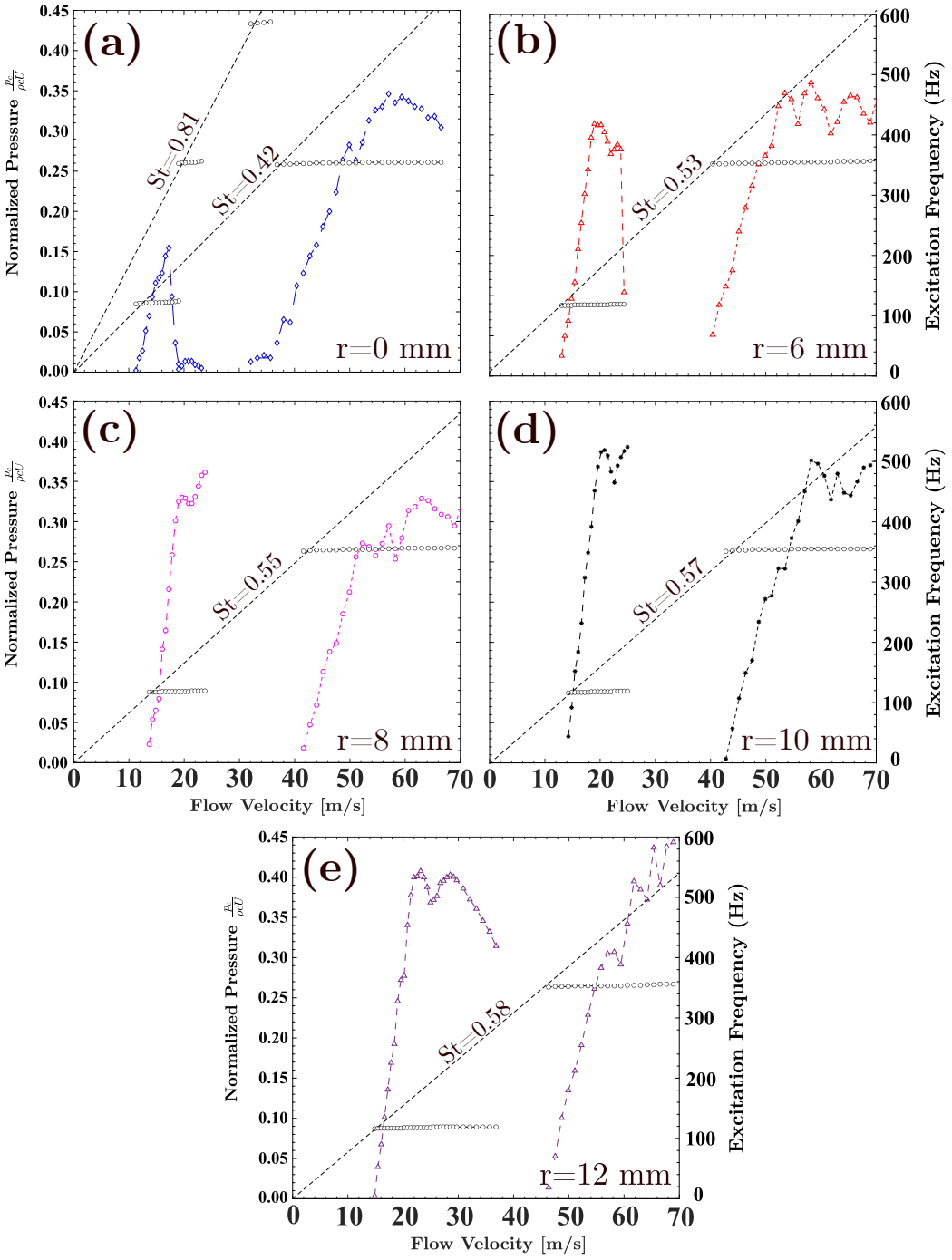

Figure 5.6: Aeroacoustic response of different edges rounding radii over a flow velocity range from 0 to $70 m/s$.

5.1.3 The Effect of Different Edge Rounding Radii on the Aeroacoustic Response

It is widely acknowledged that the aeroacoustic characteristics of cavities are susceptible to substantial alterations due to minor modifications in the geometry of the cavity. The incorporation of rounding at co-axial junctions, while occasionally mandated by manufacturing or welding requirements in industrial applications, is one factor that can prompt these modifications. Figure 5.6 visually presents the aeroacoustic response as a function of the mean flow velocity in the main pipe, represented on the x-axis, and is denoted by normalized acoustic pressure on the y-axis. This graphical representation includes the sharp-edge case as well as four additional cases with varying edge-rounding radii. The primary objective is to discern the impact of edge rounding on the interaction between the shear layer and the acoustic modes, as well as the degree of influence exerted by varying levels of rounding. In the case featuring sharp edges, the first hydrodynamic mode instigates the excitation of the first, and third acoustic modes, while the second hydrodynamic mode triggers the excitation of the third and fifth acoustic modes, with all excitations occurring at the point of frequency coincidence. Considering the first rounding ratio, it is apparent that the second hydrodynamic mode is completely suppressed. When examining the second round of the sound source spiral depicted in figure 5.3, which exhibits an imaginary component equal to zero (Im(s)=0) and a lesser positive real value, it can be inferred that this sound source spiral indicates that the second hydrodynamic mode could only be excited in a system characterized by low impedance, minimal damping, and a diminutive attenuation constant. This condition can be attained by either amplifying the system's static pressure or by curtailing the system's damping, as discussed earlier. Furthermore, the peak of the acoustic pressure during the excitation of the

first mode is doubled and displays a broader range of flow velocities compared to the sharp edge case. This can be attributed to the prolongation of impingement and intensification of vortex formation and coherence resulting from rounding. As the degree of rounding augments, a simultaneous increase in both the peak pressure and the lock-in range is observed. The amplified vortex formation, a direct consequence of rounding intensification, significantly influences the acoustic properties, leading to an escalation in peak pressure and expansion of the lock-in range. The peak acoustic pressure during the excitation of the third mode is marginally higher and possesses a broader lock-in range compared to the first mode excitation for all cases. This can be attributed to the reduced damping and wall vibrations, as it represents a higher resonant frequency and it locks in at an increased flow velocity, where inherently greater flow energy is present.

5.2 Features of the Aeroacoustic Sound Source for Co-axial Cavities with Chamfered Edges

The presence of chamfered edges, as a typical transitional geometry in industrial pipelines, makes the study of sound sources within such configurations pivotal for aiding the design process in mitigating acoustic resonance within industrial environments. A noteworthy research work conducted by Xiao et al. (2021) [73] scrutinized the influence of chamfer on a single side branch, contrasting it with the effect of rounding for a chamfer to diameter ratio of $c/d = 0.22$. Their investigation found that the excitation process was largely indifferent to chamfer when compared to the configuration with sharp edges, while the rounding significantly amplified the pulsation pressure.

In this section, this line of inquiry is extended by examining the impact of chamfers

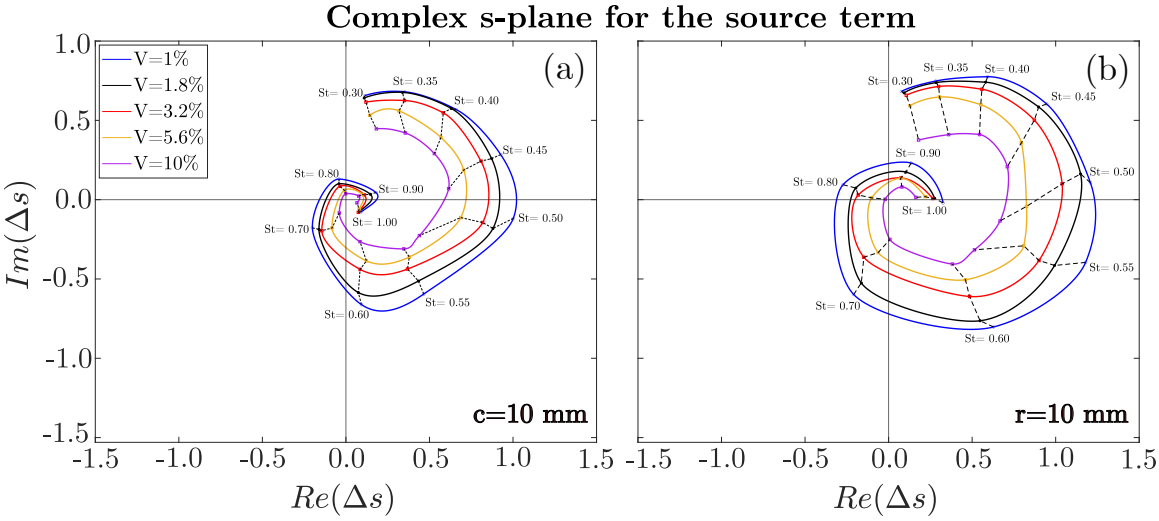

Figure 5.7: The aeroacoustic sound source maps for the 10 mm rounding and chamfer configurations for the low and moderate excitation amplitudes.

on the aeroacoustic sound source, comparing it to the edge rounding configuration. This is followed by a validation of the predicted aeroacoustic response against a set of experimental data to ensure the reliability and applicability of the findings. Subsequently, the aeroacoustic responses associated with different chamfers are presented, informed by an investigation of the aeroacoustic source term and its implications. This comprehensive analysis will not only shed light on the interplay between geometrical modifications and the aeroacoustic response but also provide meaningful insights that can be applied to optimize industrial pipeline designs to better avoid acoustic resonance.

5.2.1 The Effect of Different Edge Chamfers on the Aeroacoustic Sound Source

Upon comparing the aeroacoustic source term for the 10 mm rounding and the 10 mm chamfered configurations, as illustrated in Figure 5.7, a noticeable disparity in the magnitude of the source term for the two cases is found. Specifically, the source

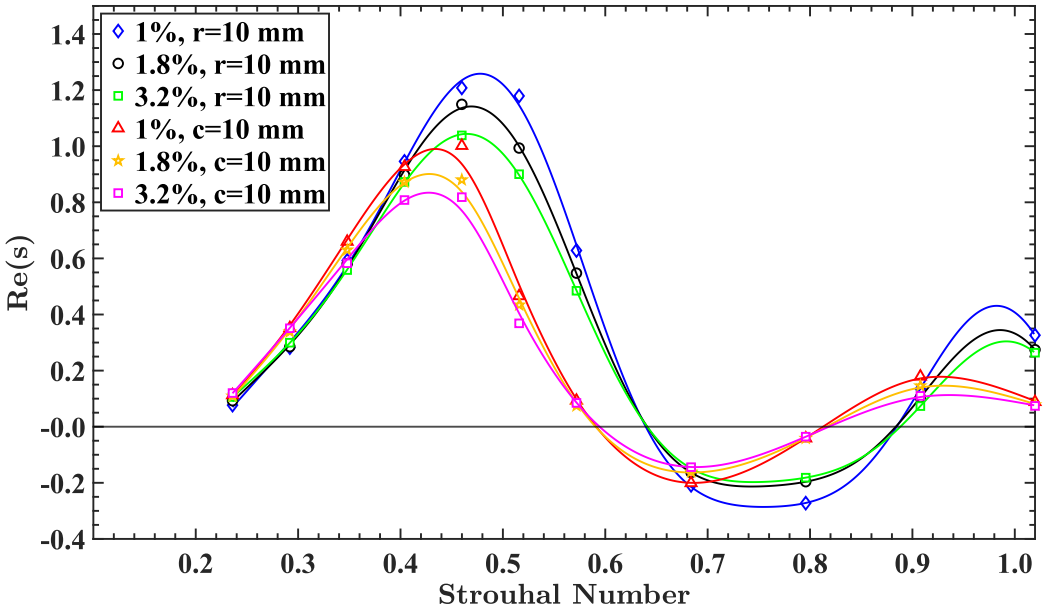

Figure 5.8: The real component of the aeroacoustic sound source for the 10 mm rounding and 10 mm chamfer configurations at excitation levels of 1%, 1.8%, and 3.2%.

term magnitude for the chamfered case is considerably lower than that of the rounded case across all Strouhal numbers and excitation levels.

As previously noted, this reduction in magnitude renders the system less vulnerable to large pressure pulsations. This is because it necessitates a smaller acoustic impedance for the system to prompt significant pulsation levels. Consequently, a smaller source term magnitude implies enhanced system stability, translating into diminished pressure pulsations.

A noteworthy similarity between the two configurations is that their source term magnitudes are both smaller than that of the sharp-edge case. Moreover, the magnitude of the source term for the second round of the sound source spiral in both the chamfered and rounded configurations is markedly lower than in the sharp-edge configuration. This observation substantiates the predicted suppression of the second hydrodynamic mode excitation in these cases.

When the active component of the aeroacoustic sound source (represented by the real component $Re(s)$) between the chamfered and rounded cases is compared, as illustrated in Figure 5.8, it is noticed that the real component of the chamfered edge is smaller across the three excitation levels presented. In addition, the peak amplitude for the real component of the chamfered case occurs at a lower Strouhal number when compared with the rounded cases. This implies that the peak excitation pressure for the chamfered case would occur at a slightly higher flow velocity.

However, a lesser range of Strouhal numbers exists within the positive domain for the chamfered case when compared with the rounded cases. This can be interpreted as a suggestion that the lock-in range for the chamfered cases would be narrower since the potential range of excitable Strouhal numbers is diminished.

Furthermore, the magnitude of the source term for the second positive range (i.e., for St=0.82-1) for the chamfered case is significantly smaller than that of the rounded cases. This indicates that the excitation of the second hydrodynamic mode is more challenging for the chamfered edges in comparison with the rounded edges.

Despite these differences, it is important to note that under the current setup, neither the rounded nor chamfered edges self-excited this mode, as discussed in the subsequent subsection. This observation holds true when the system operates under typical conditions, which inherently suggests a high absorption coefficient. These insights are invaluable in understanding the implications of edge modifications on the aeroacoustic response and can provide key design insights for industrial pipelines where acoustic resonance is a critical factor.

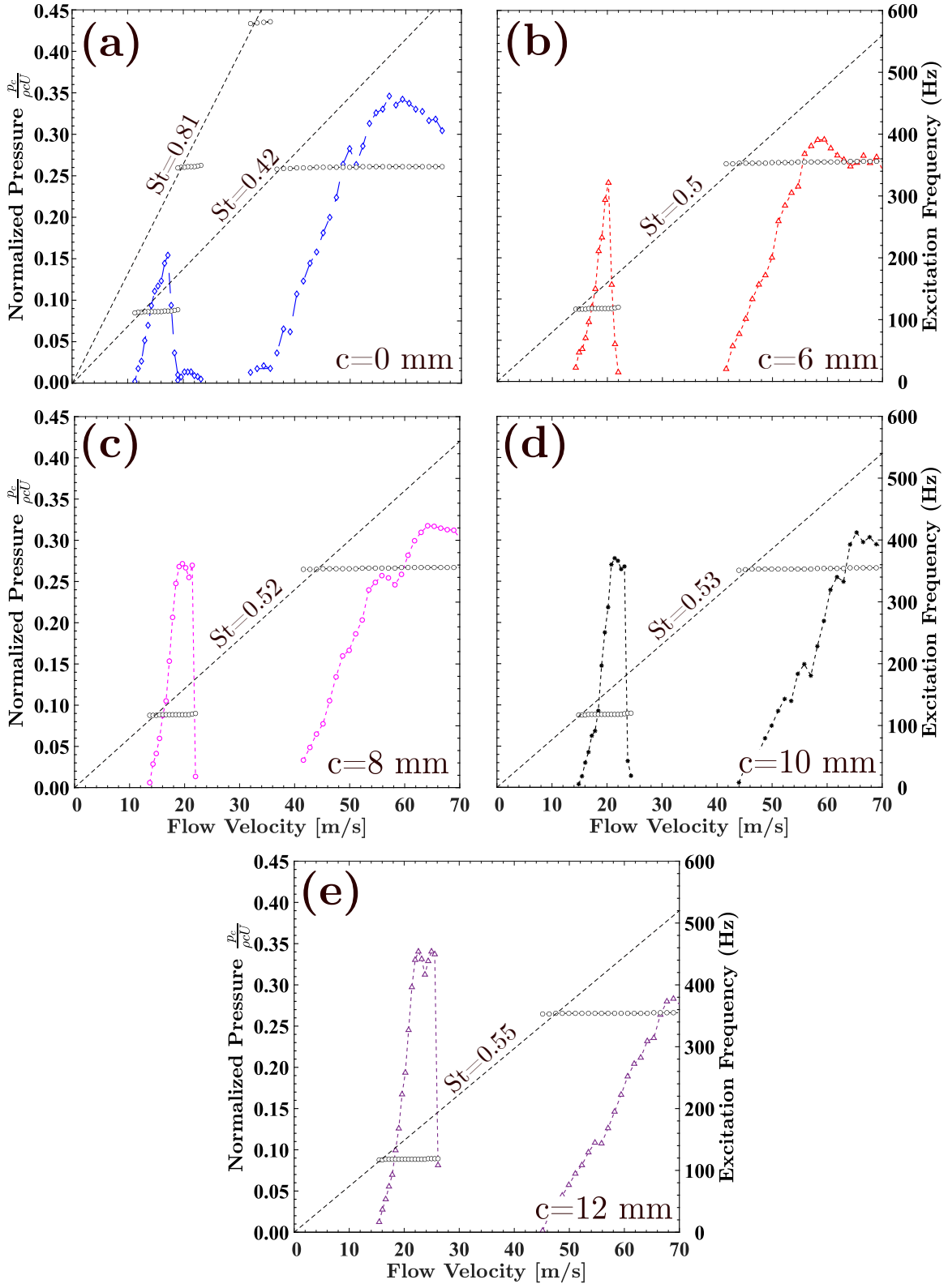

Figure 5.9: Aeroacoustic response of different edges chamfers over a flow velocity range from 0 to 70m/s.

5.2.2 The Effect of Different Edge Chamfers on the Aeroacoustic Response

Chamfering is frequently employed as a geometric alteration to junction edges due to its practical advantages in manufacturing and design. In this study, various chamferings have been applied to investigate their impacts on the aeroacoustic response of the system. As delineated in Figure 5.9, chamfering mirrors the effects of edge rounding in terms of suppressing the second hydrodynamic mode and significantly amplifying the peak pressure of the first acoustic mode. Yet, there is a noticeable difference in the lock-in range for the first and third acoustic modes, with the rounding cases demonstrating a significantly wider range compared to their chamfered counterparts. This phenomenon is attributed to the well-defined separation point in the chamfered cases, which renders the hydrodynamic wavelength of the shear layer constant, and thus unable to modulate adaptively with the acoustic field during resonance. Conversely, for the rounded edges, the absence of a definitive separation point allows the shear layer to separate at various points, tuning the hydrodynamic wavelength to create favourable phasing with the acoustic field. This synchronization facilitates a broader lock-in range for the shear layer frequency with the acoustic field across a wider span of flow velocities. Upon comparing chamfered and rounded edge cases with their sharp-edged counterpart, the latter exhibits a narrower lock-in range and significantly lower peak acoustic pressure under resonant conditions. This is ascribed to the influence of edge modifications, rounding or chamfering, on the shear layer's trajectory. By promoting a smoother path transition for the shear layer, these modifications mitigate abrupt changes in velocity gradients, thereby reducing shear stress at the interface. Such junction-edge modifications minimize turbulence and potentially resulting in a reduced shear layer thickness. Collectively, these alterations foster

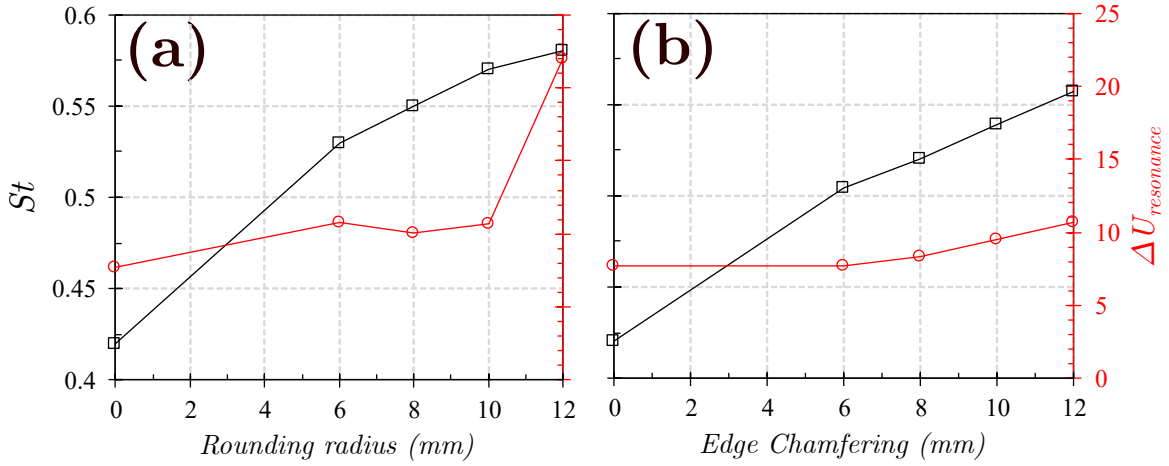

Figure 5.10: The Strouhal number and first acoustic mode lock-in range trend for (a) Different edges rounding radii; (b) Different edges chamfering

enhanced vortex coherence and correlation during resonance, subsequently leading to higher acoustic pressures under resonant conditions.

Figure 5.10 presents a comparative analysis of the critical Strouhal number for the first hydrodynamic mode and the lock-in velocity range for both edge rounding and chamfering modifications. The introduction of rounding or chamfering to the edge prompts a sharp increase in the critical Strouhal number, leaping from a value of 0.42 to 0.53 and 0.5 for the initial rounding and chamfering cases, respectively. This precipitous rise is ascribed to the alteration in impingement length resulting from the edge modification. As the degree of chamfering or rounding amplifies, the Strouhal number demonstrates a linearly increasing trend. It's crucial to highlight that the critical Strouhal number is determined by the slope of a line that intersects the starting point of the lock-in range. This point has been selected because it defines the Strouhal number that corresponds to the onset of resonance, a critical parameter to ascertain from an industrial perspective where it is vital to predict the flow velocity at which resonant conditions may occur. The lock-in range also displays an increasing trend commensurate with the augmentation of chamfering and rounding. However,

a noteworthy leap in the lock-in range is evident for the case with a rounding radius of 12mm. This observation elucidates a significant alteration in the behaviour of the shear layer at this specific rounding radius, leading to the manifestation of a hydrodynamic wavelength that has favourable phasing with the acoustic pressure cycle.

In this chapter, the impact of edge geometry on the aeroacoustic sound source and response within coaxial cavities has been extensively investigated. Through the experimental study, it has been verified that modifications to the junction edge rounding radii and chamfers significantly affect the shear layer's phasing with the acoustic field, which in turn affects the aeroacoustic sound source. These changes have been tested by focusing on four different rounding radii and four different edge chamfers.

The results show that edge rounding directly influences the excitation and resonance behavior of the aeroacoustic system. It is found that the source term in the rounded case exhibits a smaller amplitude for the same Strouhal number compared to the sharp edge case. Furthermore, disparities between the aeroacoustic sources of the sharp edge case and the rounded cases become more noticeable with an increase in the rounding radius.

The computational methodology, designed to predict the aeroacoustic response for each of the four considered rounded cases, aligns well with the self-excited experimental data. it is observed that an expansion in the lock-in range with larger rounding radii, demonstrating the substantial impact of edge rounding on the aeroacoustic response.

Moreover, it is found that the extent of rounding directly affects the peak pressure and lock-in range. As the rounding radius increases, an increase in both these parameters is observed. The amplification of vortex strength due to rounding significantly influences the coupling with the acoustic field, leading to heightened peak pressure

and an expanded lock-in range.

Then, the study extended the analysis of chamfered edges and their influence on aeroacoustic sound sources in comparison to rounded edges. It was observed that the magnitude of the aeroacoustic source term in chamfered configurations was significantly lower than in rounded cases, implying a greater system stability and reduced pressure pulsations. However, both configurations presented smaller source term magnitudes than sharp-edge configurations for the second round of the sound source spiral, indicating similar behaviour of suppressing the second hydrodynamic mode excitation, which is more pronounced in the chamfered cases.

Upon examining the real component of the aeroacoustic sound source, it was found that the chamfered case had a smaller real component across all excitation levels. The peak amplitude for the chamfered case occurred at a lower Strouhal number, implying higher flow velocity for peak excitation pressure. Moreover, the potential range of excitable Strouhal numbers was narrower in the chamfered case. These suggestions were confirmed by the self-excited data for the chamfered configurations.

When comparing the aeroacoustic response of the chamfered and rounded cases, chamfered cases exhibited a noticeably narrower lock-in range for the first and third acoustic modes compared to rounded ones. The well-defined separation point in the chamfered cases caused the hydrodynamic wavelength of the shear layer to remain constant, limiting its ability to adaptively modulate with the acoustic field during resonance. This contrasted with rounded edges, where the absence of a definitive separation point enabled a broader lock-in range and higher acoustic pressures under resonant conditions due to improved vortex coherence. Comparative analysis of critical Strouhal numbers for the first hydrodynamic mode and lock-in velocity range for edge rounding and chamfering modifications indicated a linear increase in the Strouhal number with increasing chamfering or rounding. This is important in

industrial settings for predicting the onset of resonant conditions.

Chapter 6

Conclusions and Future Work

6.1 Summary and conclusions

In conclusion, this comprehensive study sheds light on the nuanced influence of acoustic terminations, the configuration of upstream pipes, and edge geometry on the aeroacoustic behavior within coaxial cavities.

The current study shows that the acoustic terminations of main pipes may not drastically impact the acoustic modes within coaxial cavities, however, end conditions significantly influence the aeroacoustic response and the aeroacoustic sound source. The insertion of a muffler, mimicking an open-end condition, notably altered key variables such as the maximum normalized pressure pulsation, the critical Strouhal number initiating the aeroacoustic resonance, and the lock-in range. These findings highlight the need to consider the impact of end conditions during design processes, despite the fact that these alterations do not strictly function as a suppression technique.

Moreover, the study underscored that variations in the downstream acoustic boundary conditions considerably impact the acoustic field within the pipeline and the

aeroacoustic sound source. The open-open configuration, in comparison to the open-anechoic one, revealed a decrease in nonlinearity and pressure pulsations.

This study elaborates on the impact of varying upstream distances on the aeroacoustic resonance of a coaxial side branch. It is evident that an extension of upstream distance prompts the velocity distribution to progressively resemble fully developed turbulent flow. Varying the upstream distance influences the complex sound source term with noticeable differences between configurations. The research confirms that the non-developed flow configuration exhibits a distinct self-excitation mechanism for the aeroacoustic resonance in deep coaxial cavities. Reducing the upstream distance below the threshold for fully developed flow results in decreased peak acoustic pressure and critical Strouhal number. Notably, the fully developed flow configurations exhibited identical acoustic responses. These findings present critical insights into the behavior of pipeline systems under different upstream distance variations.

This study also undertook an in-depth examination of the effects of modifying the junction edge rounding radii and chamfers on the aeroacoustic sound source and response within coaxial cavities. It was ascertained that these alterations considerably impact the shear layer's phasing with the acoustic field. The study revealed that edge rounding directly modifies the excitation and resonance behavior of the aeroacoustic system, with the source term in the rounded case showing a more compact spirals for the same excitation levels than in the sharp edge case.

The study also demonstrated the significant influence of edge rounding on the aeroacoustic response and established that the extent of rounding directly affects the peak pressure and lock-in range. Furthermore, the investigation analyzed the effects of chamfered edges, revealing that the magnitude of the aeroacoustic source term in chamfered configurations was markedly lower than in rounded cases. These observations are revealed in the aeroacoustic response as lower peak pressure pulsations and

smaller lock-in range when compared to the rounded cases.

Overall, this thorough investigation, driven by meticulous experiments and predictive modeling, has generated crucial insights into the aeroacoustic behavior within coaxial cavities. The findings have profound implications for the design of industrial applications where control and mitigation of aeroacoustic resonance is crucial, and contribute to the understanding of the mechanisms underlying the aeroacoustic sound source and response.

6.2 Major contributions

The research presented in this thesis extended the knowledge in the literature in the field of modeling the aeroacoustic coupling and the flow excited acoustic resonance by making the following contributions:

1. Pioneered an advanced version of the sound source method, tailor-made for industry applications, capable of forecasting the onset of acoustic resonance and predicting pulsation amplitudes across diverse cavity geometries.

2. Demonstrated that the acoustic termination and the velocity profiles of the main pipe influences the aeroacoustic response, even in acoustically trapped modes such as co-axial cavities.

3. Established that edge modifications (rounding and chamfering) of the co-axial cavity amplify the flow-excited acoustic resonance and expand the lock-in range, with rounding exerting a more pronounced effect.

6.3 Future Work

This study has significantly broadened the understanding of flow-excited acoustic resonance, the interplay between flow and acoustic fields, and the vital role of phasing between the oscillations of the shear layer and the acoustic particle velocity. Moreover, the research expanded the sound source modeling technique, elucidating the impact of various geometrical modifications on the aeroacoustic sound source. This study will provide a solid foundation for future research aimed at enhancing the comprehension of flow-sound interactions in the following aspects:

1. Further investigations are required on the acoustic boundary conditions of the main pipe using controlled radiation boundaries. This is critical in order to better assess their impact on the aeroacoustic sound source term. A comprehensive understanding of these effects will contribute to more precise predictive models and effective design strategies for mitigating unwanted aeroacoustic responses.

2. It's crucial to investigate the impact of diameter ratio on the aeroacoustic sound source of various configurations such as single, tandem, and co-axial deep side branches. This research needs to be combined with the findings presented in this study to form a comprehensive design methodology. This methodology will enable us to predict the aeroacoustic response considering various parameters, including different cavity configurations, edge modifications, upstream velocity distributions, and acoustic boundary conditions of the main pipe. This inclusive approach will allow for a more thorough understanding of the aeroacoustic behavior of these systems and inform more effective mitigation strategies.

3. The sound source model could be extended to include a wider variety of cavities and systems that are acoustically vulnerable due to shear layer excitations. The

goal is to create a non-dimensional source map that could be utilized in modeling aeroacoustic responses. This will provide the basis for strategies to avoid such responses during operation.

Bibliography

[1] Abdelmwgoud, M., and Mohany, A. Control of the self-sustained shear layer oscillations over rectangular cavities using high-frequency vortex generators. *Physics of Fluids 33*, 4 (04 2021), 045115.

[2] Aly, K., and Ziada, S. Flow-excited resonance of trapped modes of ducted shallow cavities. *Journal of Fluids and Structures 26*, 1 (2010), 92–120.

[3] Alziadeh, M., and Mohany, A. Passive noise control technique for suppressing acoustic resonance excitation of spirally finned cylinders in cross-flow. *Experimental Thermal and Fluid Science 102* (2019), 38–51.

[4] Alziadeh, M., and Mohany, A. Vorticity shedding and acoustic resonance excitation of two tandem spirally finned cylinders in cross-flow. *Journal of Pressure Vessel Technology 143(2)* (2021), 021405.

[5] Alziadeh, M., and Mohany, A. Flow structure and aerodynamic forces of finned cylinders during flow-induced acoustic resonance. *Journal of Fluids and Structures 119* (2023), 103887.

[6] Arafa, N., and Mohany, A. Aeroacoustic response of a single cylinder with straight circular fins in cross-flow. *Journal of Pressure Vessel Technology 137(5)* (2015), 051301.

[7] Arafa, N., Tariq, A., Mohany, A., and Hassan, M. Effect of cylinder location inside a rectangular duct on the excitation mechanism of acoustic resonance. *Canadian Acoustics 42*, 1 (Mar. 2014), 33–40.

[8] Blevins, R., and Bressler, M. Experiments on acoustic resonance in heat exchanger tube bundles. *Journal of Sound and Vibration 164* (1993), 503–533.

[9] Blevins, R. D. The effect of sound on vortex shedding from cylinders. *Journal of Fluid Mechanics 161* (1985), 217–237.

[10] Bruggeman, J., Hirschberg, A., van Dongen, M., Wijnands, A., and Gorter, J. Self-sustained aero-acoustic pulsations in gas transport systems: Experimental study of the influence of closed side branches. *Journal of Sound and Vibration 150*, 3 (1991), 371–393.

[11] Bruggeman, J. C., van Dongen, M. E. H., Wijnands, A. P. J., Gorter, J., and Hirschberg, A. Flow induced pulsations in gas transport systems: Analysis of the influence of closed side branches, 1989.

[12] Chorin, A. J., and Bernard, P. S. Discretization of a vortex sheet, with an example of roll-up. *Journal of Computational Physics 13*, 3 (1973), 423–429.

[13] Coltman, J. W. Sounding Mechanism of the Flute and Organ Pipe. *The Journal of the Acoustical Society of America 44*, 4 (07 2005), 983–992.

[14] Davies, P. Flow-acoustic coupling in ducts. *Journal of Sound and Vibration 77*, 2 (1981), 191–209.

[15] Davies, P. Plane wave reflection at flow intakes. *Journal of Sound and Vibration 115*, 3 (1987), 560–564.

[16] Davies, P. Practical flow duct acoustics. *Journal of Sound and Vibration 124*, 1 (1988), 91–115.

[17] Davies, P., Bhattacharya, M., and Coelho, J. L. B. Measurement of plane wave acoustic fields in flow ducts. *Journal of Sound and Vibration 72* (1980), 539–542.

[18] Demetz, F., and Farabee, T. *Laminar and turbulent shear flow-induced cavity resonances.*

[19] Dequand, S., Hulshoff, S., and Hirschberg, A. Self-sustained oscillations in a closed side branch system. *Journal of Sound and Vibration 265*, 2 (2003), 359–386.

[20] Doherty, J., Ngan, P., Monty, J., and Chong, M. The development of turbulent pipe flow. In *16th Australasian Fluid Mechanics Conference (AFMC)* (2007).

[21] Duan, Y., Koch, W., Linton, C. M., and McIver, M. Complex resonances and trapped modes in ducted domains. *Journal of Fluid Mechanics 571* (2007), 119–147.

[22] Elder, S. A. The mechanism of sound production in organ pipes and cavity resonators. *Journal of the Acoustical Society of Japan (E) 13*, 1 (1992), 11–23.

[23] Föller, S., Polifke, W., and Tonon, D. *Aeroacoustic Characterization of T-Junctions Based on Large Eddy Simulation and System Identification.*

[24] Gaster, M. A note on the relation between temporally-increasing and spatially-increasing disturbances in hydrodynamic stability. *Journal of Fluid Mechanics 14*, 2 (1962), 222–224.

[25] Geveci, M., Oshkai, P., Rockwell, D., Lin, J.-C., and Pollack, M. Imaging of the self-excited oscillation of flow past a cavity during generation of a flow tone. *Journal of Fluids and Structures 18*, 6 (2003), 665–694. Flow-Acoustic Interactions.

[26] Gloerfelt, X., Bailly, C., and Juvé, D. Direct computation of the noise radiated by a subsonic cavity flow and application of integral methods. *Journal of Sound and Vibration 266*, 1 (2003), 119–146.

[27] Graf, H. R., and Ziada, S. Excitation source of a side-branch shear layer. *Journal of Sound and Vibration 329* (7 2010), 2825–2842.

[28] Hanna, M., and Mohany, A. Aeroacoustics and shear layer characteristics of confined cavities subject to low mach number flow. *Journal of Fluids and Structures 121* (2023), 103949.

[29] Hourigan, K., Welsh, M., Thompson, M., and Stokes, A. Aerodynamic sources of acoustic resonance in a duct with baffles. *Journal of Fluids and Structures 4*, 4 (1990), 345–370.

[30] Howe, M. The dissipation of sound at an edge. *Journal of Sound and Vibration 70*, 3 (1980), 407–411.

[31] Howe, M. S. Contributions to the theory of aerodynamic sound, with application to excess jet noise and the theory of the flute. *Journal of Fluid Mechanics 71*, 4 (1975), 625–673.

[32] Karlsson, M., and Åbom, M. Aeroacoustics of t-junctions—an experimental investigation. *Journal of Sound and Vibration 329*, 10 (2010), 1793–1808.

[33] Kergomard, J., Debut, V., and Matignon, D. Resonance modes in a one-dimensional medium with two purely resistive boundaries: Calculation methods, orthogonality, and completeness. *The Journal of the Acoustical Society of America 119*, 3 (03 2006), 1356–1367.

[34] Kooijman, G., Hirschberg, A., and Golliard, J. Acoustical response of orifices under grazing flow: Effect of boundary layer profile and edge geometry. *Journal of Sound and Vibration 315*, 4 (2008), 849–874.

[35] Kook, H., and Mongeau, L. Analysis of the periodic pressure fluctuations induced by flow over a cavity. *Journal of Sound and Vibration 251*, 5 (2002), 823–846.

[36] Krasny, R. A study of singularity formation in a vortex sheet by the point-vortex approximation. *Journal of Fluid Mechanics 167* (1986), 65–93.

[37] Lafon, P., Caillaud, S., Devos, J., and Lambert, C. Aeroacoustical coupling in a ducted shallow cavity and fluid/structure effects on a steam line. *Journal of Fluids and Structures 18*, 6 (2003), 695–713. Flow-Acoustic Interactions.

[38] Lucas, M. *Handbook of the Acoustic Characteristics of Turbomachinery Cavities*. ASME Press, 1997.

[39] Lympany, S. V., and Ahuja, K. K. Methodology for measuring higher-order acoustic modes in uniform heated flows. *AIAA Journal 58*, 9 (2020), 3978–3986.

[40] Martínez-Lera, P., Schram, C., Föller, S., Kaess, R., and Polifke, W. Identification of the aeroacoustic response of a low Mach number flow through a T-joint. *The Journal of the Acoustical Society of America 126*, 2 (08 2009), 582–586.

[41] Michalke, A. On spatially growing disturbances in an inviscid shear layer. *Journal of Fluid Mechanics 23*, 3 (1965), 521–544.

[42] Miksad, R. W. Experiments on the nonlinear stages of free-shear-layer transition. *Journal of Fluid Mechanics 56*, 4 (1972), 695–719.

[43] Mohamed, S., and Eng, B. Sound waves excitation by flow in a pipe housing a shallow cavity, 2015.

[44] Mohamed, S., Graf, H. R., and Ziada, S. Measurement of the Excitation Source of an Axisymmetric Shallow Cavity Shear Layer. *Journal of Pressure Vessel Technology 140*, 3 (04 2018), 031304.

[45] Mohany, A. *Flow-sound interaction mechanisms of a single and two tandem cylinders in cross-flow.* PhD thesis, Mc-Master University, 2007.

[46] Mohany, A., Alziadeh, M., and Hassan, M. Vorticity Shedding and Acoustic Resonance Excitation of a Square Tube Array: Effect of Flow Approach Angle. *Journal of Pressure Vessel Technology 145*, 1 (08 2022), 011401.

[47] Mohany, A., and Ziada, S. Flow-excited acoustic resonance of two tandem cylinders in cross-flow. *Journal of Fluids and Structures 21*, 1 (2005), 103–119.

[48] Monkewitz, P. A., and Huerre, P. Influence of the velocity ratio on the spatial instability of mixing layers. *The Physics of Fluids 25*, 7 (07 1982), 1137–1143.

[49] Morita, R., Takahashi, S., Okuyama, K., Inada, F., Ogawa, Y., and Yoshikawa, K. Evaluation of acoustic- and flow-induced vibration of the bwr main steam lines and dryer. *Journal of Nuclear Science and Technology 48* (5 2011), 759–776.

[50] Morse, P., and Ingard, K. *Theoretical Acoustics*. International series in pure and applied physics. McGraw-Hill, 1968.

[51] Munjal, M. L. *Acoustics of Ducts and Mufflers with Application to Exhaust and Ventilation System Design*. John Wiley & Sons, 1987.

[52] Nelson, P., Halliwell, N., and Doak, P. Fluid dynamics of a flow excited resonance, part i: Experiment. *Journal of Sound and Vibration 78*, 1 (1981), 15–38.

[53] Nelson, P., Halliwell, N., and Doak, P. Fluid dynamics of a flow excited resonance, part ii: Flow acoustic interaction. *Journal of Sound and Vibration 91*, 3 (1983), 375–402.

[54] NRC. Additional flow-induced vibration failures after a recent power uprate. Tech. rep., NRC Information Notice 2002-26, Supplement 2, January 9, 2004, US Nuclear Regulatory Commission, Washington, D.C., United States.

[55] Omer, A., Arafa, N., Mohany, A., and Hassan, M. The effect of upstream edge geometry on the acoustic resonance excitation in shallow rectangular cavities. *International Journal of Aeroacoustics 15*, 3 (2016), 253–275.

[56] Omer, A., Mohany, A., and Hassan, M. Effect of impingement edge geometry on the acoustic resonance excitation and strouhal numbers in a ducted shallow cavity. *Wind and Structures 23* (01 2016), 91–107.

[57] Oshkai, P., and Yan, T. Experimental investigation of coaxial side branch resonators. *Journal of Fluids and Structures 24* (2008), 589–603.

[58] Powell, A. On the Edgetone. *The Journal of the Acoustical Society of America 33*, 4 (07 2005), 395–409.

[59] Radavich, P. M., Selamet, A., and Novak, J. M. A computational approach for flow–acoustic coupling in closed side branches. *The Journal of the Acoustical Society of America 109*, 4 (04 2001), 1343–1353.

[60] Rashwan, S., Mohany, A., and Dincer, I. Investigation of self-induced thermoacoustic instabilities in gas turbine combustors. *Energy 190* (2020), 116362.

[61] Rayleigh, L. On the Stability, or Instability, of certain Fluid Motions. *Proceedings of the London Mathematical Society s1-11*, 1 (11 1879), 57–72.

[62] Rockwell, D. Oscillations of impinging shear layers. *AIAA Journal 21*, 5 (1983), 645–664.

[63] Rockwell, D., and Knisely, C. The organized nature of flow impingement upon a corner. *Journal of Fluid Mechanics 93*, 3 (1979), 413–432.

[64] Rockwell, D., Lin, J.-C., Oshkai, P., Reiss, M., and Pollack, M. Shallow cavity flow tone experiments: onset of locked-on states. *Journal of Fluids and Structures 17*, 3 (2003), 381–414.

[65] Rockwell, D., and Naudascher, E. Review—Self-Sustaining Oscillations of Flow Past Cavities. *Journal of Fluids Engineering 100*, 2 (06 1978), 152–165.

[66] Sadek, O., Shaaban, M., and Mohany, A. Suppression of acoustic resonance in piping system using passive control devices. *Canadian Acoustics - Acoustique Canadienne 42(3)* (2014), 58–59.

[67] Shaaban, M., Abdelmwgoud, M., Arafa, N., Sachedina, K., Mohany, A., and Hassan, M. Measurement of acoustic admittance of piping systems at different flow velocities.

[68] Shabaan, M., and Mohany, A. A. passive control of flow-excited acoustic resonance in rectangular cavities using upstream mounted blocks. *Exp Fluids 56*, 72 (2015).

[69] Shoukry, A., and Mohany, A. Direct measurements of the dynamic lift force acting on rectangular rods in cross-flow during acoustic resonance excitation. In *Proceedings of the 12th International Conference on Flow-Induced Vibration* (07 2022), C. Habchi and P. Moussou, Eds., p. 255–261. ISBN: 979-10-699-9682-3.

[70] Stoltenkamp, P. W., Bergervoet, J. T., Willems, J. F., van Uittert, F. M., and Hirschberg, A. Response of turbine flow meters to acoustic perturbations. *Journal of Sound and Vibration 315* (8 2008), 258–278.

[71] Tonon, D., Hirschberg, A., Golliard, J., and Ziada, S. Aeroacoustics of pipe systems with closed branches. *International Journal of Aeroacoustics 10* (6 2011), 201–275.

[72] White, F. *Viscous Fluid Flow.* McGraw-Hill series in mechanical engineering. McGraw-Hill, 1991.

[73] Xiao, Y., Zhang, W., Li, J., Gao, X., Huang, C., and Gu, H. Effects of edge geometry on the flow-induced acoustic resonances in closed side branches. *Annals of Nuclear Energy 160* (2021), 108372.

[74] Ziada, S. A flow visualization study of flow- acoustic coupling at the mouth of a resonant side-branch. *Journal of Fluids and Structures 8*, 4 (1994), 391–416.

[75] Ziada, S. Flow-excited acoustic resonance in industry. *Journal of Pressure Vessel Technology, Transactions of the ASME 132* (2 2010), 0150011–0150019.

[76] Ziada, S., and Bühlmann, E. Self-excited resonances of two side-branches in close proximity. *Journal of Fluids and Structures 6*, 5 (1992), 583–601.

[77] Ziada, S., Ng, H., and Blake, C. Flow excited resonance of a confined shallow cavity in low mach number flow and its control. *Journal of Fluids and Structures 18*, 1 (2003), 79–92.

[78] ZIADA, S., and SHINE, S. Strouhal numbers of flow-excited acoustic resonance of closed side branches. *Journal of Fluids and Structures 13*, 1 (1999), 127–142.